Rehabilitating mangroves with a sediment nourishment

M.G.A. Bles
4463188

Faculty of Civil Engineering and Geosciences
Hydraulic Engineering
April 1, 2022

Van Oord
Marine ingenuity

TU Delft

Rehabilitating mangroves with a sediment nourishment

An initial assessment using a schematised model

In partial fulfilment of the requirements for the degree of

Master of Science in Civil Engineering

at the Delft University of Technology.

by

M.G.A. (Matthijs) Bles

April 1, 2022

Student number:	4463188	
Thesis committee:	prof. dr. ir. S.G.J. Aarninkhof	TU Delft, chair
	ir. E.M.M. van Eekelen	Van Oord, supervisor
	dr. ir. B.C. van Prooijen	TU Delft
	dr. B.K. van Wesenbeeck	TU Delft
	R.J. Terry-Tyson MEng	Van Oord

Van Oord
Marine ingenuity

TU Delft

Abstract

Mangroves are productive ecosystems. Degradation of mangroves has been observed since the 1970s, due to a variety of reasons. Successful rehabilitation focuses on restoring conditions suitable for mangroves. Sediment availability has been shown to positively impact mangrove growth. Therefore, it can likely play a role in mangrove rehabilitation. This research aims to explore if the rehabilitation of coastal mangroves is possible using a sediment nourishment.

A process analysis is performed, to identify the processes driving sedimentation on a mangrove coast. This analysis uses a schematised, cross-shore, one-dimensional model, based on global data of mangrove coasts. Convex, linear and concave bottom profiles are used. The forcing on the coasts consists of three different wave heights, tidal ranges, and sea level rise rates. A homogeneous mangrove forest is present above mean sea level.

Sedimentation within the mangrove forest is caused by a combination of processes. Waves pick up the sediment, which is transported by the tide. Tidal asymmetry then drives the actual sedimentation in the forest. An increase in asymmetry results in increased sedimentation. Mangroves increase the flood dominance of slack water asymmetry, but also cause an ebb dominant peak flow velocity and duration asymmetry. Dependent on the tidal range, the influence of mangroves on net sedimentation can either be null, negative or positive. Sea level rise increases sedimentation within the mangrove, by enhancing slack water asymmetry.

The main tipping point identified is the gradient of the bed slope in cross-shore direction. If the slope becomes milder towards the shore, i.e. a convex coast, this value is negative. If the slope becomes steeper, which is the case for concave coasts, it is positive. The tipping point is when the slope does not change towards the shore. The gradient of the slope then is zero. The net sedimentation is considerably less for concave coasts than for convex coasts.

Sediment nourishments can increase sedimentation in the mangrove forest. Four nourishment designs were simulated, using the same model as for the process analysis. The designs varied in location and achieved depth across the coast. Three design considerations for a successful sediment nourishment have been identified, which are firstly the obtained bed level by the nourishment, secondly the slope of the original bed, and thirdly the location of the nourishment. First, the obtained bed level by the nourishment influences the quantity of sediment pick-up. Higher bed levels increase the sedimentation within the mangrove, by increasing sediment mobilisation rates. Second, the slope of the original bed largely influences the feasibility of a nourishment. Due to mild bed slopes, the construction of a nourishment is difficult and large volumes for a nourishment are required. Finally, the location of the suppletion should be close to the mangrove. If the nourishment is located far offshore, the sediment is not transported towards the mangrove. Rather, it then is transported away from the coast. This thesis has shown the rehabilitation of mangroves using a sediment nourishment is possible.

Preface

This thesis concludes my Master of Science in Hydraulic Engineering at the Delft University of Technology. The research was carried out at Van Oord. It gave me the possibility to help in upscaling mangrove rehabilitation efforts. This is a very interesting and relevant topic, which I enjoyed working on and am grateful for the experience I had.

First, I would like to thank my graduation committee for the guidance, support, and supervision during this process. Then, I would like to thank my Environmental Engineering colleagues at Van Oord for their support during the thesis.

I want to dedicate this space to thanking the people close to me. Friends from the freshly formed crater, thank you for not distracting me even more during my thesis. I'd like to thank Jan Mudman, aka msd, for his feedback on my work. Then, I'd like to thank Erik for the many coffee breaks at civiel, his valuable feedback, and the many fruitful discussions. Finally, I would like to thank my parents, family, and my girlfriend Evelien for their continuous support throughout my life. Thank you all.

Matthijs Bles
Rotterdam, April 2022

Contents

Chapter 1

Introduction

Mangroves are productive ecosystems, providing utility to both humans and the environment. They function as carbon sink, nursery for fish, water purification system, and supply of timber (Barbier et al., 2011). Furthermore, mangroves function as coastal protection. They stabilise the coast by trapping sediment and by attenuating waves with their typical root system (Winterwerp et al., 2020). This typical root system is shown on figure 1.1. The latter ecosystem service is rather important, as globally more and more people move to the coasts (Bouma et al., 2014). These people require coastal protection, offered by the mangroves.

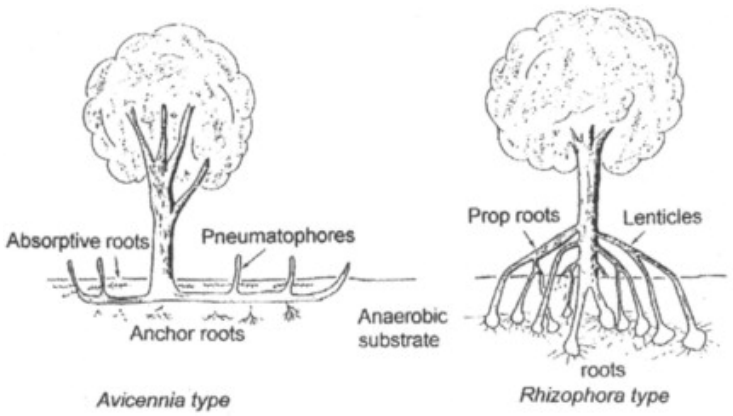

Figure 1.1: Left: *Avicennia* root system. Right: *Rhizophora* root system system (Janssen-Stelder et al., 2002)

Since the 1970s, global mangrove area decline has been observed. Annual degradation rates varying between 1-3% are often cited (Friess et al., 2019). To fight mangrove degradation, many countries have laws in place to protect these ecosystems (Lugo et al., 2014). Furthermore, rehabilitation efforts to increase mangrove cover are undertaken, albeit with varying success rates (Dale et al., 2014). Despite these efforts, mangroves have continued degrading in the 21st century (Friess et al., 2019).

Five reasons for mangrove degradation can be identified (Friess et al., 2019). These are: habitat conversion, harvesting of trees, pollution, extreme weather events, and relative sea level rise (r-SLR). Successful mangrove rehabilitation focuses on restoring suitable conditions for mangroves (Lewis, 2009). This thesis aims to find if sediment nourishments can contribute to rehabilitating mangroves.

1.1 Background information on mangroves

1.1.1 Mangrove degradation

Since the 1970s, mangrove decline has been observed. About 25-30% of global mangrove extent has been lost over the past 50 years (Polidoro et al., 2010). Five reasons for mangrove degradation can be identified. These are: habitat conversion, harvesting of trees, pollution, extreme weather events, and relative sea level rise (Friess et al., 2019).

When mangroves are degraded, two import functions are lost. First and foremost, the ecosystem services they provide are gone. Secondly, soil surface elevation can also be lost (Cahoon et al., 2003). After an event of mass mangrove extinction peat, thus the soil, collapsed. This hinders re-establishment of mangroves, as they require their habitat to be above MSL (Ricklefs & Latham, 1993).

Mangrove losses are both human and naturally induced (Thomas et al., 2017). For example, when mangrove habitat is converted, people use the land for another purpose. Apart from the cutting of mangrove trees, the abiotic conditions change such that mangroves cannot establish themselves anymore (Winterwerp et al., 2013). Next to the fact that degradation occurs because of a change in biotic or abiotic conditions, it can be a social issue (Friess et al., 2019). However, the social aspect of mangrove degradation is not considered for this research. Humans can also contribute to the rehabilitation of mangroves, offsetting their negative impact on mangroves, which is covered in subsection 1.1.2.

1.1.2 Mangrove rehabilitation

Successfully rehabilitating mangroves can be achieved by reinstating the conditions in which they can prevail (Lewis, 2009). This is called Ecological Mangrove Rehabilitation. If the reason for degradation is not removed, replanting mangroves will lead to the loss of the newly planted trees (Kodikara et al., 2017). For every reason of degradation, it holds true that rehabilitation is easier when the mangroves have not yet completely vanished (Lewis III et al., 2016). Next to the fact that ecosystem services are higher when mangroves are present, rather than gone, is that the growth and establishment of a rehabilitated mangrove can take up to five years (Mazda et al., 1997). Therefore, rehabilitation should be undertaken before mangroves are gone entirely.

In practice, mangrove rehabilitation projects success rates vary a lot. Some projects report a 90%+ mangrove survival rate, whereas others see all mangroves dying within a short time span (Lovelock & Brown, 2019; Kodikara et al., 2017). This is because mangrove rehabilitation projects are often seen as ‘one-off projects’, with little knowledge being transferred to other projects (Lewis III et al., 2019). Projects often fail due to a disregard for the hydrodynamic criteria of mangroves: they are planted on coasts with the wrong conditions, e.g. in the wrong tidal zone or in high-energy wave areas (Primavera & Esteban, 2008).

Surface elevation has been found to be essential in the re-establishment of mangroves in aquaculture ponds (Oh et al., 2017). Lower elevations lead to an increase of inundation. This reduces seedling establishment and hinders growth rates (Krauss et al., 2008). However, higher elevation levels lead to relatively higher growth rates. Increasing surface elevation within a mangrove can therefore contribute towards their rehabilitation.

Measures to rehabilitate mangroves, by enhancing sedimentation, consist in the form of permeable dams. These constructions have been investigated in both Demak, Indonesia and

in the Lower Mekong Delta, Vietnam (Winterwerp et al., 2013; Albers & Schmitt, 2015). By constructing respectively a permeable and a T-shaped dam, sedimentation was enhanced on the tidal flat. Due to surface level gain, mangroves were able to regrow on these locations (Winterwerp et al., 2020). A soft solution, using sediment, however, has not yet been investigated.

1.1.3 Soil surface elevation within mangroves

Mangrove surface elevation is not only made up of sediment, but also consists of biological and geological components (McIvor et al., 2013). The geological components, such as changes to the sea level due to El Ninõ and isostatic adjustments, are regional longer-term processes. Their timescales are three to four years and decadal respectively (Moy et al., 2002; Spada, 2017). The short term is governed by biological and sedimentary processes. Sediment and roots play a major role, but there are six known processes that govern short term surface elevation (McIvor et al., 2013), shown on figure 1.2.

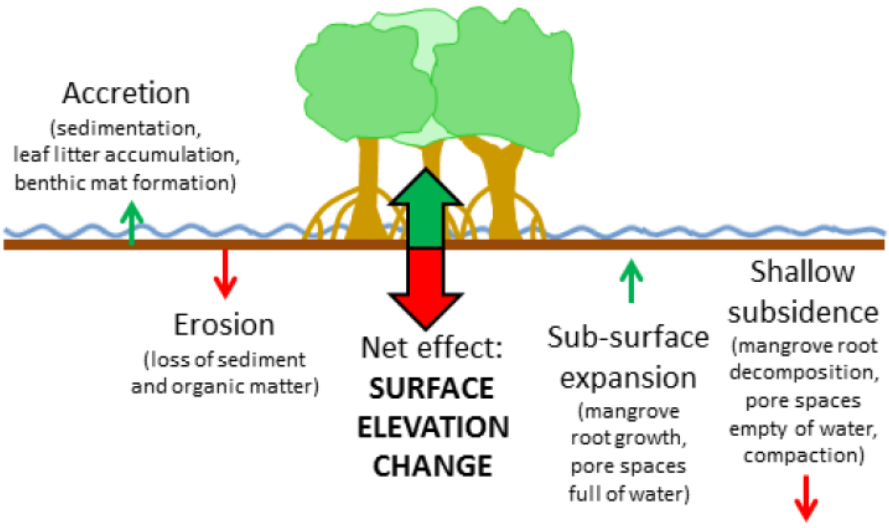

Figure 1.2: (Sub)surface processes influencing surface level elevation (McIvor et al., 2013)

Short term changes in surface elevation come from processes on the surface of the soil, i.e. accretion and erosion, or from processes on the sub-surface of the soil, i.e. expansion and shallow subsidence. The accretion and erosion of material can be both organic and inorganic matter, e.g. roots or sediment respectively. Sub-surface processes consist of the consolidation or expansion of soil, due to a change in water content in the pores, the growth or decomposition of roots, and the compaction and rebound of soils under the weight of the matter above. The relative effect these processes have, determine the rates of elevation change within a mangrove (McIvor et al., 2013).

Biotic soil processes in mangroves are not understood well. They have an inherent variability, due to ecological differences, e.g. in growth rates (Lambers & Poorter, 1992). Under equal conditions, one root system might grow more rapidly than the other, resulting in different elevation gains. Another reason for the limited understanding is the large variation within species. Some 73 species exists (Spalding et al., 2010), the global distribution of mangrove species is shown on figure 1.3, which makes that not all mangrove forests are created equal. Considering

the inherent variability of mangroves, the focus of this research will lay on the abiotic, meaning non-biological, processes.

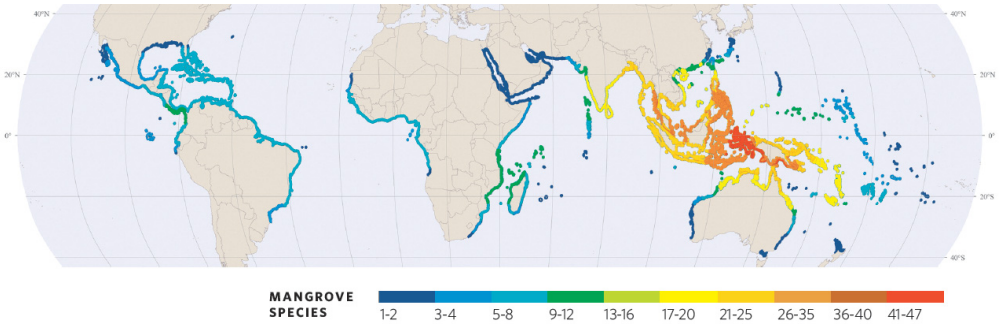

Figure 1.3: Global mangrove species distribution

Sediment plays a significant role in surface elevation level and in mangrove growth in general. After storms, large sedimentation rates are observed. However, under regular conditions the sediment often erodes again (Smith et al., 2009). This is not to state that under regular conditions, sedimentation cannot occur. In New Zealand, several mangroves are expanding due to an increase in sediment availability (Horstman, Lundquist, et al., 2018). In the Mekong Delta in Vietnam, during the wet season in summer, sediment deposition occurs. During the winter monsoon, sediment erosion takes place (Nardin et al., 2016). Krauss et al. (2014) found that in regions with sufficient sediment supply, mangroves kept pace with sea level rise. Furthermore, data has shown that in areas with sediment available, surface elevation is maintained relative to sea level rise (Lovelock, Cahoon, et al., 2015). Under what conditions sediment is eroded or is able to accrete, during both regular and extreme events, has not yet been described.

Van Maren & Winterwerp (2013) state that the main generator of sediment transport in cross-shore direction on an intertidal flat is tidal asymmetry. This is due to the combination of fine sediment properties and the hydrodynamic asymmetries. Two lag effects are scour lag and settling lag (Van Maren & Winterwerp, 2013). Settling lag is the distance a particle travels when the flow has fallen below the critical shear stress for erosion, before settling on the bed. Scour lag is the difference between the greater critical shear stress for erosion than for suspension, which causes a net sedimentation effect. SLR has a damping effect on tidal asymmetry. Due to greater depths on the intertidal, both the peak current asymmetry and slack water asymmetry are reduced (Guo et al., 2018).

When large quantities of sediment are supplied, mangroves may be buried (Terrados et al., 1997; Ellison, 1999). If the pneumatophores, or aerial roots, are fully covered, the tree usually dies, due to low oxygen levels. If the sedimentation rate is such that the roots are not completely buried, but buried significantly, growth is retarded. Exact rates of maximum sedimentation have not been defined, as this depends on local factors and on sediment characteristics (Ellison, 1999). Very fine sediment is more harmful than coarser sediment (Ellison, 1999). Terrados et al. (1997) found mortality of seedlings increased and growth reduced for *Rhizophora* sp. when a sudden sediment layer is deposited.

Understanding how and if sediment can play a role in solving r-SLR, as well as understanding the tipping points for which behaviour changes, is the main goal of this thesis. It has been shown sediment availability can prevent mangroves from drowning due to sea level rise. However, how these processes work has yet to be understood more thoroughly.

1.2 Problem statement

Mangroves are productive ecosystems, providing vital ecosystem services. However, since the 1970s, degradation of mangroves has been observed. Rehabilitation efforts are undertaken, albeit with varying success rates. Sediment can likely play a role within mangrove rehabilitation. Surface elevation has been shown to be key to mangrove establishment. Furthermore, in places with abundant sediment supply mangroves are expanding.

How sediment can be used has not yet been investigated. To do so, first an understanding of the coasts typical for mangroves is required. This is obtained by performing a process analysis. Using the results, possible sediment nourishment strategies are investigated and evaluated.

1.3 Aim & objectives

Considering the problem statement, the following aim of this thesis has been defined:

The aim of this research is to determine if and how the rehabilitation of coastal mangroves using a sediment nourishment is possible.

To reach the research aim, three objectives have been formulated. These are:

Objective 1. To identify the processes driving sedimentation on a mangrove coast.

Objective 2. To identify tipping points, for which sedimentation behaviour changes drastically across the coast.

Objective 3. To determine the possibilities and design considerations of a sediment nourishment, to influence the sedimentation within the mangrove.

1.3.1 Approach

Objective 1. To identify the processes driving sedimentation on a mangrove coast, a process analysis is performed. This allows for an understanding of the interactions between the hydrodynamic processes and sediment transport.

The process analysis will be performed in a schematised model, following a step-wise approach. A schematised model is used, rather than a case location. That allows knowledge transfer to several locations rather than being valid for a single site. Gradually, complexity is added by including more hydrodynamic forcings in the model. This step-wise approach enables an understanding of the processes by themselves, but also their interaction with one another.

Objective 2. Tipping points are identified by determining where behaviour identified in the process analysis changes drastically. The results of the process analysis are carefully analysed and interpolated. This allows for the identification of tipping points found on mangrove coasts.

Objective 3. Several nourishment designs will be tested on a mangrove coast, to compare and analyse their behaviour. The nourishment designs are created using limitations of dredging vessels. The analysis of the design is based on the resulting sedimentation within the mangrove forest, the nourishment volume required to obtain that sedimentation, and the constructability of the nourishment.

1.4 Scope

The scope of this study is limited to the hydrodynamic processes of the mangrove coasts. The behaviour is investigated under regular, non-extreme event, conditions on a schematised coast. Ecological processes are not considered in the research. The time-scale is 1 month. Feedback interactions on the intertidal are not considered, due to short-time scale model and the quantity of scenarios investigated.

1.5 Reader guide

In chapter 2, the schematised model is presented, to investigate the processes driving sedimentation within the mangrove. Chapter 3 covers the various scenarios simulated, and then presents the results of the process analysis. Chapter 4 gives a global overview of processes on a mangrove coast, and aims to identify tipping points for which behaviour changes. A discussion on the obtained results is also presented. Furthermore, a conceptual model for mangrove coasts is presented. In chapter 5, several nourishment designs are tested and compared, to evaluate possible nourishment strategies for mangrove coasts. The conclusion is presented in chapter 6. Finally, in chapter 7, recommendations are made for applications and future research.

Chapter 2

Methodology

In this chapter, the model to perform the process analysis is presented. First, the model is described in section 2.1. Then, in section 2.2, the model is validated. Section 2.3 performs a sensitivity analysis. Section 2.4 concludes the chapter by summarising the model.

2.1 Model description

The schematised model for the process analysis should simulate the behaviour of mangrove coasts with a shallow foreshore. The model is one-dimensional in the cross-shore, and is made using global data observed at mangrove coasts. One dimension is appropriate, as mangrove coasts coasts experience forcing mainly in the cross-shore direction, due to their shallow foreshore (Le Hir et al., 2000). Furthermore, a one-dimensional model is the least complex, allowing a thorough understanding of the basic processes and their interactions. The global data allows for a description of generic mangrove coasts, with conditions that are commonly found on these types of coasts. These three characteristics - bottom profile, tide, waves, and sea level rise - are chosen such that they represent observed conditions. The values for these characteristics are presented in chapter 3.

Delft3D is chosen as an appropriate modelling program, since it is able to simulate the behaviour on a mangrove coast. In this section, first Delft3D will shortly be discussed. Then, model settings will be given. After the model settings, boundary conditions are stated. Then, initial conditions are discussed.

2.1.1 Delft3D

The schematised model of the coast is created in Delft3D, a process-based software package developed by Deltares, which can simulate hydrodynamics, sediment transport, waves, and morphodynamics. Delft3D consists of several modules that can be run either independently or jointly. The modules used for the process analysis are a flow and a wave module, named Delft3D-FLOW and Delft3D-WAVE respectively.

Flow module The flow module is a multi-dimensional (2D or 3D) hydrodynamic and sediment transport simulation program, which calculates non-steady flow and transport phenomena. The non-steady flow can result from meteorological, i.e. wind, and tide, forcing. Furthermore,

forcing can come from pressure gradients due to free surface gradients or density gradients. It is calculated on a boundary fitted grid (Deltares, 2021a).

Delft3D-FLOW calculates the flow and transport by solving the horizontal equations of motion, the continuity equation and the transport equation for conservative constituents. The flow is calculated by using the one-dimensional shallow water equations. Sediment transport in Delft3D can be modelled for cohesive and non-cohesive sediment types. As this concerns a mud coast, cohesive sediment is selected. Cohesive sediment transport is based on the Partheniades-Krone formula. It compares computed bed shear stresses versus the critical bed shear stress to calculate erosion fluxes. Deposition is calculated using the concentration, settling velocity, and a dimensionless reduction factor (Deltares, 2021a).

Wave module The wave module in Delft3D is based on the SWAN (Simulating WAves Nearshore) model of the TU Delft, in which waves are described using a two-dimensional wave action density spectrum. The wave action density is the wave energy density divided by relative frequency, $N(\sigma,\Theta) = E(\sigma,\Theta)/\sigma$. It seems possible to predict waves with reasonable accuracy using the spectral distribution of the second order moment of the waves, albeit not sufficient to fully describe the waves statistically (Deltares, 2021b).

The evolution of the wave spectrum is described by the spectral action balance equation. In SWAN, waves are generated by wind. Dissipation of waves occurs by white capping, bottom friction and depth-induced breaking. Furthermore, wave energy is shifted between frequencies by non-linear wave-wave interactions, i.e. as triads and quadruplets.

2.1.2 Settings

The model settings are important, as this concerns a schematised model. The influence of all settings on the results should be understood. Furthermore, the model should be reproducible. In table 2.1, all model parameter settings are presented. All settings are presented and some important ones are highlighted.

Table 2.1: Parameter settings for Delft3D

Parameter		Value	Unit	Description
Flow module parameters				
dt		0.0125	min	Time step
dx offshore		150	m	Grid dimension on offshore boundary
dx intertidal		5	m	Grid dimension in the intertidal boundary
C		65	$m^{1/2}/s$	Chézy roughness parameter
ρ		1025	kg/m^3	Water density
HEV		1	m^2/s	Horizontal eddy viscosity
HED		10	m^2/s	Horizontal eddy diffusivity
d_{min}		0.01	m	Minimum depth for flow calculation
gammax		0.5	-	Additional parameter to limit wave height
Advection scheme		Cyclic	-	Advection scheme for momentum
Flag for velocity output		#glm#	-	Lagrange flow velocities output
Sediment transport parameters				
ρ_{hs}		1600	kg/m^3	Reference density for hindered settling
ρ_s		2650	kg/m^3	Specific density
ρ_s		500	kg/m^3	Dry bed density
w_s		$1 \cdot 10^{-4}$	m/s	Settling velocity
$\tau_{cr,e}$		$1 \cdot 10^{-1}$	Pa	Critical bed shear stress for erosion
$\tau_{cr,s}$		$1 \cdot 10^{3}$	Pa	Critical bed shear stress for sedimentation
M		$1 \cdot 10^{-2}$	$kg/m^2/s$	Erosion parameter
$d_{min,sed}$		0.1	m	Minimum depth for sediment calculation
Wave parameters				
Wave direction		270	°	Wave direction
T_p		4	s	Peak wave period
γ		3.3	-	JONSWAP peak enhancement factor
d_{min}		0.1	m	Minimum depth for wave calculation
γ		0.5	-	Depth induced breaking parameter
Mangrove parameters				
Stem	C_d	1.0	-	Stem drag coefficient
	Nplants	0.7	$1/m^2$	Number of stems per m^2
	Height	4.5	m	Stem height
	Diameter	0.3	m	Stem diameter
Root	C_d	0.8	-	Root drag coefficient
	Nplants	125	$1/m^2$	Number of roots per m^2
	Height	0.2	m	Root height
	Diameter	0.01	m	Root diameter

Advection scheme for calculation The advection scheme is the numerical method to calculate the advection terms in the momentum equation. Three options exist: Cyclic, Flood or Waqua. The first two are possible choices for this model.

On first hand, the Flood scheme may seem logical: it can accurately calculate flooding and drying of cells. However, this scheme is more appropriate for short term runs, such as a dike

breach, with a limited time span and small time step. This is due to the fact that the integration of the advection term is explicit, and therefore the time step is restricted by the Courant number.

The Cyclic scheme on the other hand, integrates the advection term implicitly. Thus, the time step is not limited by the Courant number. This means a larger time step can be used, without losing stability in the model. Therefore, the Cyclic scheme is used.

Minimum depth for flow calculation The minimum depth for flow calculation is a balance between the Flow model stability and realistic flow velocities. If a small depth is chosen, e.g. < 0.01 m, then a small time step is required to have no model instabilities. However, if a large minimum depth is chosen, then computed flow velocities in the intertidal area become unrealistically large. This is due to the fact that a cell that changes from dry to flooded needs to fill the entire volume of the cell. Therefore, a value of 0.01 m has been chosen.

Minimum depth for wave calculation The minimum depth for waves is based on a choice of realism versus stability. On one hand, waves propagate into small - but not tiny - depths when using a small depth, i.e. 0.1 m. However, wave calculations in even smaller depths, such as 0.01 m, result in unstable numerical calculations. The wave height then exceeds the breaker criterion, due to numerical artefacts. Therefore, 0.1 m has been chosen.

Depth induced breaker parameter The wave breaker criterion for shallow coasts has been investigated to be 0.5 for slopes of 1:1000 (Salmon et al., 2015). Therefore, this value is chosen in both the Flow model, as gammax, and in the Wave model, as γ.

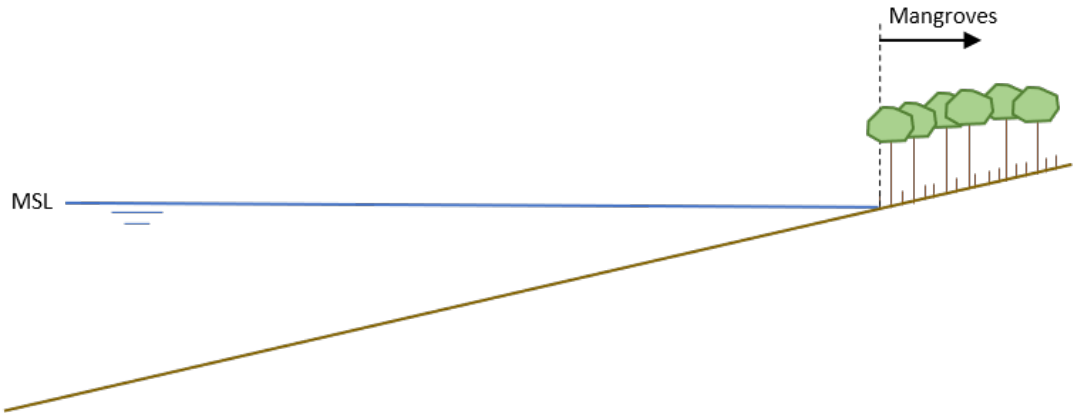

Figure 2.1: Cross-shore location of mangroves in the model

Mangrove parameters A homogeneous mangrove distribution is present above MSL, of mangrove species *Avicennia marina*, as shown on figure 2.1. This is a pioneer-type mangrove species, which grows in a variety of conditions. The species is found on many locations around the globe (Alvarez Cruz, 2008). The mangrove vegetation is schematised as cylinders.

The root density per m^2 has been observed to be varying between 50-250 (Norris et al., 2017; Horstman, Bryan, et al., 2018). A value in the middle of the range, being 125, is chosen. Roots have a C_d that varies between 0.5-1.0, and have a height of 0.2 m. For the C_d, a value of 0.7 is assumed. The stem diameter varies between 0.1-0.4 m, and has a C_d of 1.0 (Alvarez Cruz, 2008; Volvaiker et al., 2018). The trees can grow up to 10 meters high (Alvarez Cruz, 2008).

2.1.3 Grid

The Flow module and the Wave module each require a computational grid. They have been visualised on figure 2.2.

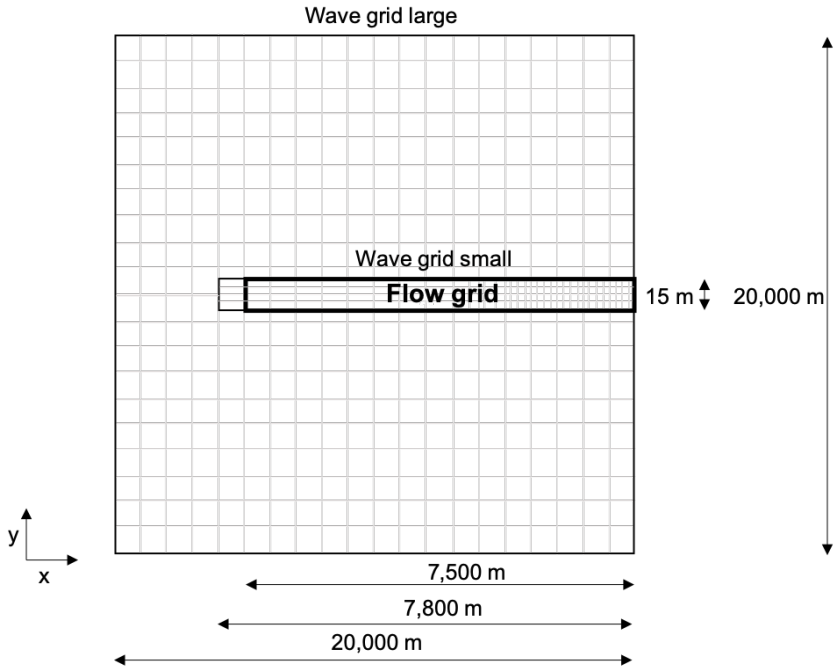

Figure 2.2: Flow and wave grids (not to scale)

Flow grid Delft3D requires a 2D flow grid. However, the interest lays in a 1D model. Therefore, a quasi-1D model is used. In cross-shore direction, the model is 7,500 m, whereas in the longshore direction, the model is 15 m. Thus, the cross-shore dimension is way larger than the longshore dimension, and a quasi-1D model is obtained. The flow grid has a dimension dx of 150 meters in the offshore and in the intertidal a cell size dx of 5 m. The width dy is equal for each cell, and is 5 meters. The refinement between the intertidal and the offshore is gradual, the cell size reduces with steps of $dx_{i+1} = dx_i/1.2$, which is the limit set in the Flow user manual (Deltares, 2021a). This refinement is required, as larger grid cells cause an instability due to a combination of drying/flooding of cells with the falling/rising of the water level. However, having small cells in the offshore cells leads to large calculation times.

Wave grid Two wave grids are used for the wave module. A large, 20 x 20 km, grid, and a small grid, which is 15 x 7,800 m. The large grid consists of 50 x 50 cells, all are 400 x 400 m. The large grid requires these dimensions for two reasons. First, in the x-direction, the waves should enter the model on offshore conditions. That is because the wave data consists of offshore conditions. Deep water waves hold true when:

$$h > 0.5 * L_0 \quad L_0 = \frac{gT^2}{2\pi} = \frac{9.81 \cdot 4^2}{2\pi} = 25 \text{ m} \quad h_{req} = 0.5 \cdot 25 = 12.5 \text{ m}$$

Extrapolating the convex profile slope on the boundary requires a wave grid of 20 km to fulfil this criterion. Secondly, the width or y-direction, should be this wide due to ‘shadow effects’,

which means that wave energy is lost through the boundaries. Using a sufficiently wide computational grid moves the 'shadow effects' outside the flow grid, which is the area of interest (Deltares, 2021b).

The small, nested model has cells exactly equal to the flow grid, but with two extra cells in the x-direction on the offshore boundary. This accounts for the 'shadow zone', which has some inaccuracies in the wave height. The zone is not a problem if it is outside of the area of interest, which is the flow model, thus these two extra cells are necessary.

In the wave grid, it is specified how and what Flow module quantities should be used. It is chosen to not use any flow quantities on the large grid, as it lays mostly outside the flow model. For the small wave grid, the hydrodynamics, being water level, current, and bathymetry, are used and extended to the wave grid.

2.1.4 Boundary conditions

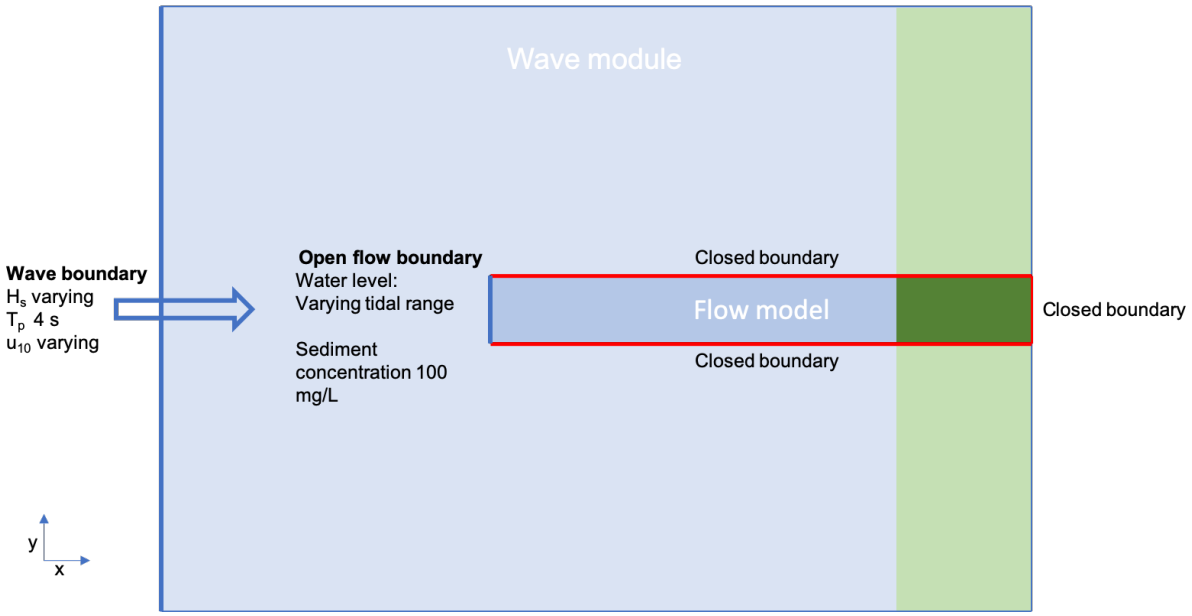

Figure 2.3: Boundary conditions for Flow and Wave module

Flow boundaries The flow model has four boundaries. Three of those, shown in red on figure 2.3, are closed boundaries, meaning flow cannot enter or exit the model. The interest is in the cross-shore direction, which allows for the closed boundaries in dx direction. On the open boundary condition a water level is imposed, which consists of the tide and sea level rise, and a sediment concentration.

The water level is expressed in terms of an M2 component, an S2 component, and if sea level rise is included in the model, an A0 component. Their values are presented in chapter 3, section 3.1.

The sediment boundary is added as a constant concentration of 0.1 kg/m^3, which equals 100 mg/L. This is a value commonly cited as present on mangrove coasts (Furukawa et al., 1997).

Wave boundary The wave module consists of four open boundaries, wave energy can enter and exit the model through all the boundaries. One boundary condition is applied, on the 'eastern' boundary. There, the wave conditions as specified in table 3.1 are applied.

2.1.5 Initial conditions

Water level The initial water level is set to the spring tide water level. This is to make sure all cells have been wet once, which results in less initial instabilities. Furthermore, starting at high water reduces the spin-up time in the model.

Sediment concentration The initial sediment concentration in the model is set to 0 kg/m^3. Combined with a spin-up time, this results in the most realistic sediment distribution in the model (Van Maren, n.d.).

2.1.6 Key assumptions

Morphostatic simulations It is chosen not to include morphodynamics, nor an erodible bottom, in the model. Sediment that settles and be picked up and moved within the model, but no sediment can be eroded from the fixed bed layer. Furthermore, the bed level does not change when sediment settles on the bed. There are a couple of reasons to not include a varying bed level.

The first is that the forcing, by the tide and waves, on the profile does not necessarily correspond to the equilibrium profile for that forcing. This comes from the fact that global databases have been used to select the boundary conditions. If morphodynamics would be included, the profile would first shift to its equilibrium profile, thereby influencing the observations and sedimentation rates.

The second reason is that a choice is made to investigate short term behaviour, rather than long term behaviour. This is done, as a sediment strategy usually is for the short term. Updating bed levels is not as relevant on this short term, as it is on a longer term simulation.

Finally, morphodynamics are interesting to look into feedback loops. However, the feedback is investigated by looking into the different profiles, rather than having a longer-term simulation for one coastal profile.

Having sediment pickup in the model, without having morphodynamics, could cause unrealistic sedimentation rates. Due to the absence of morphodynamics, negative feedback loops are not present. Any damping effect they have on sediment transport is not included. This could lead to non-realistic sediment transport rates.

Ecology It is assumed that the mangrove forest is present above the 'original' mean sea level, and is homogeneous in its vegetation. When sea level rise is added, the location of the mangroves is not changed. The reasoning for this assumption is that if the mangrove forest would change with SLR, it would only change the location of where the processes occur, rather than showing new interactions. A homogeneous forest is assumed, as detailed data of mangrove distribution in a forest is lacking, thus the model is made based on data of other research. Ecological processes, such as the growth of trees and roots, are not included in this research.

Fine sediment dynamics The fine sediment dynamics are schematised. This means a constant critical bed shear stress is used, whereas in reality consolidation of bed material would occur. As morphodynamics are excluded, the absence of consolidation is not an issue. Flocculation has not been included, as this depends on local factors such a salinity and turbulence (Kranck, 1973; Winterwerp, 2002).

The formation and streaming of fluid mud has been shown to be a considerable driver of respectively wave damping and sedimentation (Winterwerp et al., 2020). However, much remains unknown about these fluid mud processes.

Considering the purpose of the process analysis, which is to understand the processes driving sedimentation, flocculation, consolidation, and the formation of fluid mud, are excluded from the model. They are important factors in the exact behaviour, but they are not expected to be the drivers of sedimentation. Therefore, they are excluded from the model.

Model duration A single model run will be 1 month and 4 days long. This consists of a hydrodynamic spin-up time of 4 days, and two spring-neap tidal cycles. The first spring-neap tidal cycle is to allow the sediment to spread through the model, whereas the second is used for the analysis.

A relatively short model duration of roughly one month, rather than a longer duration, is most appropriate for this research. Given that the boundary conditions are constant, and the quantity of model combinations, a longer model duration would result in excessive computing time. Over one spring-neap tidal cycle all phenomena on the coast have occurred. A longer model duration would be appropriate for feedback loops, however these are not the area of interest of this research.

Extreme events and barotropic currents It is assumed no extreme events occur during the model simulation. This is due to the fact that this model has been created for regular conditions. For a storm event, model setting most likely have to change. Barotropic currents are not considered. These depend on salinity, temperature, and set-up due to wind, which are all local effects. Therefore, they are not added to this schematised model.

2.1.7 Model output

The main output of the process analysis will be an overview of the abiotic processes acting on the mangrove coast, with their standalone effect and the influence they have on each other and the mangrove coast. To assess the abiotic processes, flow velocities and sediment fluxes require investigation. These are analysed per model simulation, by creating overview plots. The overview plots are cross-shore snapshots in time during spring tide, over a 12 hour period, with various water levels, accompanied by maximum bed shear stresses, flow velocities, and sediment transport rates. Maximum bed shear stresses are used, rather than mean bed shear stresses, as this is a more relevant measure for fine sediment pick-up (Deltares, 2021a).

Tidal asymmetry is analysed, as this is a significant driver of sediment transport (Van Maren & Winterwerp, 2013). Tidal asymmetry is investigated by evaluating the flow velocity and sediment transport rates over a 12 hour period during spring tide, on 4 bed levels. The bed levels are -5.0, -0.5, +0.0, and +0.5 m. Net sediment fluxes are evaluated by integrating the sediment transport at one location, for a spring-neap tidal cycle. Net intertidal sedimentation is

computed by integrating the sediment transport at LAT. The net sediment transport above MSL is computed by integrating net sediment transport at MSL.

Using the aforementioned data and analyses, the hydrodynamic processes driving sedimentation, and tipping points can be evaluated.

2.2 Model validation

Usually, a model is calibrated and validated based on a real-life data set. However, as this is a schematised model, such a data set does not exist. Therefore, the model cannot be validated nor calibrated based on a real-life scenario, but it will be validated using an analytical calculation.

Calibration means tweaking the parameters such that model behaviour is equal to real-life behaviour. In this situation, with a schematised model, calibration therefore is not required. Understanding the impact of model parameters on the results is, though. Therefore, a sensitivity analysis is performed in section 2.3.

The model is validated by calculating flow velocities analytically, and comparing these to the observed flow velocities in the model run without any waves. Analytical flow velocities on a shallow bed can be calculated by (Le Hir et al., 2000):

$$u(x) = \frac{\pi R}{\beta T_{tide}} \tag{2.1}$$

With $u(x)$ the flow velocity, R the tidal range, β the slope, and T_{tide} the tidal period. As seen on figure 2.4, the flow velocity in the model is almost exactly equal to the calculated flow velocity, below MSL. For values above MSL, the formula does not hold true. There, the flow velocity reduces until it reaches zero (Le Hir et al., 2000). This behaviour is seen in the model.

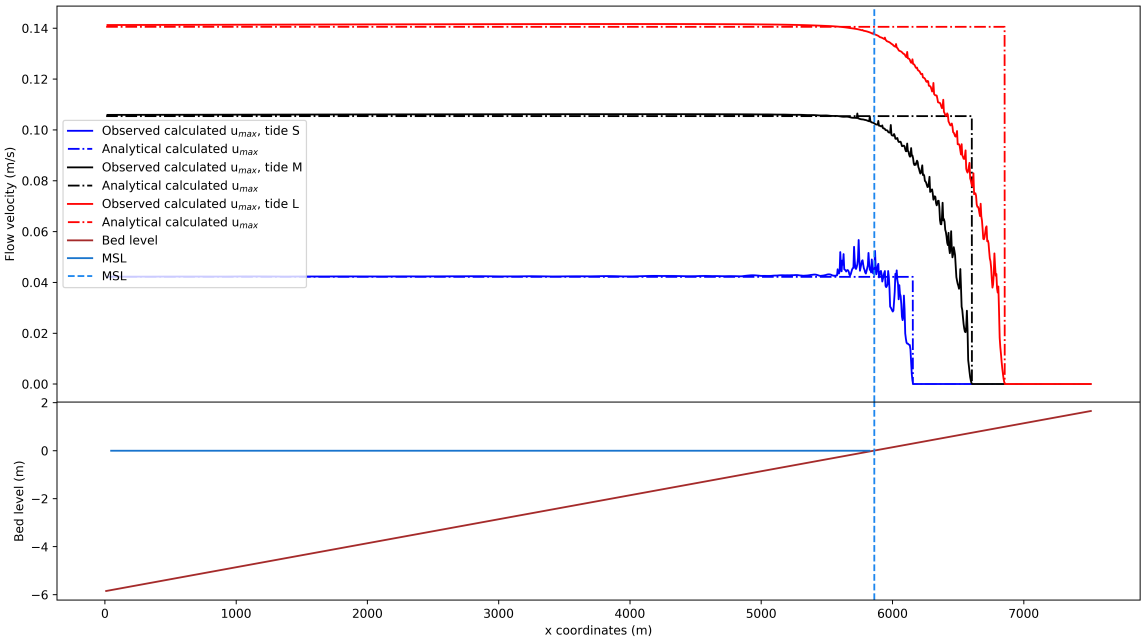

Figure 2.4: Model validation by comparing analytically calculated maximum flow velocities with observed maximum flow velocities in the model

Some model artefacts can be seen in around MSL, in the form of a noisy maximum flow velocity signal. These artefacts cause a slight variation within the model behaviour. These do not form a problem for the model results, as these errors are in the order of 0.01 m/s. This means that their influence on the sediment flux is minor. Therefore, it can be concluded that the model works appropriately.

2.3 Sensitivity analysis

In this section, the sensitivity analysis is performed. Hydrodynamic, sediment transport and mangrove parameters are tested on their influence on net sedimentation. Some of the parameters influence the stability of the model, which has been discussed in section 2.1, others influence the model behaviour quantitatively. The parameters that influence the stability of the model are discussed qualitatively, whereas the parameters that influence behaviour quantitatively are compared on their relative influence on net sedimentation in the intertidal and above MSL.

The net sedimentation is defined as the sediment transport, integrated on either LAT for intertidal sedimentation, or at MSL for MSL sedimentation. All sensitivity analysis runs have been performed on a linear coast, with a tidal range of 0.8-1.5 m, and a significant wave height H_s of 0.6 m. Three values per parameter are tested: the one used in the report (denoted by M in the tables), a larger value (L) and a smaller value (S). In appendix A, plots are presented of the sensitivity to the varying parameters.

2.3.1 Hydrodynamic sensitivity analysis

The parameters tested in the hydrodynamic sensitivity analysis are presented in table 2.2.

Table 2.2: Sensitivity analysis: hydrodynamic parameters

Parameter	S	M	L	Unit
Minimum calculation depth for flow	0.001	0.01	0.1	[m]
Grid dimension dx	1.5	5	30	[m]
Calculation scheme for momentum	Flood		Cyclic	[-]
Chézy parameter C	40	65	90	$[m^{\frac{1}{2}}/s]$

Minimum calculation depth for flow The minimum calculation depth for flow is a parameter that influences the model stability. A larger minimum depth for flow calculations, such as 0.1 m, leads to unrealistic slack water. The flow velocity goes from 0 m/s to its maximum almost instantly. For the smaller value of 0.001 m, the model become unstable. 0.01 m is a value that does not have significant instabilities, but does show slack water behaviour.

Grid dimension dx The grid dimension dx impacts the model stability. Increasing the grid dimension dx scales the computation time inversely proportional. 5 m leads to 7 hours, a 1.5 m grid results in 15 hours, whereas 30 m leads to 1 hour. However, a dx of 30 m does not capture the rising tide correctly. Flow velocities are rather high on the front of the tidal wave. This

comes from the way cells are flooded: when going from dry to wet, the flow velocity depends on the volume required to fill the cell. A large dx therefore gives high flow velocities going from dry to wet. On the other end of the spectrum is the small dx, of 1.5 m. This leads to an unstable model, giving a saw tooth velocity profile.

Calculation scheme for momentum The calculation scheme for momentum is a stability parameter. For equal model settings, the flood scheme is unstable, whereas the cyclic scheme is stable. The cyclic scheme has an implicit time step, while the flood scheme has an explicit time step. The explicit time step imposes a restriction on the length of the time step for a stable calculation, resulting in a longer simulation time (Deltares, 2021a). Therefore, for a longer simulation time, the cyclic scheme is appropriate.

Chézy parameter C The Chézy parameter influences model behaviour quantitatively, by changing the influence of the bed on the flow. The higher value , 90 $m^{\frac{1}{2}}/s$, is found in literature for several mud coasts (Van Rijn, 2020). The lower value of 40 $m^{\frac{1}{2}}/s$ is cited for estuaries, where mangroves are also observed (Toffolon et al., 2006).

An increase of 40%, from 65 to 90 $m^{\frac{1}{2}}/s$, leads to an increase of the net sedimentation above MSL by 69%, and in the intertidal of 200%. A reduction of 40%, from 65 to 40 $m^{\frac{1}{2}}/s$, increases the net sedimentation above MSL by 17%. Sedimentation within the intertidal is reduced by 13%.

The variation of the net sedimentation with varying Chézy parameters means that the bottom roughness is of significant influence on the results.

2.3.2 Sediment transport sensitivity analysis

The parameters for the sensitivity analysis of sediment transport are shown in table 2.3 below.

Table 2.3: Sensitivity analysis: sediment transport parameters

Parameter	S	M	L	Unit
w_s	0.05	0.1	0.5	[mm/s]
$\tau_{cr,e}$	0.05	0.1	0.5	[N/m^2]
M	0.001	0.01	0.1	[kg/m^2/s]
c_b	0.05	0.1	0.5	[kg/m^3]

Sediment parameters do not influence hydrodynamics, they only change the quantity of the sedimentation. This is due to the fact that this concerns a morphostatic model, where no feedback is present between the bed and the forcing. All parameters are quantitative parameters.

Settling velocity w_s A larger settling velocity, increasing by 400%, reduces net sediment import above MSL by 39%. It increases net sediment transport by 17% within the intertidal. The reason for this reduction in the mangrove, but an increase in the intertidal, can be found in the fact that sediment is able to settle in the intertidal, where it is not mobilised anymore due to lower maximum bed shear stresses. It then does not reach the mangrove anymore, thereby reducing the net sedimentation in the mangrove (Van Maren & Winterwerp, 2013). A smaller

settling velocity, reducing by 50%, reduces net sediment transport rates above MSL by 8%. Within the intertidal, a smaller settling velocity decreases net sediment transport by 18%. This reduction in sedimentation can be found in the fact that during larger tides, the sediment is not able to settle altogether (Van Maren & Winterwerp, 2013).

Critical bed shear stress for erosion $\tau_{cr,e}$ A larger critical bed shear stress, increasing by 400%, increases net sediment transport above MSL by 57%. Within the intertidal, sediment transport increases by 259%. Reducing the critical bed shear stress by 50% increases net sediment transport above MSL by 9%. Net sediment transport within the intertidal reduces by 8%.

Erosion parameter M Increasing the erosion parameter M by 900%, does not change the results. Net sediment transport within the intertidal and above MSL remain constant. A reduction of 90% of the erosion parameter increases net sediment transport above MSL by 18%. It increases net sediment transport within the intertidal by 22%.

Sediment boundary concentration c_b A larger sediment concentration, increasing by 400%, increases the intertidal and MSL net sediment transport by 400%. Reducing the sediment boundary concentration by 50% reduces both the intertidal and MSL net sediment transport by 50%.

2.3.3 Mangrove parameter sensitivity analysis

The mangrove parameters analysed are shown in table 2.4. The values for the mangrove parameters have been cited in literature as appropriate values for *Avicennia marina* (Alvarez Cruz, 2008; Norris et al., 2017; Horstman, Bryan, et al., 2018). The large values are the upper end of the range, whereas the small values are on the low end.

Table 2.4: Sensitivity analysis: sediment transport parameters

Parameter	S	M	L	Unit
Roots				
Number of plants	50	125	200	[m^{-2}]
C_d	0.5	0.7	0.9	[-]
Stem				
Number of plants	0.33	0.7	1.0	[m^{-2}]
C_d	0.8	1.0	1.2	[-]
Diameter	0.15	0.3	0.45	[m]

Root parameters

It has been found that varying the root parameters does not influence the net sediment transport in the intertidal, nor above MSL. They do influence model behaviour.

Stem parameters

It has been found that varying the stem parameters does not influence the net sediment transport in the intertidal, nor above MSL. They do influence model behaviour.

2.3.4 Influential parameters

Three parameters are identified that influence net sediment transport significantly. These are the Chézy parameter, the critical bed shear stress $\tau_{cr,e}$, and the sediment boundary condition c_b.

2.4 Model summary

In summary, a schematised 1D model has been created. The reason to chose for a 1D model is due to the cross-shore dominance on shallow foreshores (Le Hir et al., 2000). The main assumptions underlying the schematised model are that there are no morphodynamics. The mangroves are fixed and homogeneous above MSL. The grid size used in the dx direction in flow model varies from 150 m in the offshore towards 5 m within the intertidal. The dy cell dimension is 5 m. The sediment boundary consists of a fixed concentration of 0.1 kg/m^3.

The sensitivity analysis has shown that the Chézy parameter, sediment boundary concentration, and critical bed shear stress for erosion influence the net sediment transport most significantly.

Using these model settings, a stable model has been created. It allows for an investigation in the abiotic processes driving sedimentation in mangroves.

Chapter 3

Results

In this chapter, the scenarios for the model simulations are covered. Afterwards, the results are presented. The goals of this chapter are to find out how the processes work at different mangrove mud coasts and to investigate which hydrodynamic processes drive sedimentation in a mangrove. Several figures are shown, explaining model behaviour. For overviews of all model simulations, the reader is referred to appendix B.

The scenarios are presented in section 3.1. The system behaviour without mangroves is discussed in section 3.2. Section 3.3 discusses the impact of mangroves on the coast. In section 3.4, the impact of SLR is shown. Finally, section 3.5 presents the main findings.

3.1 Process analysis scenarios

For the process analysis, a step-wise approach is used, which gradually adds complexity. This allows an understanding of the processes by themselves and the influence they have on each other. The different steps are:

1. Tide
2. Tide and waves
3. Tide, waves, and mangroves
4. Tide, waves, mangroves, and sea level rise

SLR is added lastly, to be able to first analyse how the coasts behave under regular conditions and to then see the impact of SLR on the behaviour of the coast. SLR is tested on one bottom profile, to reduce calculation time. It is expected that the changes in behaviour due to SLR do not change per coast (Guo et al., 2018).

In each of the steps, characteristics are varied on three bottom profiles. The characteristics are based on global data, and are presented in subsection 3.1.1 below. This results in a variety of model simulations, which are presented in subsection 3.1.2.

3.1.1 Characteristics

The schematised model consists of boundary conditions and bottom profiles that are varied per run. Three values are chosen for each of the varying characteristics. In table 3.1, all the values are presented. The discretisation of the characteristics found on mangrove coasts is described in this subsection.

Table 3.1: Characteristics for schematised model

Condition	**Small**	**Medium**	**Large**
Bottom profile	Concave	Linear	Convex
Average bed slope	1:1000		
Tidal range R	0.4 - 0.6 m	0.8 - 1.5 m	1.0 - 2.0 m
M2 component	0.5 m	1.15 m	1.5 m
S2 component	0.1 m	0.35 m	0.5 m
Significant wave height H_s	0.3 m	0.6 m	1.0 m
Peak wave period T_p	4 s	4 s	4 s
Wind speed u_{10}	2.5 m/s	5 m/s	7.5 m/s
Sea level rise	0.2 m	0.4 m	0.6 m

Bottom profile The most commonly observed average bed slope for mangrove coasts is 1:1000, as shown on figure 3.1a (Athanasiou et al., 2019). The most common closure depth, which is the depth for which no significant change in bottom profile is observed during a time interval, associated with these slopes is 6 m. This is shown on figure 3.1b (Athanasiou et al., 2019). The bed slope of 1:1000 and the closure depth of 6 m are used as characteristic values in the model.

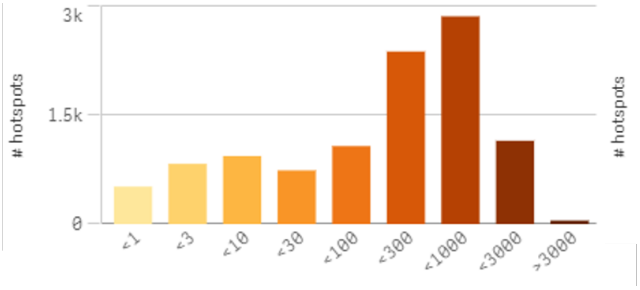

(a) Common bed slopes for mangrove coasts

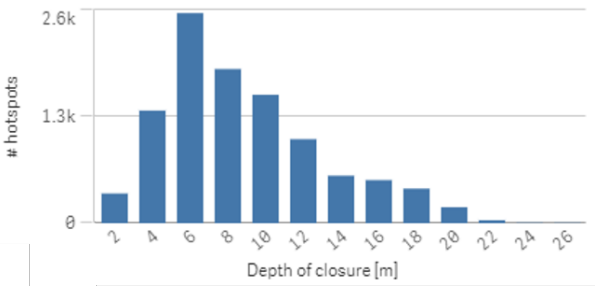

(b) Closure depth for bed slope 1:1000

According to Winterwerp et al. (2013), the offshore shape of the coast determines if a mangrove coast is either stable or unstable. A stable coast keeps its shape constant, which allows for mangrove colonisation. An unstable coast on the other hand has a shape that changes and does not allow for mangrove colonisation. A convex coast is assumed to be stable, whereas a concave coast is assumed to be unstable. The instability comes from an interaction of near-shore wave-induced mobilisation of the sediment, which is transported offshore by the tide. For a convex coast it is exactly the other way around: waves mobilise sediment offshore, which is transported onshore by the tidal current. For this research, it is interesting to understand what the role of the shape of the foreshore is in terms of r-SLR rates. Therefore, three bottom profiles shapes haven been chosen, as shown on figure 3.2.

The bottom profiles chosen are concave, linear, and convex. The shapes of these profiles is shown on figure 3.2. The exact shapes are based on (Van Maren & Winterwerp, 2013). The profiles in the model all start at -6 m on the offshore boundary. The onshore boundary is at +1.65 m. With a slope of 1:1000, this results in a model of 7650 m.

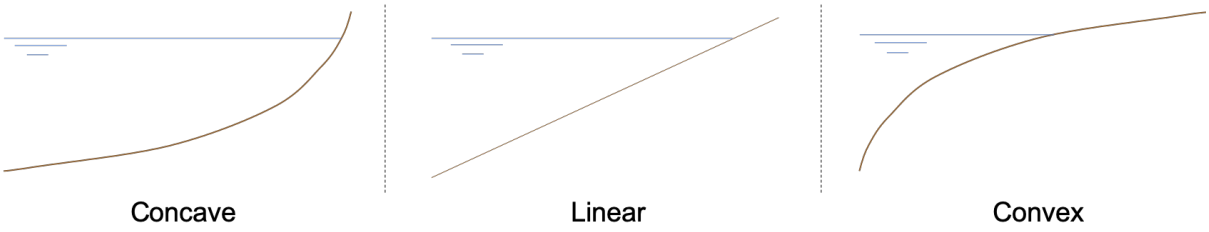

Figure 3.2: Bottom profiles, not to scale

Tide Three different tidal ranges have been defined: 0.4-0.6 m, 0.8-1.5 m, and 1.0-2.0 m. They are defined by an M2 and S2 component. The values have been based on tidal ranges from different locations around the globe, from research by Lovelock, Cahoon, et al. (2015); McIvor et al. (2013); Albers & Schmitt (2015); Winterwerp et al. (2020). Furthermore, a global tidal database, filtered on mangrove coasts, has also been used, to quickly evaluate if the tidal ranges by these researchers are in the correct range (Ray & Center., 1999).

Waves Along mangrove coasts, different significant wave heights are observed. For this research, the offshore significant wave heights chosen are $H_s = 0.3$, $H_s = 0.6$, and $H_s = 0.9$ m. All have a peak wave period T_p of 4 s (Ray & Center., 1999; Lovelock, Cahoon, et al., 2015; McIvor et al., 2013; Albers & Schmitt, 2015; Winterwerp et al., 2020). It has been chosen to vary the wave heights, but keep the peak period constant, to see the effect of a varying wave height. A shorter peak period would result in higher bed shear stresses on equal depths compared to a longer peak period, given that wave heights are equal.

Usually, wave heights vary over time, due to changing wind conditions. However, for this model, a constant wave height is set at the boundary. The wind speed u_{10} that accompanies each wave height is 2.5 m/s for 0.3 m, 5 m/s for 0.6 m and 7.5 m/s for 1.0 m. These have been based on observations of wind velocities accompanying wave heights (NOAA, 2006).

One important note is that the wave height is not a constant wave height set at the boundary. The waves are described by a JONSWAP-spectrum, with a peak coefficient γ of 3.3, with its peak at the H_s given.

Sea level rise Many different sea level rise prognoses exist, such as Bamber et al. (2019), Le Bars et al. (2017), and the commonly known IPCC report (Oppenheimer & Hinkel, 2019). They all predict varying rates of sea level rise by the year 2100. Lots of uncertainty exists within each scenario, due to varying emission rates, the contribution of the melting of ice sheets and differences in locations, but all agree that sea level rise will exceed historic rates and that it is probable that sea level rise will be at least +1.0 m by 2100.

Due to the variety in scenarios and variability per location, it is chosen to use three levels of sea level rise: 0.2, 0.4, and 0.6 m. These rates will probably all be exceeded in the future, but the exact moment in time is not yet known, as that depends on the local and global influences. Furthermore, r-SLR rates rates also vary per location, due to different bed level subsidence rates. This would make an analysis in time impossible. Due to the variability, the rates are added as an instant change in MSL. Using these three rates of sea level rise, an analysis based on a scenario is possible.

3.1.2 Model variations

The different model combinations that are obtained from the variations in characteristics, are presented in table 3.2. First, model runs are performed with just a tide on a bottom profile. Then, waves are added. Afterwards, mangroves are included in the model. Finally, model simulations are performed with SLR. The SLR simulations are performed on just the convex coast, as literature has shown this is a stable, importing coast (Winterwerp et al., 2013). Therefore, SLR on concave or linear coasts is not expected to present itself in reality. Thus, no simulations are performed for these types of coasts.

In table 3.2, the S denotes 'small', M stands for 'medium', and L means 'large'. The values for these characteristics are shown in table 3.3.

Table 3.2: Scenarios

Bottom profile	Tide	Waves	Mangroves	Sea level rise (only convex)		
				20 cm	40 cm	60 cm
Concave and Linear and Convex	R: *S* H_s: 0	R: *S* H_s: *S*	R: *S* H_s: *S*	R: *S* H_s: *S*	R: *S* H_s: *S*	R: *S* H_s: *S*
		R: *S* H_s: *M*	R: *S* H_s: *M*	R: *S* H_s: *M*	R: *S* H_s: *M*	R: *S* H_s: *M*
		R: *S* H_s: *L*	R: *S* H_s: *L*	R: *S* H_s: *L*	R: *S* H_s: *L*	R: *S* H_s: *L*
	R: *M* H_s: 0	R: *M* H_s: *S*	R: *M* H_s: *S*	R: *M* H_s: *S*	R: *M* H_s: *S*	R: *M* H_s: *S*
		R: *M* H_s: *M*	R: *M* H_s: *M*	R: *M* H_s: *M*	R: *M* H_s: *M*	R: *M* H_s: *M*
		R: *M* H_s: *L*	R: *M* H_s: *L*	R: *M* H_s: *L*	R: *M* H_s: *L*	R: *M* H_s: *L*
	R: *L* H_s: 0	R: *L* H_s: *S*	R: *L* H_s: *S*	R: *L* H_s: *S*	R: *L* H_s: *S*	R: *L* H_s: *S*
		R: *L* H_s: *M*	R: *L* H_s: *M*	R: *L* H_s: *M*	R: *L* H_s: *M*	R: *L* H_s: *M*
		R: *L* H_s: *L*	R: *L* H_s: *L*	R: *L* H_s: *L*	R: *L* H_s: *L*	R: *L* H_s: *L*

With

Table 3.3: Values for scenario

	Tidal range (R)	Significant wave height (H_s)
S	0.4 - 0.6 m	0.3 m
M	0.8 - 1.5 m	0.6 m
L	1.0 2.0 m	1.0 m

3.2 System behaviour without mangroves

This section investigates the behaviour of the coasts without mangroves present. Both the simulations with just a tide and those for tide & waves are investigated.

The tide, for all tidal ranges and all profiles, does not allow for sedimentation in the mangroves. Bed shear stresses remain below the critical bed shear stress, meaning that no sediment is picked up. Sediment transport, which is the lower right panel on figure 3.3, is only present on the offshore boundary of the model. Sediment enters the model on the boundary, due to the boundary condition imposed. Some sediment, below a certain water depth, settles. The rest is exported.

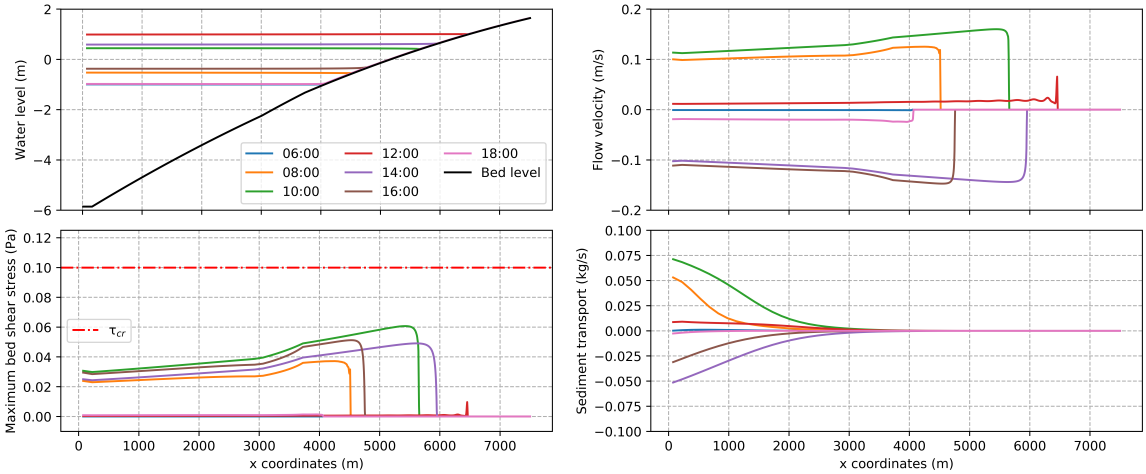

Figure 3.3: Cross-shore overview of tidal run during spring tide on convex profile. Tidal range of 1.0-2.0 m, significant wave height of 0.6 m.

The flow velocity profile varies depending on the coastal shape. A concave bottom has a decelerating flow velocity towards the coast, a linear bottom has a constant flow velocity, whereas on the convex bottom flow accelerates towards the shore. This is shown on figure 3.4.

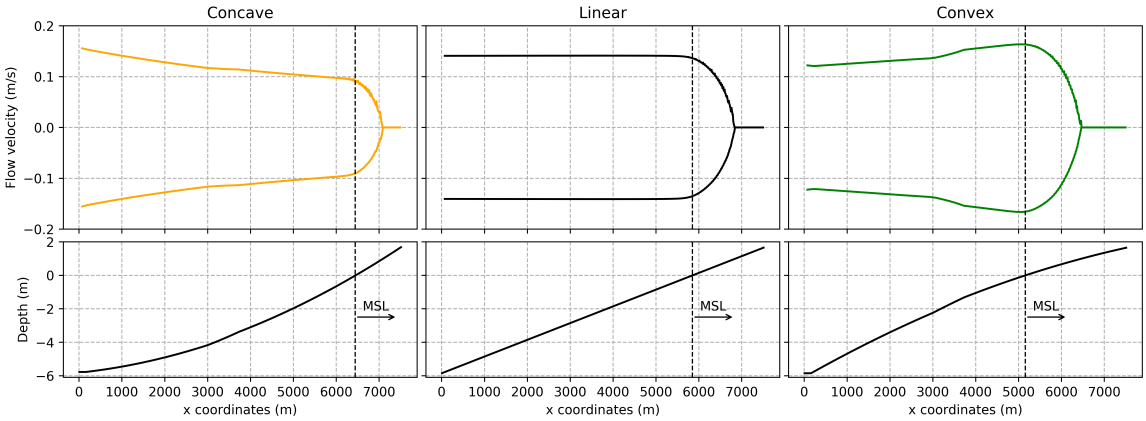

Figure 3.4: Cross-shore observed maximum flow velocities for concave (left), linear (middle), and convex (right) profiles, for a tidal range of 1.0-2.0 m.

Waves pick up sediment, as seen on figure 3.5. The critical bed shear stress is exceeded across the entire domain, which mobilises sediment and keeps it in suspension. On the bottom right panel, it is seen that over the entire model stretch, sediment is transported.

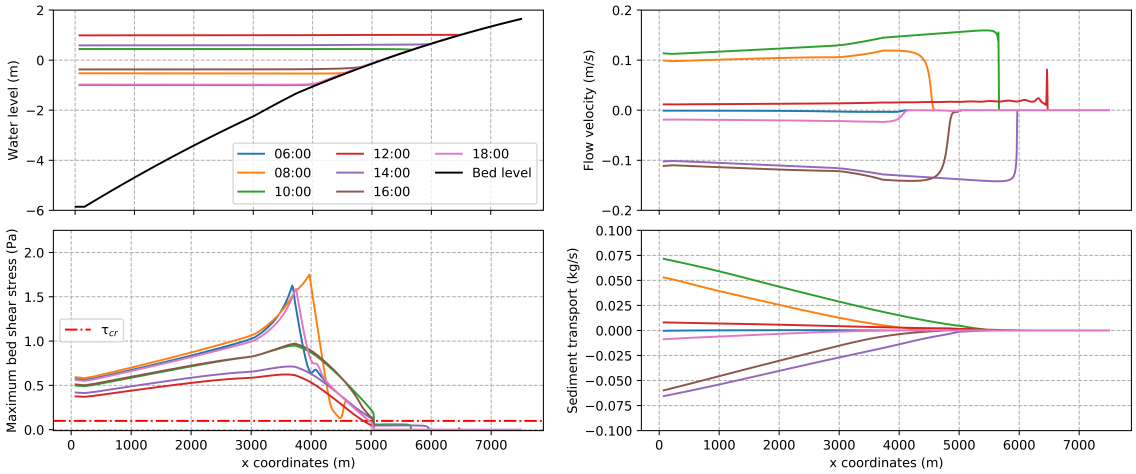

Figure 3.5: Cross-shore overview of tide and wave run during spring tide on convex profile. Tidal range of 1.0-2.0 m, H_s of 0.6 m.

For waves with a height of 0.3 m, not all sediment is kept in suspension, as seen on figure 3.6. At 12:00, on the landward boundary, $\tau < \tau_{cr}$. Then, sediment is able to settle. If waves are larger than 0.6 m, the bed shear stress exceeds the critical bed shear stress all the time everywhere, except for in the intertidal. If the critical bed shear stress is exceeded, no sediment is able to settle.

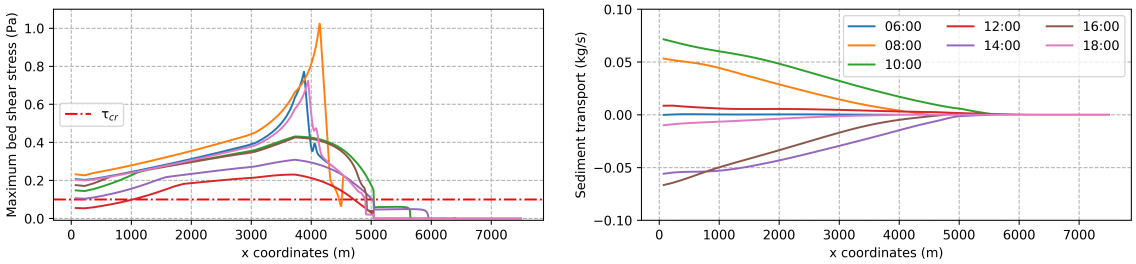

Figure 3.6: Cross-shore overview of bed shear stresses and sediment transport of tide and wave run during spring tide on convex profile. Tidal range of 1.0-2.0 m, H_s of 0.3 m. Water level and flow velocity equal to figure 3.5.

Figure 3.7 shows the differences in net sediment import above MSL during one spring-neap tidal cycle. It is visible that for the different coastal profiles, net sediment import changes. Furthermore, larger tidal ranges lead to an increase in net sediment import compared to smaller tidal ranges. These differences can be attributed to the variations in tidal asymmetry.

Another observation is that waves of 0.3 m, with the lowest H_s ratio, cause more sedimentation than larger waves of either 0.6 or 1.0 m. An explanation for this can be found in the fact that the smaller waves do not exceed the critical bed shear stress in the deep end all the time. That results in some sediment being able to settle, which is then picked again, when the critical bed shear stress is exceeded. For the larger waves, the maximum bed shear stress exceeds the

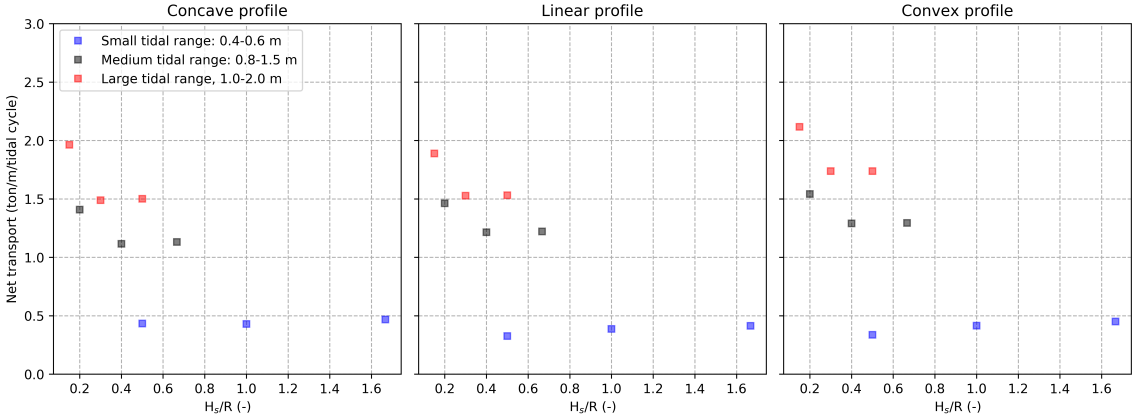

Figure 3.7: Net transport of sediment above MSL during a spring-neap tidal cycle for three bottom profiles, no mangroves. H_s/R is the ratio of significant wave height over tidal range.

critical bed shear stress all the time. Therefore, this settlement is not observed, resulting in a larger outflow of sediment on the offshore boundary. Due to the sediment not flowing out of the offshore boundary with waves of 0.3 m, it can end up in the intertidal. This causes the difference between sedimentation for smaller waves of 0.3 and larger waves of 0.6 m and 1.0 m. The difference between sediment transport on the offshore boundary is shown on figure 3.8.

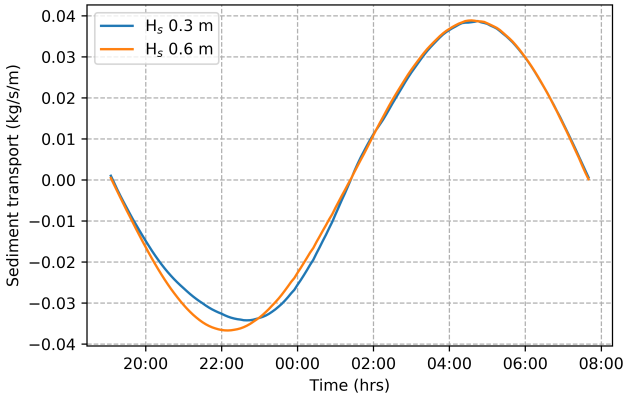

Figure 3.8: Variations in sediment transport on offshore boundary due to varying wave heights, for a convex profile with a tidal range of 0.8-1.5 m. Arbitrary moment in time.

Tidal asymmetry without mangroves

The tidal asymmetry has been plotted for a tidal range of 1.0-2.0 m, and a wave height of 0.6 m, at -5.0, -0.5, +0.0, and +0.5 m, on figure 3.9.

In deep water, at -5.0 m, the velocity and sediment transport profiles are all symmetrical. Sediment transport follows the flow velocity, however delayed by 30 minutes.

At -0.5 m, the tide is not symmetrical anymore. Ebb holds on for longer, creating ebb dominance. However, the flow reversal is flood favoured, shown by the skewness of the flow velocity profile. This creates flood dominance. By looking at the sediment transport, it is seen that the overall system is flood dominant. More sediment is transported towards the intertidal

due to the flood dominance. A convex coast is able to transport more sediment than a concave coast, which can be attributed to larger slack water asymmetry for a convex than a linear and concave coast. The duration of flow reversal is equal, but the flow velocity differences between the convex coast are larger than the concave coasts.

At MSL, the asymmetry change is the as seen at -0.5 m. The tidal duration increases in ebb dominance, but slack water asymmetry also increases. Slack water asymmetry increase can be seen in the increase in skewness. The net result is a stronger flood dominance.

For +0.5 m, the same holds true as at MSL. Ebb duration is longer than flood duration, and skewness again increases.

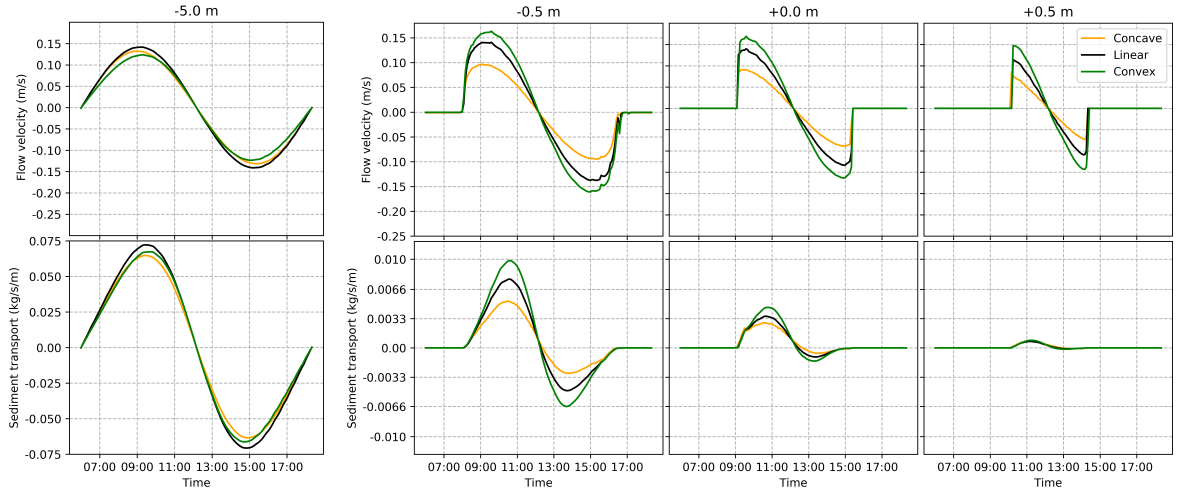

Figure 3.9: Tidal asymmetry for concave, linear and convex profiles, during spring tide without mangroves present. Tidal range of 1.0-2.0 m, significant wave height of 0.6 m. Shown at depths of -5.0 m (outer left), -0.5 m (middle left), +0.0 m (middle right), and +0.5 m (outer right).

Summary of the system behaviour without mangroves

In short, the tide is able to transport sediment, but does not pick it up. Waves pick up sediment, which the tide then transports. Depending on the coastal shape, flow velocities towards the intertidal change, which result in varying sedimentation rates.

3.3 Impact of mangroves

Mangroves add roughness to the water column, with their roots and stems. Over the entire domain, results are similar to when waves are present, but in the intertidal, the influence of mangroves is visible. Their influence can be seen on figure 3.10, from x-coordinates 3,000-6,200 m. The water level contains a gradient, and flow velocities as well as bed shear stresses are changed.

Due to the added roughness, water cannot flow freely in and out of the mangrove forest. This reduces flow velocities, and induces a water level gradient. The water level gradient causes acceleration and deceleration of the water, which influences tidal asymmetry. Furthermore, the mangroves cause a variation in sedimentation. This is shown on figure 3.11.

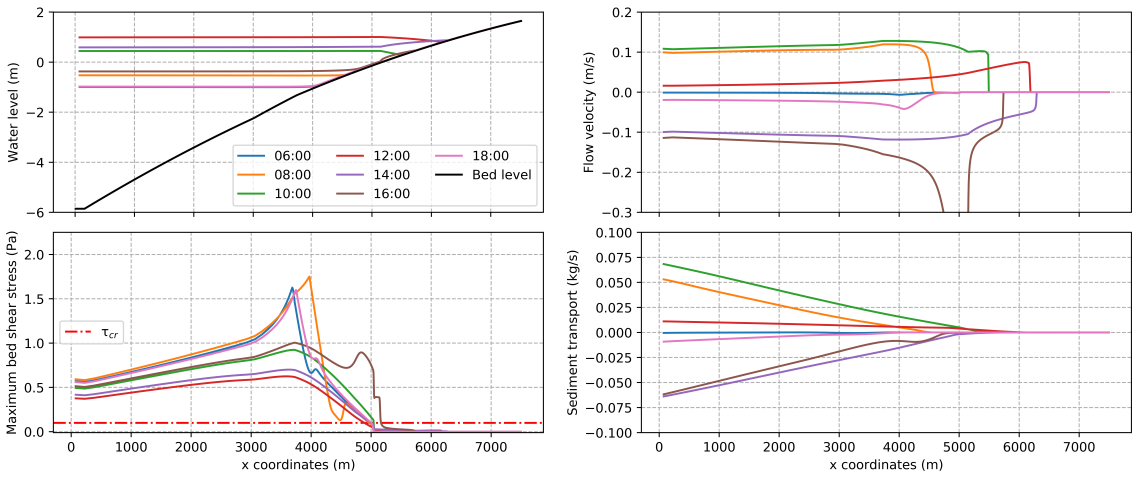

Figure 3.10: Cross-shore overview of mangrove run during spring tide on convex profile. Tidal range of 1.0-2.0 m, significant wave height of 0.6 m.

The impact of mangroves on net sediment transport depends on the hydrodynamic conditions coast. For a large tide on a convex coast, more sediment is transported above MSL with mangroves than without. However, on the same coast with a medium tide, the impact of mangroves is negative. Then, less sediment is imported, compared to a coast without mangroves. The net import rates of the various combinations is shown on figure 3.11. Differences in sedimentation are caused by variations in tidal asymmetry and in bed shear stresses. Variations in bed shear stresses within the forest depend on the length the flow travels through a mangrove, as shown in table 3.4.

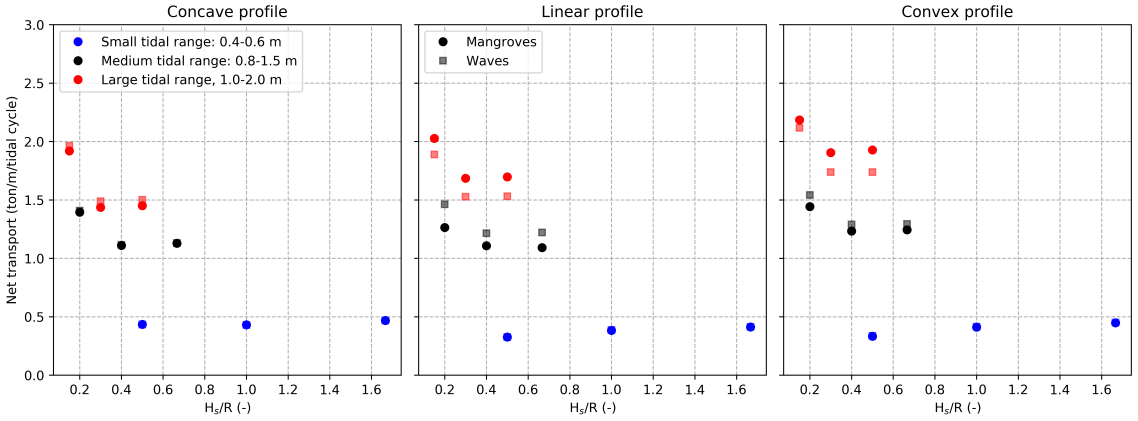

Figure 3.11: Net transport of sediment above MSL during one spring-neap tidal cycle for three bottom profiles, with mangroves included. H_s/R is the ratio of significant wave height over tidal range.

Tidal asymmetry with mangroves

The tidal asymmetry has been plotted for a tidal range of 1.0-2.0 m, and a wave height of 0.6 m, at -5.0, -0.5, +0.0, and +0.5 m, on figure 3.12.

In deep water, at -5.0 m, there are no changes compared to waves. The signals are symmetrical, with a delay of 30 minutes for the sediment transport.

In the intertidal at -0.5 m, the influence of mangroves becomes visible. The ebb duration is longer than the flood duration, creating ebb dominance. Furthermore, the peak velocity also becomes ebb dominant: the peak ebb velocity is larger than the peak flood velocity. This peak ebb velocity asymmetry is caused by the outflow acceleration, due to the water level gradient. Slack water asymmetry increases, compared to the no-mangrove situation. The latter asymmetry dominates. The total system is flood dominant, causing a net import in the system.

At MSL, the same asymmetries are observed. A peak, ebb dominant, flow velocity asymmetry is present. The tidal duration is also ebb dominant. Slack water is flood dominant. However, the asymmetry has increased. Slack water is dominant over the asymmetries, creating a net importing, flood dominant system. The impact of mangroves is clearly visible, when compared to the no mangrove situation. Maximum flood velocities have reduced, due to the increased roughness in the water column. Maximum ebb velocities increase, due to the water level gradient.

In the mangrove, at +0.5 m, no export occurs, whereas import is seen. The mangroves hinder flow: during flood the flow velocity of 0.1 m/s, rather than 0.15 m/s. Asymmetries are enhanced by the mangrove, peak velocity and duration asymmetries have become more ebb dominant. Slack water has increased in its flood dominance. The system remains flood dominant.

Similarly to the situation with no mangroves, the system is flood dominant. It imports more sediment than it exports.

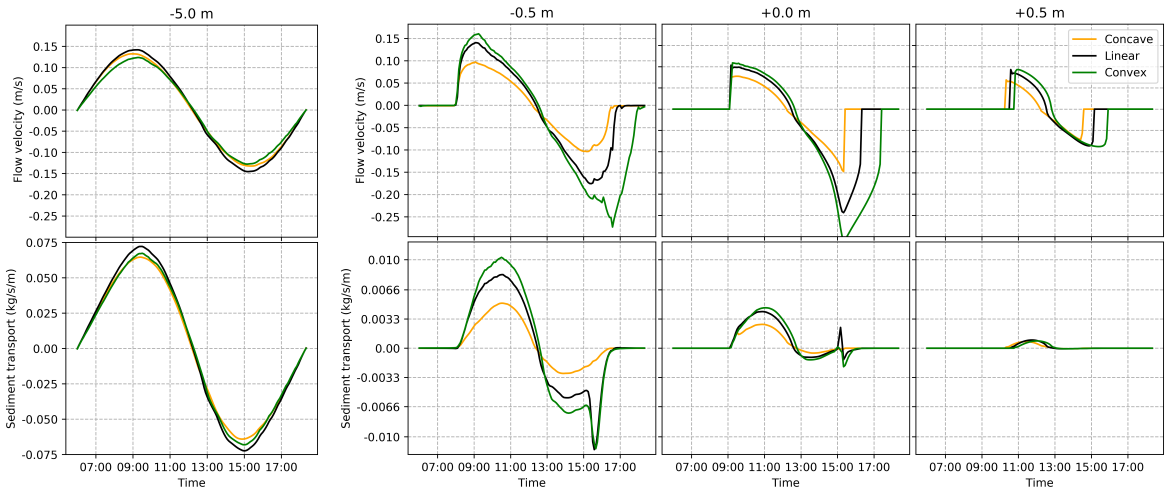

Figure 3.12: Tidal asymmetry for concave, linear and convex profiles, during spring tide with mangroves present. Tidal range of 1.0-2.0 m, H_s of 0.6 m. Shown at depths of -5.0 m (outer left), -0.5 m (middle left), +0.0 m (middle right), and +0.5 m (outer right).

Bed shear stresses in the mangrove

Bed shear stresses above MSL change for the situation with and without mangroves, causing a variation in sedimentation within the mangrove area. Similarly as for the situation without mangroves, tidal asymmetry is the main driver for differences in net sediment transport.

However, the tidal asymmetry does not explain the differences in sedimentation between tidal ranges. The bed shear stresses in the mangrove forest are influenced by the vegetation, and depend on the distance the flow travels through the forest and the flow velocities. Dependent on the bottom profile and tidal range, the length of the flow through the mangrove varies. The lengths of the flow through the mangrove, during spring tide, has been shown in table 3.4.

Table 3.4: Length of the flow through the mangrove during spring tide

Bottom profile	Tidal range		
	0.4-0.6 m	0.8-1.5 m	1.0-2.0 m
Concave	200 m	490 m	645 m
Linear	300 m	750 m	1000 m
Convex	365 m	960 m	1310 m

The influence of vegetation on the bed shear stresses is plotted of figure 3.13. For a flow that travels a small distance through vegetation, during the tidal range of 0.4-0.6 m, bed shear stresses are almost equal between runs with and without mangroves. The mangrove has not yet influenced the flow. However, the differences can be seen at tidal ranges of 0.8-1.5 and 1.0-2.0 m. For 0.8-1.5 m, bed shear stresses are reduced. Due to the slowing of the flood, bed shear stresses hold on for longer. This can be seen as more non-zero lines being plotted in the middle bottom panel, compared to the middle upper panel of figure 3.13. If a tidal range of 1.0-2.0 m, is present, the same behaviour holds observed. Bed shear stresses are reduced, albeit a stronger reduction, and hold on for longer.

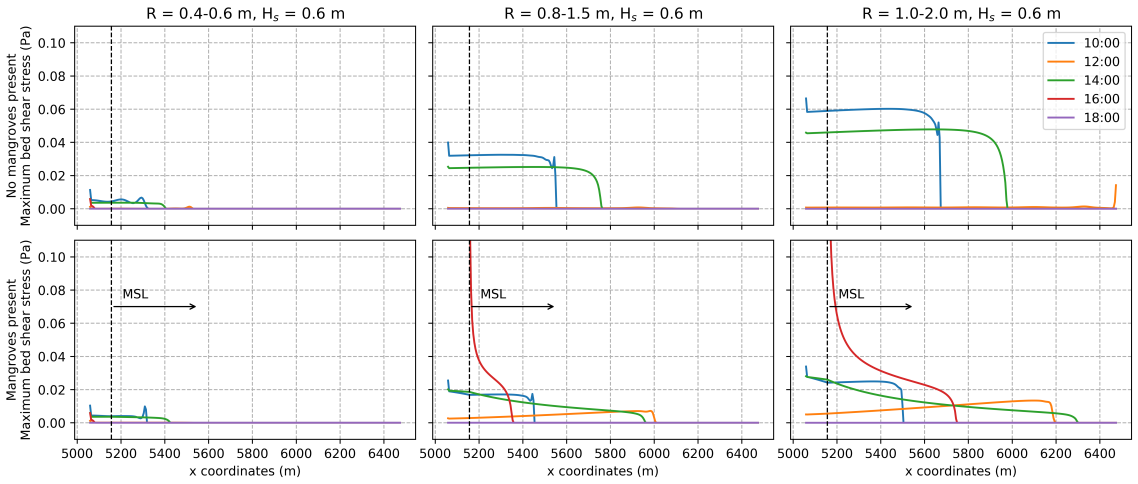

Figure 3.13: Cross-shore comparison of bed shear stresses in the intertidal for runs with (bottom panels) and without mangroves (upper panels), on a convex coast with tidal ranges of 0.4-0.6 m (left panels), 0.8-1.5 m (middle panels), and 1.0-2.0 m (right panels) during spring tide.

The outflow acceleration reduces sedimentation on the intertidal, shown on figure 3.14, compared to a coast without mangroves. For the convex coast, which has a longer distance of flow through the mangrove, the difference is largest. This results in a larger decrease in intertidal sedimentation. For the concave coast, the outflow acceleration is not as strong. The negative flow velocity is smaller compared to that of the convex coast. This explains the smaller differences between intertidal sedimentation for concave coasts with and without mangroves.

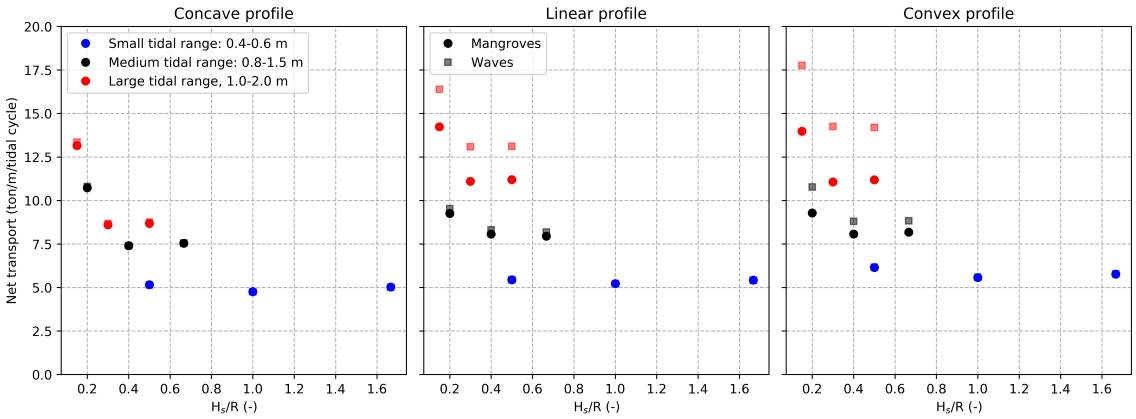

Figure 3.14: Net transport of sediment above LAT, during one spring-neap tidal cycle for three bottom profiles scenarios, mangroves included. H_s/R is the ratio of significant wave height over tidal range.

Summary of the system behaviour with mangroves

Summarising, dependent on the tidal range, mangroves change the behaviour of the coast. The added roughness caused by mangroves increases ebb velocities at MSL and reduces flood velocities above MSL. For small tidal ranges, the mangroves do not impact the behaviour. However, for large tidal ranges, mangroves can either have a negative or positive impact on the net sedimentation, compared to a coast without mangroves. This depends on the distance the flow travels through the mangrove, which depends on the tidal ranges. For a longer distance the effect is positive, whereas it is negative for a shorter distance.

3.4 Impact of sea level rise

Sea level rise increases water depths, thereby changing the coast's behaviour. Due to the increased water depths, the influence of the bottom on the water is reduced. This can be seen in a reduction in bed shear stresses, as shown on figure 3.15. Furthermore, sedimentation rates increase.

Sedimentation rates increase due to SLR. This is visible on figure 3.16. The sediment boundary condition is applied as a concentration in kg/m^3. An increase in sea level increases the volume of water. Therefore, the amount of sediment that enters the model also increases. However, it can be seen that the change in net sedimentation differs for varying tidal ranges and rates of SLR. For example, for a medium tidal range and small waves, the increase in net sedimentation is smaller than for a large tidal range. This can be attributed to changes in the tidal asymmetry, which are explained below.

Another change caused by SLR is the reduction in maximum bed shear stresses, due to increased water depths. For no-SLR, critical bed shear stresses are not exceeded on the offshore boundary of the model for waves with H_s = 0.3 m. This effect increases with SLR rates, resulting in an increase in import, as shown on figure 3.17. The export, or negative transport, of waves with H_s = 0.3 m is smaller than waves with H_s = 0.6 m, whereas the import is equal. This explains the increasing difference between the net import for smaller waves of 0.3 m and larger waves of 0.6 m and 1.0 m, seen on figure 3.16.

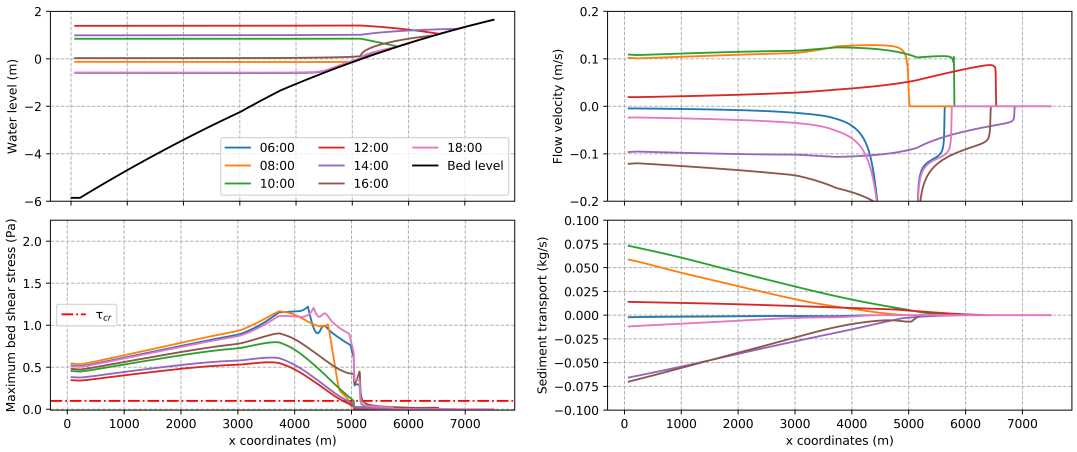

Figure 3.15: Cross-shore overview of 0.4 m SLR run during spring tide on convex profile. Tidal range of 1.0-2.0 m, significant wave height of 0.6 m.

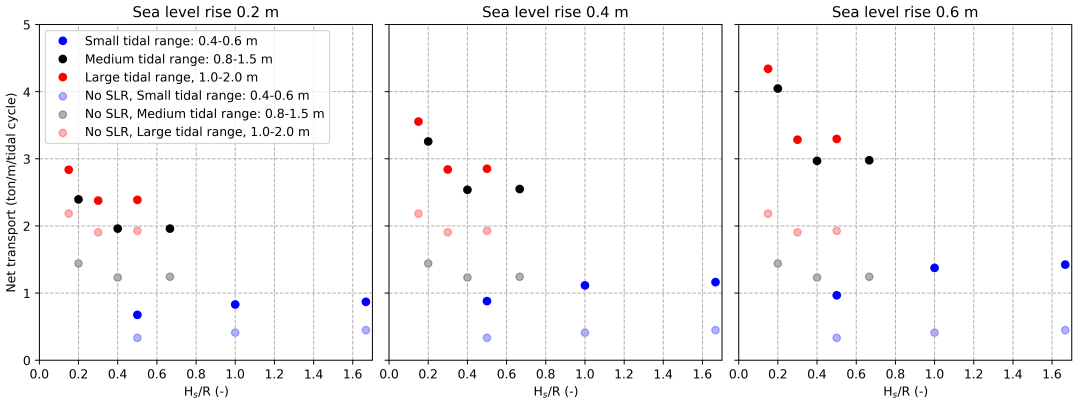

Figure 3.16: Net transport of sediment into the mangrove during one spring-neap tidal cycle on a convex profile, with mangroves, at a bed level of 0.0 m. Three SLR rates, 0.2 m left, 0.4 m middle, 0.6 m right. H_s/R is the ratio of significant wave height over tidal range.

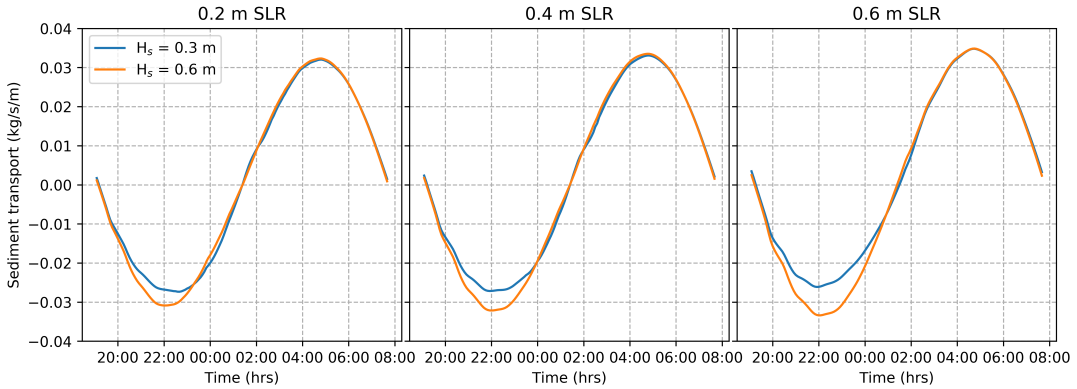

Figure 3.17: Variations in sediment transport on offshore boundary due to varying wave heights, for a convex profile with a tidal range of 0.8-1.5 m and SLR of 0.2 (left), 0.4 (middle), and 0.6 m (right). Arbitrary moment in time.

Increasing SLR rates lead to higher sedimentation rates, but not to a change in sediment distribution. The distribution of sediment in the mangrove does not change, as shown on figure 3.18. Most sediment ends up at the seaward edge of the forest, while at the landward side less sedimentation is observed.

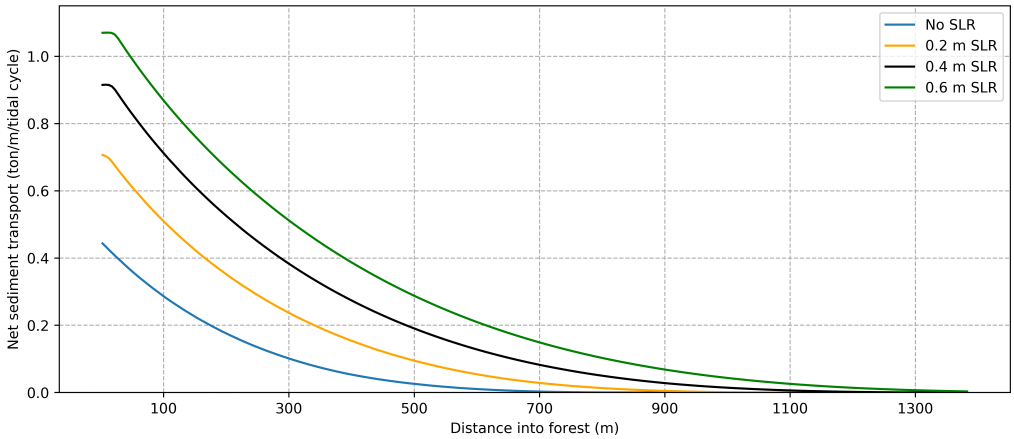

Figure 3.18: Cross-shore overview of net sediment transport into the mangrove forest during one spring-neap tidal cycle, for varying SLR rates. Convex profile, tidal range 0.8-1.5 m and $H_s = 0.6$ m.

Tidal asymmetry with sea level rise

The tidal asymmetry has been plotted for a tidal range of 1.0-2.0 m, and a wave height of 0.6 m, at -5.0, -0.5, +0.0, and +0.5 m, on figure 3.19. This allows for comparison of the three different SLR scenarios on the convex coast.

It can be seen that on the deep end, no change in flow velocity is present, and the signal remains symmetrical. The water depth has increased, thus the bed has less influence on the flow. Therefore, this is to be expected. The amount of sediment transported has increased, due to the boundary condition being applied as kg/m^3. The sediment transport remains delayed.

At -0.5 m, the asymmetry changes. Slack water asymmetry remains dominant. For increasing SLR rates, the slack water asymmetry increases. The flow velocity gradient increases per rate of SLR, when going from ebb to flood. It decreases from flood to ebb. The ebb duration and peak ebb flow velocity asymmetry both increase, compared to no SLR. With increasing SLR, the peak ebb velocity increases and is delayed. The system remains flood dominant, transporting more sediment towards the shore than offshore.

At MSL, tidal asymmetry again changes with varying rates of SLR. The ebb duration increases with increasing SLR, as well as the peak in flow ebb flow velocity. Slack asymmetry also increases. More export is observed, however import also increases. For all rates of SLR the flow remains flood dominant.

At +0.5 m, flood dominance prevails. The flood slack duration decreases with increasing SLR rates, thereby increasing the slack water asymmetry. However, the ebb duration also increased. The slack water asymmetry is dominant over the longer ebb duration, which is seen in the sediment transport. thus the system remains flood dominant. Almost no export is observed.

The enhancement of tidal asymmetries for increasing rates of SLR can be attributed to the larger distance the flow flows through the mangrove forest. The effect of the mangrove increases, as more flow experiences resistance.

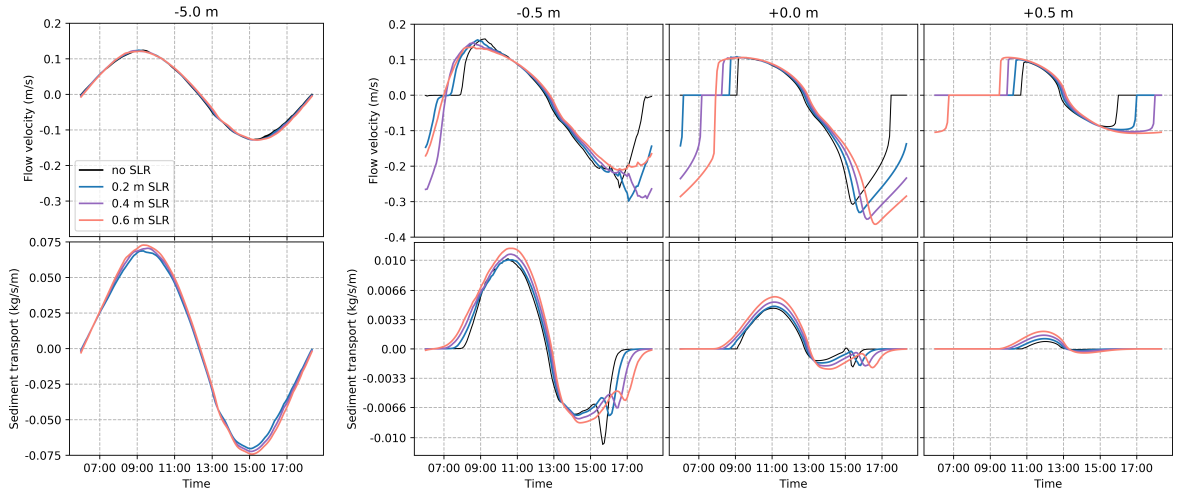

Figure 3.19: Tidal asymmetry for 0.2, 0.4 and 0.6 m SLR, during spring tide with mangroves present. Tidal range of 1.0-2.0 m, significant wave height of 0.6 m. Shown at depths of -5.0 m (outer left), -0.5 m (middle left), +0.0 m (middle right), and +0.5 m (outer right).

Summary of the system behaviour with sea level rise

Concluding, SLR changes how much the flow feels the bottom, and increases sedimentation rates. Tidal asymmetries are increased due SLR: slack water increases in flood dominance, but both peak flow and duration asymmetry increase in their ebb dominance. Sea level rise does not change the spatial sediment distribution across the mangrove.

3.5 Summary of results

Using this process analysis, a generic understanding of the abiotic processes on a mangrove coast is obtained. The tide is able to transport sediment, but does not pick it up. Sediment pick-up is caused by waves, after which the sediment can be transported by the tide. Depending on the coastal shape, flow velocities towards the intertidal change, which result in varying sediment transport rates. These varying transport rates are caused by changes in tidal asymmetry. Mangroves increase roughness in the water column. Dependent on the length of the flow through the mangroves, this effect causes either a net increase or decrease in sedimentation. Sea level rise increases water levels, which reduces the bottom influence on the waves and therefore reduces bed shear stresses. More water flows through mangroves, thereby increasing tidal asymmetry.

Chapter 4

Analysis of results

Using the knowledge obtained in chapter 3, the results are analysed. An overview of interactions discovered is presented in section 4.1. Then, tipping points are identified in section 4.2. Section 4.3 discusses the model results and behaviour. Lastly, section 4.4 presents a conceptual model of mangrove coasts.

4.1 Overview of processes

On figure 4.1, the interactions discovered in chapter 3 are presented. The arrows showing interactions are numbered. Then, the numbers are listed, which explain the effect that the processes have on each other.

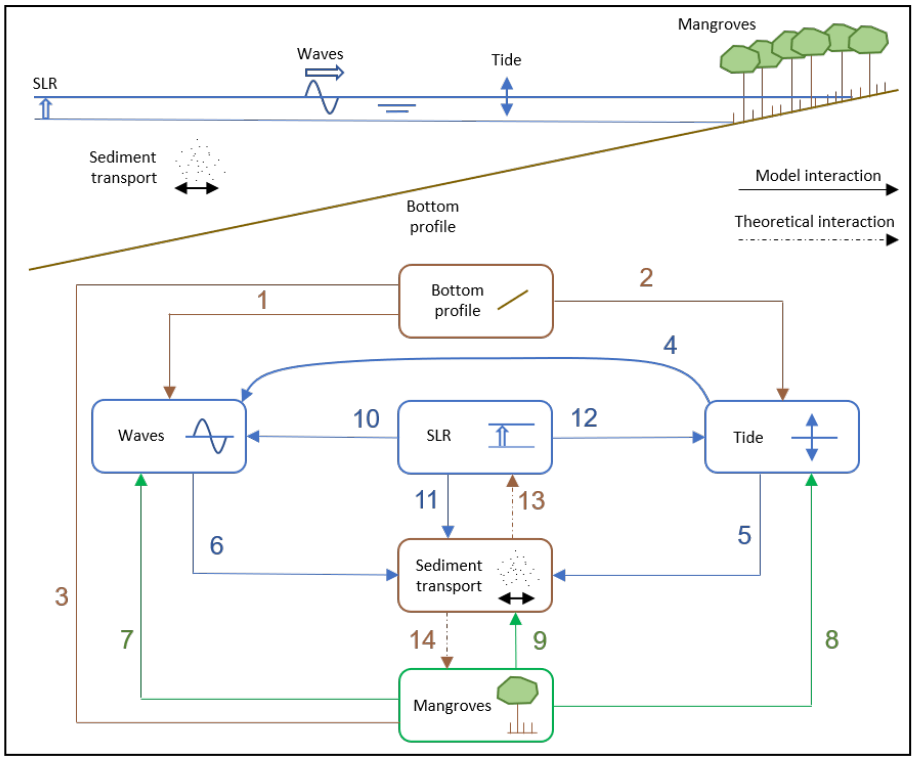

Figure 4.1: Interactions overview map

1. **Bottom profile - Waves:** The bottom profile influences where the largest part of wave reduction occurs. Dependent on the slope and depth, it influences over which distance waves do not 'feel' the bottom, which enables a larger difference in import between smaller and medium wave heights. In reality, when waves do not influence the bed, no changes in bed level would be observed.

2. **Bottom profile - Tide:** The bottom profile influences tidal velocities by variations in the bottom slope. A milder slope increases flow velocities, whereas a steeper slope reduces them. This also influences tidal asymmetry, by increasing slack water asymmetry. In this manner, the slope indirectly influences sediment transport. Furthermore, if the slope becomes milder/steeper in the cross-shore direction, the flow velocities increase/decrease accordingly. This enhances tidal asymmetry.

3. **Bottom profile - Mangroves:** The bed slope, thus the bottom profile, influences how much mangrove forest prevails above MSL. As mangroves habit the intertidal above MSL, a flatter slope in the intertidal results in a larger mangrove habitat.

4. **Tide - Waves:** The tide influences water levels, which influences where and how much the waves feel the bottom. A small tidal range results in a more consistent location of the bed shear stresses, whereas a large tidal range increases the variability of bed shear stresses. Furthermore, waves come closer to the mangrove with a larger tide.

5. **Tide - Sediment transport:** The tide is the main transporter of sediment. A larger tidal range causes more sedimentation, whereas a smaller tidal range results in less sedimentation. This can be attributed to flow velocities. Larger flow velocities, caused by both an increase in tidal range and a flatter bed slope, increase sediment transport. Furthermore, a larger tidal range allows for sediment to intrude further into the mangrove. The tide itself does not influence tidal asymmetry, this is caused by the bed and mangroves. Enhanced flood dominant tidal asymmetry increases sedimentation.

6. **Waves - Sediment transport:** Waves pick up sediment, by causing maximum bed shear stresses in excess of the critical bed shear stress. Furthermore, waves keep sediment in suspension by exceeding the critical bed shear stress.

7. **Mangroves - Waves:** Mangroves allow for less wave intrusion on the intertidal. This results in lower bed shear stresses on the intertidal. Added roughness in the water column due to vegetation and lower bed shear stresses on the intertidal, results in different behaviour.

8. **Mangroves - Tide:** Mangroves hinder tidal flows by adding roughness to the water column. This induces a water level gradient, resulting in acceleration and deceleration of the water in and out of the mangrove. Depending on the distance of the flow through the forest, the acceleration increase or reduces. The accelerating water influences the tidal asymmetry, thus tidal behaviour.

9. **Mangroves - Sediment transport:** Mangroves influence the sediment transport by altering tidal asymmetry. Due to the acceleration of water out of the forest, the impact of mangroves on intertidal sedimentation is negative. Within the upper intertidal, above MSL, the impact of mangroves can either be zero, negative or positive. This depends on

the distance the flow travels through the mangrove, which alters bed shear stresses. If the flow is sufficiently long through the forest, mangroves provide a 'sheltered area' in which sediment can settle more easily, compared to a coast without mangroves. However, for flows that travel a shorter distance through the forest, bed shear stresses are not reduced, but they do hold on for a longer duration.

10. **SLR - Waves:** Sea level rise causes waves to have less influence on the bottom. If the wave height does not cause suspension of sediment all the time, as is the case with waves of 0.3 m, this results in more net import in the system in these simulations. This is due to the fact that the settled sediment is re-suspended, and then transported towards the mangrove. Another effect SLR has on the waves is that it shifts the area in which they influence the bed further landwards.

11. **SLR - Sediment transport:** Sea level rise influences sediment transport in two manners. Firstly, due to the sediment boundary condition - applied as kg/m^3 - more sediment enters the model. This is because a larger volume of water is present on the offshore boundary. The extra sediment finds its way towards the shore, thereby increasing sedimentation. However, in reality however the total quantity of sediment available will most likely not increase. Secondly, SLR influences sediment transport by varying the tidal asymmetry. This results in slight changes in sedimentation rates.

12. **SLR - Tide:** SLR shifts the intertidal further into the mangrove, causing flows deeper within the forest. This results in more flow being hindered by the mangrove vegetation, causing variations in tidal asymmetry. The changes in tidal asymmetry are seen by an increase in flood dominance of slack water asymmetry, as well as an increase in ebb dominance in tidal duration asymmetry and peak ebb velocity. Two reasons are identified for the change. The first is that, due to the assumption of a mangrove not moving with SLR, flows through the mangrove are longer. The second reason is that increase in water level reduces the bed's influence on the flow.

13. **Sediment transport - SLR:** In this model, sediment transport does not influence sea level rise. However, in reality, increased sediment transport towards the mangrove reduces r-SLR.

14. **Sediment transport - Mangroves:** This interaction is not included in the model, but should be stated for completeness. Mangroves require sediment transport to exist, as they require surface level elevation.

4.2 Tipping points

Having identified the cross-shore behaviour of mangrove coasts, tipping points can be identified. Tipping points are certain values for which an exceedance of that value changes the behaviour significantly (Van Nes et al., 2016). Tipping points should therefore be sought for values for which the regular behaviour does not hold true anymore. The tipping points will be investigated by comparing the observed characteristics, such as flow velocities, bed shear stresses and sedimentation rates between coasts. First, the tipping points for the bottom profile are presented. Then, the tide is discussed. Afterwards, the wave tipping point is covered. Thirdly, the tipping points for mangroves are touched upon. Finally, sea level rise is covered.

4.2.1 Bottom profile

The bottom profile influences the flow velocities and the sediment transport capacities on the shore. As seen in equation 2.1, the flow velocity depends on the tidal range and the bed slope. A gradually decreasing slope towards the coast therefore has an increasing flow velocity towards the coast. It has been shown that a concave coast imports less sediment than a linear coast, and a linear coast imports less sediment than a convex coast, given that they have equal hydrodynamic conditions. The slack water duration is equal for all coasts, but with larger flow velocities are observed, depending on the slope of the coast. This increases the dominance of the slack water, and therefore net sedimentation.

Therefore, the tipping point identified is the gradient of the slope in cross-shore direction, shortly denoted as $d\beta/dx$, in which β is the bottom slope. If $d\beta/dx < 0$, flow velocities increase towards the shore and sedimentation increases above MSL. If $d\beta/dx > 0$, flow velocities are reduced and less sediment is imported. The tipping point is $d\beta/dx = 0$, which is when the cross-shore gradient of the bed slope goes from positive to negative.

4.2.2 Tide

The tide moves the water, resulting in flow velocities. The flow causes bed shear stresses, as well as sediment transport. It has been shown that without waves, the tide does not pick-up sediment. The tide only transports sediment. Two tipping points are defined, for which behaviour changes across the coast.

Firstly, the tidal range reduces or is completely damped. This stops the flow of water, reducing sediment available and ultimately a complete starvation of sediment. An example of where this happened is the Oosterschelde, where tidal barriers blocked tidal flows such that a tidal reduction took place (Nienhuis & Smaal, 1994). This tipping point is also seen in the process analysis. With reducing tidal range, the net sediment transport reduces in the mangrove. Thus, when the tide is damped, it does not cause any flow velocities, and therefore does not move any sediment.

The second tipping point for this behaviour is the tidal range such that the flow velocities cause bed shear stresses in exceedance of the critical bed shear stress, $\tau_b \geq \tau_{cr}$. Then, the tide can pick-up sediment.

In reality, a morphodynamic response is expected when either of these tipping points is exceeded (Maan et al., 2015). If tidal ranges are small, a milder slope will most likely form. If the tidal range is such that $\tau_b \geq \tau_{cr}$, then a steeper slope of the bed will be formed. Therefore, these are theoretical tipping points that will most likely not occur in practice.

4.2.3 Waves

Waves cause large bed shear stresses, which mobilises sediment and keeps it in suspension. The sediment can then be transported towards the mangrove. The large bed shear stresses causes exceedance of the critical bed shear stress of the sediment. Two tipping points are observed, for which this behaviour changes drastically. The first is when waves are so small, the critical bed shear stress is not exceeded anywhere. Then, sediment is not picked up at all. This behaviour is seen in the simulations without waves. Sediment enters the model, due to the boundary condition, but is not kept in suspension. It all settles far offshore. No sediment is transported towards the mangrove area. The second tipping point is when the critical bed shear stress is

not exceeded on the offshore boundary during low tide, but is exceeded during flood. Sediment settles and is not exported out of the model. The sediment is mobilised again during flood and then transported towards the mangrove. This is observed for wave heights H_s = 0.3 m, explaining the higher quantity of net sedimentation for smaller waves.

These tipping points explain the observed model behaviour. In reality, feedback interactions are expected, which damps this behaviour (Maan et al., 2015). Sedimentation would take place such that an equilibrium is found between the critical bed shear stress and the bed shear stresses observed on the coast. Thus, it is expected that these tipping points do not occur in reality, but are seen due to the modelling approach.

4.2.4 Mangroves

Mangroves increase roughness in the water column, thereby influencing flow velocities and tidal asymmetry. Dependent on the length, the mangroves either have no effect, a net negative effect, or a net positive effect on sediment import, compared to a situation without mangroves. Therefore, two tipping points exist for mangroves, determined by the length of the flow through the mangrove.

The first tipping point is when going from a short distance of flow through the mangrove, to a 'medium' length. For small tidal ranges, mangroves have no effect on the flow, nor on the net sedimentation in the mangrove. This is the case for a flow going through the forest for less than 500 meters. This behaviour changes when the distance increases, up to 1,000 m. Then, the impact of mangroves on net sedimentation is negative compared to a no mangrove situation. This is observed for a large tidal range on a concave coast and a medium tide on a convex coast. The bed shear stresses are slightly reduced in the forest, but they hold on for a longer period. This causes the sediment to be kept in suspension. Less sedimentation occurs, compared to a no-mangrove situation.

The second tipping point is when mangroves change the behaviour from a negative to a positive effect on net sedimentation, compared to a no mangrove situation. This is the case when flow through the mangrove is sufficiently long. This is observed when the distance of flow through the mangrove exceeds 1,000 m. Then, bed shear stresses are reduced significantly. This reduction results in more sedimentation within the mangrove.

The length of the flow through the forest can be reduced or increased, resulting in different tipping point, depending on the vegetation. The mangrove influence on the flow comes from the roughness of the vegetation. If the forest has denser or stiffer vegetation, the distances found here will reduce. The influence of the vegetation then increases. Reversely, if the forest is less dense or more flexible, then the distances for which the behaviour is observed increases, or it is not observed altogether.

4.2.5 Sea level rise

Sea level rise increases water depths, and shifts the intertidal shorewards. The shift results in the movement of the intertidal area towards the mangrove area, where more roughness is present. The increased roughness in the intertidal enhances tidal asymmetry. Slack flood dominance increases, but peak flow velocity and duration asymmetry increase in ebb dominance. The result is an increase in sedimentation, for increasing rates of sea level rise.

These findings are based on a mangrove forest that does not move with increasing mean sea level. This is covered in section 4.3. Most importantly, no tipping point is observed for sea level rise.

4.3 Discussion

The discussion consists of two parts. Firstly, the model results are evaluated and compared to literature. Secondly, the model limitations are discussed.

4.3.1 Reflection on process analysis results

Hydrodynamic behaviour

The flow has been shown to be inversely proportional to the bed slope. Concave profiles have flows decelerating towards the intertidal, whereas a convex slope has a flow accelerating towards the intertidal. Within the intertidal, the flow velocities decreases. Le Hir et al. (2000) share these observations.

Mangroves have been shown to slow down flows (Janssen-Stelder et al., 2002). This can be seen on figures 3.9 and 3.12, on the panels at +0.0 and +0.5 m. When mangroves are absent, flow velocities are about 30% higher than when they are present.

Bed shear stresses reduce within the mangrove forest (Etminan et al., 2018). This is caused by the increased drag within the water column, due to the presence of vegetation. Figure 3.13 shows this. Bed shear stresses are reduced by up to 50% by mangrove vegetation.

Tidal asymmetry

Convex coasts have been shown to be importing more sediment than concave coasts. Convex coasts have an increasing flow velocity towards the shore, which enhances slack water tidal asymmetry. Winterwerp et al. (2013) state that convex coasts, with mangroves present, accrete sediment. The reason why convex coasts are more importing is mainly due to the fact that slack water asymmetry increases. This is supported by Friedrichs (2012), who states that fine sediment is most sensitive to slack water asymmetry.

Mangroves induce ebb tidal asymmetry (Mazda et al., 1995). This comes from the friction within the forest, and is controlled by the vegetation density. A reduction in vegetation density lowers tidal asymmetry, whereas an increase increases tidal asymmetry. Comparing the results for a coast with and without mangroves shows similar findings. Without vegetation, tidal asymmetry is lower than for a coast with vegetation.

It is seen that SLR results in an increase in tidal asymmetry. However, Guo et al. (2018) argues that SLR leads to a relative reduction in tidal asymmetry. This is due to the fact that an increase in water level results to a decline of the effect the bed has on the flow. Due to the assumption of mangroves not moving within the model, SLR shifts the intertidal towards a region with more roughness, thereby increasing tidal asymmetry.

The growth and decomposition of mangroves under SLR conditions, as well as SLR itself, have unknown temporal components. The time frame of the response of mangroves on sea level rise, e.g. the (de)composition of roots, is dependent on local conditions (Lovelock, Adame, et al., 2015; Sidik et al., 2016). The decomposition results in a reduction of roughness, thus to

less tidal asymmetry. Therefore, in reality, it is expected that SLR results to an increase in net sedimentation, but less than observed in the model.

Sedimentation behaviour

It has been found that waves stir up sediment, and the tide then transports the sediment. Without waves, no sediment is stirred up. This can be seen in the simulations without waves. If a tide is absent, then the sediment is not transported. Extrapolating the results for different tidal ranges shows this. This is in accordance with Winterwerp et al. (2020). They state that the tide transports sediment that is stirred up by waves.

The distribution of sediment within the mangrove in the model simulations is similar as found in literature (Janssen-Stelder et al., 2002; Van Santen et al., 2007). Sedimentation rates are highest at the seaward edge of the mangrove, and lowest at the landward edge. This results from a reduction in the current velocity within the mangrove. Furthermore, less sediment is transport to the landward edge, as this is only flooded during spring tide.

Observed net sedimentation rates are in the order of 1.5 ton/m per spring-neap tidal cycle for no SLR. As there are 26 spring-neap tidal cycles, this would mean a net sedimentation of roughly 39 ton/m/year. Assuming 1.6 ton/m^3 gives 24 m^3/m/year of sedimentation. Roughly 50 % of the sediment ends up in the first 200 meters of the mangrove, as seen on figure 3.18. This would mean that average sedimentation rates are 6 cm/year within the first 200 meters. This is in line with sedimentation rates made in the dry season on a mangrove coast in Indonesia, where rates of the order 5 cm/yr are seen (Sidik et al., 2016).

Mangrove roots have been schematised as uniformly distributed cylinders above MSL, with a diameter of 0.01 m and a height of 0.2 m. The roots enhance tidal asymmetry because they add roughness in the water column. Horstman, Bryan, et al. (2018) found that roots with a uniform height underestimate sedimentation rates in a mangrove. Roots with varying heights increase turbulence in the flow, which enhances sedimentation. In reality, roots have varying heights. Therefore, sedimentation rates are potentially higher in practice.

Historically, sedimentation rates increase with sea level rise (Lovelock, Adame, et al., 2015; Friess et al., 2019). This has also been found in these simulations. Net sedimentation increases with increasing SLR rates. The increase in net sedimentation can be partially attributed towards the increase in roughness within the intertidal. Another slight contribution to the increase in net sedimentation is the way the sediment boundary condition is applied, namely in kg/m^3. It can be seen that the models are sediment supply limited. Sediment transport rates are equal if wave height, thus sediment transport capacity, increases. This has also been shown in the sensitivity analysis, where a change in sediment boundary concentration is correlated 100% with net sedimentation. With increasing SLR, i.e. an increase in the volume of water, more sediment enters the model and more sedimentation is observed. In reality, it is expected that the sediment available does not increase with increasing water levels. Therefore, the net sedimentation rates with SLR are slightly overestimated due to the boundary condition.

It has been found that for increasing SLR rates, the net sedimentation within the mangrove increases and the distribution of the sedimentation across the mangrove stays the same. For larger sedimentation rates, it is expected that this would lead to an expansion of the intertidal in the offshore direction. An expanding intertidal does not yet have vegetation, as this needs to grow. Therefore, the roughness is less than within the mangrove. It is expected that the distribution of the sedimentation does not remain the same, sedimentation will most likely

occur on the intertidal as well. Furthermore, it is expected that on the intertidal, sedimentation will be less than within the mangrove, due to the absence of vegetation.

4.3.2 Model limitations

Fine sediment schematisation

The fine sediment in the model has been schematised without consolidation nor flocculation. Flocculation changes the settling velocity, due to the formation of larger sediment flocs (Winterwerp, 2002). Consolidation changes the critical bed shear stress over time (Torfs et al., 1996). The bed initially has a lower critical bed shear stress, which increases gradually.

Both of these properties influence net sedimentation, as seen in the sensitivity analysis in section 2.3. (Van Maren & Winterwerp, 2013) shared these observations. They found that a changing the critical bed shear stress, which consolidation does, and changing the settling velocity, which flocculation does, changes the behaviour quantitatively.

It is expected that when flocculation is included, the sedimentation above MSL decreases, but within the intertidal increases. When consolidation is included, a larger net sediment transport is expected, both above MSL and within the intertidal.

Morphodynamic response

A morphostatic bed has been assumed for these simulations, which influences the model behaviour. As stated in section 4.2, a morphodynamic response is expected when the tipping points of the tide and waves are exceeded. Above MSL, the critical bed shear stress is not exceeded often, and sediment is able to deposit. That deposition would lower deposition rates, as less water then flows towards the sedimentation location (Maan et al., 2015). Therefore, it is expected that a morphodynamic model leads to a reduction in sedimentation above MSL as defined in the model, and towards an expansion of the upper intertidal flat.

The absence of a morphodynamic response is expected to be the main reason the sediment distribution for varying SLR rates does not change. When SLR increases, the net sediment transport within the mangrove increases. However, in reality a morphodynamic feedback loop, as described above, would limit this behaviour. An expanding intertidal mud flat is expected, rather than a sediment distribution remaining equal.

Minimum depth for flow module

The minimum depth for the flow module causes model artefacts, seen as sudden increases in flow velocities, at the edge of the tidal wave. They are caused by the emptying and filling of cells. The model artefacts are rather insignificant. Their duration is short, they are present in shallow water depths, and they occur over a small distance. The impact of these artefacts on the results in minor. They do not hinder the understanding of the processes on mangrove coasts. Furthermore, their impact on the net sedimentation is small, due to their insignificance. A model without artefacts would slightly reduce net sedimentation. The artefacts increase flow velocities, therefore they increase net sedimentation. However, the artefacts are of no issue for this research.

4.4 Conceptual model

In this section, a conceptual model is presented. This gives an insight in the regular behaviour of the mangrove coasts. Furthermore, it allows for a preliminary assessment in the possible results of a nourishment in a mangrove, without performing any calculations. The model is shown on figure 4.2, and then explained below.

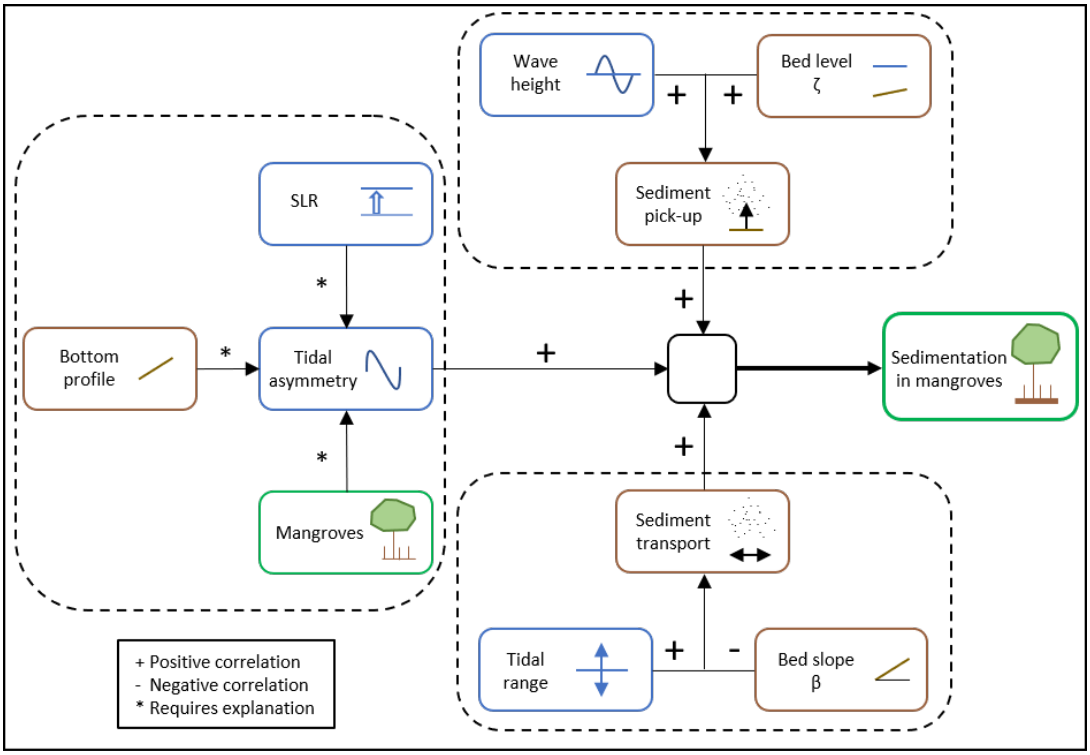

Figure 4.2: Conceptual model of mangrove coast

Three major components to sedimentation within the mangrove are identified. These, not coincidentally, are the major components of sediment dynamics (Bosboom & Stive, 2012). The components are sediment pick-up, sediment transport, and tidal asymmetry. Their combination controls the total amount of sedimentation within the mangrove.

4.4.1 Sediment pick-up

Sediment pick-up is the first component of sediment dynamics. Without sediment pick-up, no sediment would be transported towards the mangrove, as there would be an absence of sediment. Due to model limitations, sediment pick-up did not increase with an increasing maximum bed shear stresses. However, in reality, a larger maximum bed shear stress will result in more sediment pick-up. This is shown in the Partheniades-Krone formula.

The two components of sediment pick-up are wave height and the bed level elevation (ζ). The tidal range (see section 4.2) which would cause bed shear stresses in excess of the critical bed shear stress is not considered, due to the expected morphodynamic response. The combination of waves and ζ can cause large maximum bed shear stresses, which pick up the sediment.

On figure 4.2, a positive correlation between both the bed level and the wave height are shown. This means that an increase in either wave height or ζ results in an increase in sediment pick-up.

A positive correlation between sediment pick-up and sedimentation exists. If more sediment is in the water, more sedimentation can occur in the mangrove, assuming no other factors are influenced.

4.4.2 Sediment transport

Sediment transport is the second component of sediment dynamics. Sediment transport moves sediment from location to location. Two components of sediment transport are identified on mangrove coasts. The first is the tide, the second one is the bottom profile.

A larger tidal range causes larger an increase in flow velocities, which increases the sediment transport capacity. A reduction in tidal range reduces flow velocities, which reduces sediment transport.

A steeper bed slope reduces flow velocities, whereas a milder bed slope increases flow velocities. A reduction/increase in flow velocities reduces/increase sediment transport.

A positive correlation between sediment transport and sedimentation exists. If more sediment is transported towards the mangrove, more sedimentation can occur in the mangrove, assuming no other factors are influenced.

4.4.3 Tidal asymmetry

Tidal asymmetry is the main driver of sediment deposition. Tidal asymmetry requires a bit more explanation than sediment pick-up and transport, due to the different interactions the components have. The three main components that cause and change tidal asymmetry are sea level rise, the bottom profile, and mangroves.

Tidal asymmetry can be either flood or ebb dominant. A more asymmetric - flood dominant - tide results in more sedimentation within the mangrove. If the tide becomes more asymmetric in the ebb direction, sediment is exported. A more symmetric tide results in less sedimentation. All coasts, both with and without mangroves, have shown to be flood dominant, meaning they all import sediment.

Increasing rates of sea level rise cause enhanced tidal asymmetries. This is because the intertidal is shifted further into the vegetation. Slack water asymmetry becomes more flood dominant, whereas the peak flow velocity, as well as the duration asymmetry, become more ebb dominant.

The tipping point $d\beta/dx$ influences tidal asymmetry. If $d\beta/dx$ is negative, the slope reduces shorewards. This leads to increased flow velocities towards the shore. As the tidal signal does not change, this increases slack water asymmetry. When $d\beta/dx$ is positive, slack water asymmetry is reduced, compared to a negative $d\beta/dx$. Thus, $d\beta/dx$ therefore influences tidal asymmetry.

Depending on the length of the mangroves, tidal asymmetry is changed. Slack water asymmetry in general increases in flood dominance. Peak flow velocity asymmetry, however, increases in ebb dominance. No definitive answer exists for the mangrove influence on tidal asymmetry, as this greatly depends on the local conditions.

Chapter 5

Sediment nourishment on a mangrove coast

In this chapter, designs for a sediment nourishment on a mangrove coast are made and evaluated, to find design considerations.

First, the model set-up is covered in section 5.1. Then, considerations for the constructability of nourishments are given in section 5.2. Section 5.3 discusses several nourishment designs. Results are presented afterwards in 5.4. Then, in section 5.5, the different designs are evaluated. Finally, in section 5.6, design considerations for a sediment nourishment are presented.

5.1 Sediment nourishment model set-up

The model used for the sediment nourishment is largely the same as for the process analysis, presented in chapter 2. Three changes are applied to the model. The first change is that bed level updates are enabled. Enabling these updates allows for an insight in the erosion of the nourishment. The second change is that an erodible sediment layer is applied to the model, with a uniform thickness of 10 cm. This layer is required to find where erosion takes place across the coast. The third and final change to the model is a change in the erosion coefficient M. In the process analysis, it was set at 0.01 kg/m^2/s. However, this results in unstable model runs when used with an erodible layer, as shown in appendix C. In the process analysis, using 0.01 kg/m^2/s did not lead to instabilities. This is due to the fact that erosion rates are significantly lower, due to the absence of an erodible layer. However, with the erodible layer, 0.01 kg/m^2/s causes high erosion rates, and therefore instabilities. Thus, it is lowered and set at $5 \cdot 10^{-5}$ kg/m^2/s (Maan et al., 2015).

It has been shown that a concave coast is able to import less sediment than a convex coast, with equal concentrations entering the coast. Thus, applying a sediment nourishment to increase sedimentation is most relevant for a concave coast. The nourishments are therefore evaluated on a concave coast.

The tidal range used for the simulation is 0.8-1.5 m, and the waves have a significant wave height of 0.6 m. Mangroves are present above MSL. The combination of tide and wave is chosen as it has been shown in chapter 3 that this results in almost equal, but very slightly less sedimentation with mangroves present. Therefore, this is a relevant combination to enhance sedimentation.

The simulations are performed without SLR. There are two reasons for running the simulations without SLR. The first reason is that there are no tipping points observed for SLR in

the hydrodynamics. Thus, there will not be a point for which behaviour changes drastically. The second is that SLR causes increased sedimentation rates, as shown in chapter 3. However, exact rates cannot be quantified using a theoretical model. Therefore, running simulations with SLR does not result in more useful knowledge.

The model output, which is used for the analysis of the results, is similar to the process analysis. This is defined in subsection 2.1.7. The only difference is that the tidal asymmetry is evaluated at -3.0 m, rather than +0.5 m, because the nourishments are present until that depth.

Using these settings, a model is obtained that gives insight in the evolution of the sediment nourishment under regular conditions.

5.2 Constructability of nourishments

A sediment nourishment can be used in two manners: to increase sediment availability, or to change the bottom profile of the coast for a longer duration (Laboyrie et al., 2018). Increasing the sediment availability requires the disposal of sediment with similar properties as found on the coast. To change the bottom profile on a longer timescale, sediment with a higher critical bed shear stress than found on the coast is required. The former can result in increased sedimentation by increasing sediment transport rates due to increased mobilisation, whereas the latter can increase net sediment transport by changing flow velocity profiles and tidal asymmetry. The tipping point, as found in section 4.2, of the onshore direction cross-shore gradient of the bed slope $d\beta/dx$, can be influenced by changing the bottom profile.

The two types of dredgers regularly used to nourish coasts are a cutter suction dredger (CSD) and a trailing suction hopper dredger (TSHD) (Laboyrie et al., 2018). The differences lay in the way the sediment is dislodged, how the sediment is transported, and where sediment is stored temporally. For this purpose, the latter two aspects of the dredgers are interesting. The different vessels have different disposal methods.

A CSD has no way of storing sediment on board. Therefore, all dredged sediment is either pumped directly into a barge, or pumped through a pipeline to the disposal location (Laboyrie et al., 2018). The placement of the sediment is therefore limited by the draught and capacity of the barges, or by the length and location of the pipeline.

A TSHD can store sediment in its hopper. It can empty its hopper in three ways: rainbowing, pumping through pipes, and dumping through its bottom doors (Laboyrie et al., 2018). Pumping sediment through pipes requires the construction of the pipes, and requires fuel to run the pumps. This method is most expensive, but it can place sediment further onshore on shallow coasts. Rainbowing does not use pipes, but uses the pumps to dislodge sediment through a nozzle. It can place the sediment less far onshore, compared to pumping through pipes, due to draught limitations of vessels (IADC, 2014). Dumping through the doors is the cheapest option, as gravity is used to move the sediment, however this requires increased water depths. Depths are limited on mangrove coasts and the loaded maximum draught of small TSHDs is in the order of 5 meters (IADC, 2014). This further limits the nourishment designs.

The exact considerations vary per type of vessel and project. However, both a CSD and a TSHD are suitable for creating a sediment nourishment on a mangrove coast.

Various disposal strategies to increase sediment availability exist. All sediment can be placed at once, such as the Zandmotor (Huisman et al., 2021). Cross-shore flow velocities can then be influenced, changing the hydrodynamic behaviour of the coast, and a large quantity

of sediment is available. Another possibility is to perform sediment suppletions over a longer period of time, such as the Mud Motor (Baptist et al., 2019). Sediment availability increases over a longer period, but the hydrodynamics do not change. This requires a sediment importing system within the intertidal. It has been shown that the coasts investigated all are importing, meaning that this can be a viable strategy.

Considering the purpose of this research, which is to investigate the design considerations for a sediment nourishment, several nourishment designs are tested. This allows for an investigation of the obtained result versus the effort, i.e. the location, quantities, required to nourish the coast. The construction of the nourishment is not considered, as that lays out of the scope of this research. The constructability of the sediment nourishment is considered.

5.3 Sediment nourishment designs

Sediment nourishments can not only increase sediment availability, but they can also change the hydrodynamics on the coast. The latter can result in a non-linear effect in the sediment transport, thus in the sedimentation within the mangrove. The non-linear effect being that the sediment is not only used to increase sediment availability, but that it also achieves increased sedimentation, by changing hydrodynamic conditions.

For this research, it is assumed that the sediment used for the nourishment has the same properties as that found on the coast. This means that the nourishment is used to increase sediment availability. However, it might also be possible that hydrodynamics are changed temporally, thereby increasing the sediment transport capacity. To investigate if a nourishment, using the same fine sediment as found on the coast, can change the hydrodynamics requires investigation. Furthermore, the location of the nourishment might influence the obtained results. To find the design considerations, several designs are simulated.

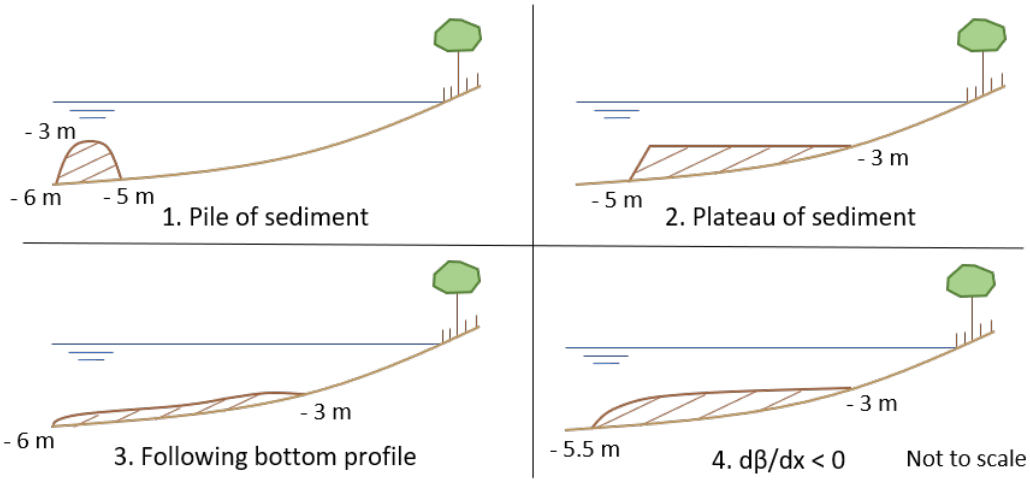

Figure 5.1: Four sediment nourishment designs. Top left: 'Pile of sediment', top right: 'Plateau of sediment', bottom left: 'Following bottom profile', bottom right: 'dβ/dx < 0'.

Four nourishment designs are presented on figure 5.1. The designs have been made for depths between -6 and -3 m. The maximum depth of -6 m has been chosen considering the coastal active profile. -3 m is considered to be the limit for constructability, due to the loaded draught of dredging vessels (IADC, 2014).

1. **Pile of sediment:** A pile of sediment is added to the mangrove coast, which lays between -6 m and -5 m, and goes up to -3 m. It is easiest to construct. The total volume of this nourishment is 1547 m^3/m
2. **Plateau of sediment:** A plateau of sediment is created, which from -5 m goes sharply to -3 m, and the remains on this height. The total volume is 5847 m^3/m
3. **Following bottom profile:** A nourishment that follows the contours of the bottom, but increases bed level with 0.7 m. This is done until a height of 3 m is reached. The required volume for this nourishment is 2624 m^3/m.
4. **$d\beta/dx < 0$:** A convex 'sub-profile' is created on the concave coast. This is done starting at -5.5 m, and goes up to -3 m. The required volume is 3692 m^3/m

The designs have been made by varying in obtained bed slope, depth, and location. The variations allows for an evaluation of the design considerations for a sediment nourishment. These four designs, and a baseline model without a nourishment, are tested and compared on the sedimentation rates within the mangrove area.

5.4 Results of sediment nourishments

The different nourishment designs lead to varying rates of sedimentation within the mangrove forest. These sedimentation rates are presented in table 5.1. Appendix C presents the cross-shore behaviour of the various sediment nourishment strategies. Designs 2 and 4 lead to the most sedimentation in the mangrove. Design 1 leads to less sedimentation in the mangroves, compared to having no nourishment.

Table 5.1: Sedimentation rates at +0.0 m and +0.2 m for the different nourishment designs

	Sed. at 0.0 m	Δ_{i-0} at +0.0 m	Sed. at 0.2 m	Δ_{i-0} at + 0.2 m
0. No nourishment	13.6 cm	-	7.4 cm	-
1. Pile of sediment	13.5 cm	- 0.1 cm	7.3 cm	- 0.1 cm
2. Plateau of sediment	13.9 cm	+ 0.3 cm	7.5 cm	+ 0.1 cm
3. Following bottom	13.7 cm	+ 0.1 cm	7.4 cm	0.0 cm
4. $d\beta/dx$	13.9 cm	+ 0.3 cm	7.5 cm	+0.1 cm

The different designs cause different erosion volumes between -6 m and -3 m, as well as accretion volumes above MSL, see table 5.2. The erodible layer of sediment has not been eroded completely anywhere. It can be seen that largest eroded volume is for design 2, and the smallest eroded volume is design 0. Design 1 has more erosion than design 0, but this does not result in an increase in sedimentation within the mangrove.

The different sedimentation rates do not cause variations in shape of sedimentation, see figure 5.2. All sediment is distributed in a similar manner, with more sediment ending up at the edge of the mangrove than within the forest. Larger sedimentation rates at the edge of the forest also translate to larger sedimentation within the mangrove. The difference in sedimentation is caused by the variations in hydrodynamics, due to the nourishments. Figure 5.3 shows the maximum bed shear stresses and maximum sediment fluxes in cross-shore direction. The differences in maximum bed shear stress explain the differences in eroded volume of the nourishment. The Partheniades-Krone formula calculates erosion rates by comparing τ and τ_{cr}.

Table 5.2: Erosion of nourishment and accretion in mangrove for the different nourishment designs

	Erosion of nourishment (m^3)	Δ_{i-0}	Accretion in mangrove (m^3)	Δ_{i-0}
0. No nourishment	226	-	21.9	-
1. Pile of sediment	236	+ 10	21.6	- 0.3
2. Plateau of sediment	298	+ 72	22.3	+ 0.4
3. Following bottom	267	+ 41	21.9	+ 0.1
4. dβ/dx	286	+ 60	22.1	+ 0.2

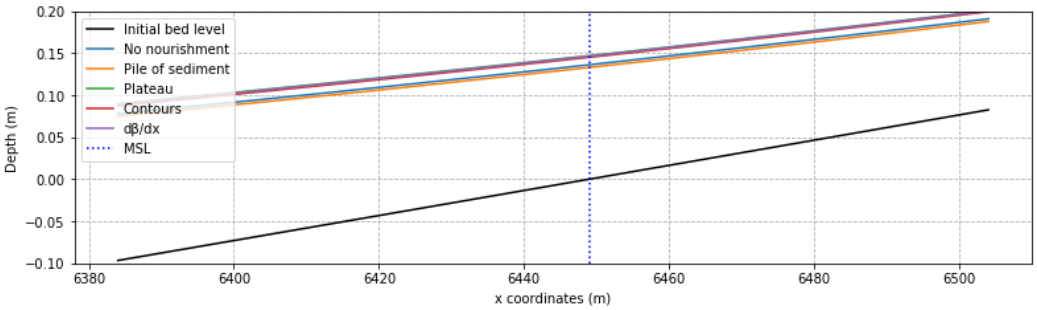

Figure 5.2: Cross-shore overview of sedimentation within the mangrove area after one spring-neap tidal cycle, varying nourishment designs. Tidal range 0.8-1.5 m, H_s of 0.6 m.

Larger bed shear stresses cause larger erosion rates. Design 2 has the largest bed shear stresses in the cross-shore direction, explaining why that design has the largest eroded volume. Design 1, pile of sediment, has a peak in the bed shear stresses, explaining why the erosion is larger than design 0. Design 1 leads to less sedimentation than no measure, because the bed shear stress envelope and the sediment transport rates (see figure 5.4) are smaller for design 1.

The different maximum sediment fluxes explain the differences in sedimentation in the mangrove. It can be seen that the maximum sediment fluxes for designs with higher bed levels are larger than those with a lower bed level.

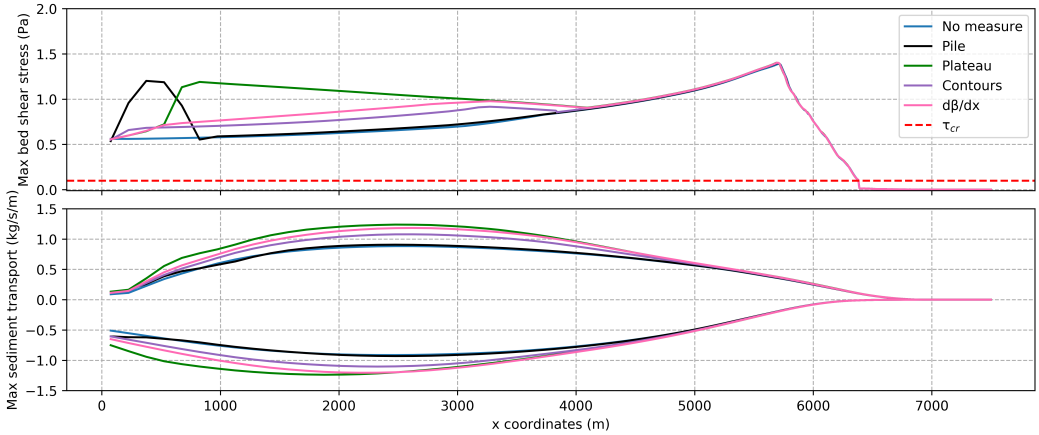

Figure 5.3: Cross-shore maximum bed shear stress and sediment transport envelope for varying nourishment designs. Tidal range 0.8-1.5 m, signifcant wave height 0.6 m.

Tidal asymmetry for sediment nourishments

To investigate if the tipping point of dβ/dx has been influenced, the tidal asymmetry across the coast is looked into. This has been shown on figure 5.4.

At -5.0 m, flow velocities vary significantly between the varying nourishment designs. For each nourishment design, the flow velocity is the equal and symmetrical. On the contrary, sediment transport is asymmetrical and ebb dominant for all designs. More sediment is transported in offshore direction than in onshore direction.

At -3.0 m, all flow velocities have the same values, and are all symmetrical. Flow velocities have not increased compared to the -5.0 m values. Designs 2 and 4 have highest onshore sediment transport rates. Design 3 transports slightly less, and designs 1 and 0 transport the least amount of sediment. For all designs, more is transported onshore than offshore.

At -0.5 m, the flow velocity profiles again are equal for all designs, but now have become asymmetrical. Again, flow velocities have not increased compared to -3.0 m and -5.0 m. Slack asymmetry appears, the flood flow reversal is faster than the ebb flow reversal. The duration of the tides is similar, and flow velocities are equal. This results in a flood dominance at -0.5 m, which also shows in the sediment transport. The nourishment design influences the quantity of sediment transport, but for all designs it holds true that more is transported towards than away from the shore.

At +0.0 m, again, for all designs the flow velocities are equal, but the sediment transport is not. Tidal asymmetries have changed. Flood reversal is quicker than ebb reversal. Ebb duration is longer than the flood duration, and peak velocities are larger for ebb than for flood. Even though the latter two asymmetries are ebb dominant, the system is flood dominant. This shows in the sediment transport, which transports more above MSL than away from MSL.

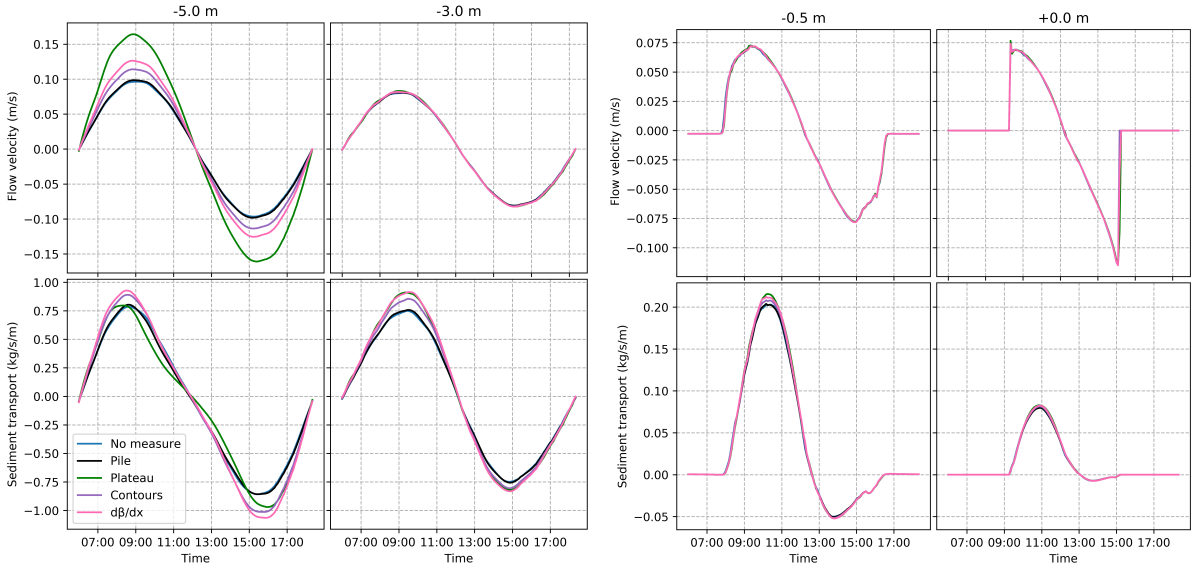

Figure 5.4: Tidal asymmetry for different nourishment designs, during spring tide with mangroves present. Tidal range of 0.8-1.5 m, significant wave height of 0.6 m. Shown at depths of -5.0 m (outer left), -3.0 m (middle left), -0.5 m (middle right), and +0.0 m (outer right)

Summary of sediment nourishment results

Using a nourishment can, but does necessarily have to, result in more sedimentation within the mangrove. The tidal asymmetry has not been influenced within the intertidal, nor has the tipping point of $d\beta/dx$ been exceeded by any of the nourishment designs. The flow velocities do not increase towards the shore. Sediment is transported towards the mangrove due to increased sediment pick-up rates. The increased pick-up is caused by higher wave influence on the bed, due to increased bed levels.

5.5 Evaluation of nourishment designs

In this section, the nourishment model and results will be evaluated. First, the model used is reflected upon. Then, the resulted are analysed. Finally, ecological considerations of nourishing a mangrove coast are discussed.

5.5.1 Reflection on sediment nourishment model

The reflection points for the sediment nourishment model are largely the same as for the process analysis, as discussed in chapter 4. This is because the model has not been changed a lot. The fine sediment behaviour remains schematised and the ecology still is fixed. However, an erodible layer on the bed is now present, as well as bed level updates. The impact of these changes is shortly presented here.

The fine sediment schematisation, without consolidation or flocculation, impacts the behaviour of sediment nourishments. When a fine sediment nourishment is applied, the critical bed shear stress first is in the order of 0.03 Pa (Torfs et al., 1996). This means not all sediment will be able to settle, but will be transported instantly, towards a location with lower bed shear stresses. Those lower bed shear stresses are found within the mangrove, meaning that sediment can settle there. Therefore, sedimentation rates within the mangrove may be higher than observed.

The mangroves within the model remain static, at the original bed level of MSL, without any growth when sedimentation occurs. This limits the behaviour of the model in two ways. First, when the upper intertidal mudflat expands offshore, i.e. the bed level of +0.0 m moves seawards, mangroves do not colonise the area. Furthermore, when sedimentation occurs within the mangrove, the roots do not grow with the sedimentation. This means that with sedimentation rates of 13 cm at the edge of the mangrove, 7 cm of roots remain above the sediment. Both of these limitations reduce tidal asymmetry. As seen in the results of the process analysis, chapter 3, a quantification of a positive or negative effect of this reduction is impossible.

The erodible layer, which has now been included in the model, has not been eroded complete anywhere in the model after a model simulation. This means that the observed behaviour has not been limited by sediment availability on the bed.

Bed level updates have now been included in the model. The bottom profile still is a non-equilibrium profile, which means that the hydrodynamic forcing does not result in the exact bottom profile, resulting in changing bed levels. However, with different nourishment designs, the erosion and accretion of sediment changes across the coast. This gives insight in the behaviour of the coast with varying nourishment designs.

The model has given insight in the behaviour of varying sediment nourishment designs. Observations of the behaviour are in line with the results of the process analysis. Even though some model limitations are present, the insight in the effect of the varying designs has been obtained, which is the purpose of this research.

5.5.2 Interpretation of sediment nourishment results

A nourishment can cause, albeit not a lot, more sedimentation within the mangrove. Depending on the design of the nourishment, varying rates of sedimentation are obtained within the mangrove. Sedimentation has been shown to positively influence mangrove growth (Horstman, Lundquist, et al., 2018). As nourishments cause an increase in sedimentation, they can be used as a method to rehabilitate mangroves. However, there are some observations that require consideration, before using a nourishment for mangrove rehabilitation. These will be discussed here.

The tested nourishment designs does not influence the tidal asymmetry within the intertidal, nor does it exceed the tipping point of $d\beta/dx$ across the coast. This can be seen on figure 5.4, by looking at the variations in flow velocities. For -5.0 m, differences are observed. However, these differences are not seen further onshore on the coast. For depths $<$ 3.0 m, the flow velocity signals have become equal. Tidal asymmetry should be influenced within the intertidal, where sedimentation occurs, to change net sedimentation rates. Sediment transport rates vary per nourishment design. Due to the absence of a variation in flow velocities and tidal asymmetry, the varying sediment transport rates come from the variations in bed shear stresses depending on the nourishment design. A non-linear effect in the sedimentation, by a change in hydrodynamic behaviour, has not been obtained by any of the designs.

The nourishment causes increased sedimentation rates by increasing bed levels, which result in more sediment mobilisation due to increased bed shear stresses. The increased bed shear stresses can be seen on figure 5.3. The envelope with the smallest maximum bed shear stresses is for 'no nourishment'. Envelopes with nourishments contain larger bed shear stresses. Increased bed shear stresses translate to larger sediment pick-up rates, as found in the Partheniades-Krone formula. These observations are made for designs 2, 3, and 4, compared to design 0. Design 1 causes an increase in bed shear stress in the offshore, but this does not result in an increase in the sediment transport.

The location of the sediment nourishment influences the obtained sedimentation rates. This observation is seen for design 1, a pile of sediment placed offshore. Onshore sediment transport is seen from the x-coordinates 2000 m and further onshore in the model. Farther offshore, sediment is transported away from the coast, rather than towards the coast. Increasing bed levels moves the point for which the sediment is transported onshore more offshore, however a significant portion is exported, as can be seen from table 5.2. Design 1 is placed offshore, close to the boundary. Design 2, for example, stretches further onshore and influences the sediment transport rates across the coast. Design 1 lays in a region where sediment is exported, meaning that this design does not increase sedimentation rates. Design 2 increases sediment pick-up both in regions where sediment is exported, as well as imported. Placing the nourishment in the region where more sediment is transported away from rather than towards the coast does not result in increased sedimentation within the mangrove. This means that sediment nourishments should be placed close to the shore.

The volumes eroded of the nourishments are significantly larger than the obtained increase

in sedimentation. This can also be attributed to the aforementioned location of the nourishments. For all designs, more sediment is transported offshore than onshore for x-coordinates less than 2000 m. As a large part of the nourishment is placed in the region of $x < 2000$ m, the sediment is eroded and not transported towards the mangrove. The shapes of the nourishments largely stay intact, meaning that they can influence the sedimentation within the mangrove for a longer duration. Design 4 obtains about the same sedimentation as design 2, whereas the volume of the nourishment is smaller. The large difference is volume is mostly seen on the seaward end of the nourishment. This extra volume is not transported towards the mangrove, but is eroded and transported offshore. Despite the larger erosion than sedimentation rates, three out of the four nourishments do increase sedimentation within the mangrove. The effectiveness of the nourishments depend on their location.

The volumes required to increase the depth for mildly sloping coasts are large, varying between 2,000 - 5,000 m^3/m. TSHDs have capacities varying between several hundreds of m^3 to 45,000+ m^3 (IADC, 2014). This limits the economic feasibility of the the nourishment as a stand alone project, due to the amount of sediment required for the nourishments. Applying a sediment nourishment on a stretch of 1,000 meters requires between $2 - 5 \cdot 10^6$ m^3 sediment, for these designs. Therefore, many trips from the dredging location to the nourishment location are required.

In the Netherlands, ranges of $3 \cdot 10^5$- $8 \cdot 10^6$ m^3 of sediment are quoted for dredging projects (Dutch Dredging, n.d.-b,-a). This means that, if all sediment is usable to rehabilitate mangroves, between 60 - 4000 meters of mangrove could be potentially nourished. The Zandmotor consisted of a nourishment of $20 \cdot 10^6$ m^3 over a distance of 2,500 m, resulting in 8,000 m^3/m (Huisman et al., 2021). For a mud motor, $4.5 \cdot 10^5$ m^3 fine sediment was nourished over a period of three months (Baptist et al., 2019). All in all, the designs are big in volume, but not impossible to execute.

Considering the volumes required, costs of a stand alone sediment nourishment project will be high. Combined with the fact that the nourishments do not result in a large increase in sedimentation, setting up a stand alone project for mangrove rehabilitation will likely be a challenge. Beneficially re-using sediment, rather than treating it as waste, appears to be a viable solution. Then, sailing distance of the dredger can possibly be reduced. This requires the combination of a dredging project with a sediment nourishment on a mangrove coast, e.g. a mud motor (Baptist et al., 2019).

Concluding, there are several important factors that play a role in the nourishing of a mangrove coast. First and foremost, nourishing a mangrove can result in an increase in sedimentation. Enhanced sedimentation rates are not obtained by influencing the tipping point of $d\beta/dx$, but by increasing bed levels. The location of the nourishment plays a significant role in the sedimentation rates. Nourishing a mangrove coast requires large volumes, limiting the feasibility of a stand alone mangrove nourishment project. However, when combining the project with another dredging project, the sediment can be re-used beneficially and a viable project can be proposed. The nourishment designs should be tested for the specific coast with the appropriate equipment, but it has been shown that increasing sedimentation within a mangrove is possible using a nourishment.

5.5.3 Ecological considerations

Two ecological aspects should be considered when applying a nourishment on a mangrove coast. These are the possible pollution of the sediment, and maximum sedimentation rates.

Contaminated material, e.g. by heavy metals or hydrocarbons, has been shown to negatively impact mangroves (Dwivedi & Padmakumar, 1983; Michel, 2000). Sediment dredged from ports, during maintenance dredging, can be contaminated (Martín-Díaz et al., 2008). The contamination of mangroves by using polluted sediment should be prevented.

The maximum sediment deposition rate for mangroves is the second ecological consideration. In the first place, the nourishment is applied to increase sedimentation rates in the mangrove. However, when placing dredged material, locally sedimentation rates increase (Erftemeijer & Lewis III, 2006). As discussed in the introduction, maximum rates of sedimentation vary between species (Ellison, 1999). Large depositions should be prevented, to make sure the roots of the mangrove are not fully buried. Burial does not appear to become a problem, however these rates do not consider consolidation nor the construction of the sediment nourishment.

5.6 Design considerations of nourishment designs

Three design considerations are identified using the evaluation of the nourishments, as well as the constructability of the nourishment. These considerations come from the impact of the nourishment on the behaviour of the coast, as well as the limits placed by the bottom profile and the equipment on the possibilities of a nourishment. The design considerations are the obtained bed level with the nourishment, the slope of the original bed, and the location of the nourishment.

The first design consideration is the obtained bed level with the nourishment. It has been shown that the nourishment does not influence tidal asymmetry, nor does it exceed the tipping point of $d\beta/dx$. Increases in sedimentation within the mangrove are obtained by increasing bed levels, which then increases sediment pick-up rates. Therefore, the nourishment should be designed such that the obtained depth is as shallow as possible.

The second design consideration is the slope of the original bed. The slope of the original bed largely determines the constructability of the nourishment. It limits the constructability by creating shallow water depths far away from the area of interest, which hinders the accessibility of the nourishment location for TSHDs. Furthermore, due to the mild slopes, large volumes are required to obtain increased bed levels across the cross-section. This further limits constructability of the nourishment. Therefore, for each nourishment design, the slope of the original bed imposes limits on the possibilities.

The final design consideration is the location of the nourishment. If the nourishment is placed too far offshore, then more sediment is transported offshore than onshore. In extreme cases, such as design 1, no sediment ends up in the mangrove. However, placing a nourishment farther offshore limits sailing distance, thereby reducing costs. The obtained effect of the nourishment should be carefully weighed against the costs of the nourishment.

In short, a sediment nourishment should be used to increase bed levels in areas where the dominant transport direction is shorewards. The design should be made such that the dredging vessel used can construct the nourishment.

Chapter 6

Conclusion

This goal of this thesis is to study whether rehabilitating coastal mangroves is possible using a sediment nourishment. Three objectives have been defined.

1. To identify the processes driving sedimentation on a mangrove coast. Identification of these processes is done by simulating mangrove coast behaviour in a schematised model.
2. To identify tipping points, for which sedimentation behaviour changes drastically across the coast. Tipping points are identified by analysing results of the simulations.
3. To investigate the possibilities and design considerations of a sediment nourishment, to influence the sedimentation within the mangrove. Several nourishment designs are tested on a mangrove coast, to compare and analyse their behaviour.

The main findings of the thesis have been based on a schematised hydro-morphodynamic model, without bed level updates. It has been shown this model functions adequately. First, the objectives are discussed shortly. Then, the final conclusion is stated.

Objective 1. The first objective of the research was to identify the processes driving sedimentation on a mangrove coast. This was done using a schematised model. The results show that the tide transports sediment and the waves mobilise sediment. The bottom profile influences tidal velocities and tidal asymmetry. Increased tidal asymmetry causes larger onshore sediment transport rates and enhance sedimentation. Mangroves influence the flow by increasing roughness in the water column, thereby altering tidal asymmetry. For small tidal ranges, which means the flow travels a short distance through the forest, the mangroves do not impact the behaviour. It then is equal to a coast without mangroves. However, for large tidal ranges, mangroves can either have a negative or positive impact on the net sedimentation, compared to a coast without mangroves. For a longer distance, i.e. a large tidal range, the effect is positive, whereas it is negative for a shorter distance, meaning a smaller tidal range.

Sea level rise changes how much the flow feels the bottom, by increasing water levels. It has been found that SLR increases tidal asymmetry, when mangroves are present, which in turn increase net sediment transport rates.

Objective 2. The second objective was to identify tipping points, for which sedimentation behaviour changes drastically across the coast. These tipping points have been identified by extrapolating behaviour observed in the model simulations. Tipping points have been found for the bottom profile, tide, waves, and mangroves. For SLR, no tipping point is found, as no drastic changes in behaviour are seen.

The bottom profile influences tidal velocities. A convex profile increases tidal velocities shorewards, which results in more sedimentation compared to a linear and concave profile. The tipping point identified is the gradient of the slope in cross-shore direction: $d\beta/dx$. The value of the tipping point $d\beta/dx$ is zero, meaning a constant bed slope across the coast. If $d\beta/dx$ is negative in the onshore direction, significantly more sedimentation is observed, compared to a positive value for $d\beta/dx$ in the onshore direction.

The tide has two tipping points, one for which the range is so small no sediment is transported towards the mangrove. The second is that the tidal range is so large, critical bed shear stresses are exceeded everywhere across the coast. For both cases, a morphodynamic response is expected.

Waves mobilise sediment. The tipping point identified is when waves do not pick-up sediment anymore, such that $\tau_{max} < \tau_{cr}$. In reality, it is expected that a morphodynamic response will occur, changing bed levels such that the bed shear stress equals the critical bed shear stress.

For mangroves, two tipping points are seen, based on the distance the flow travels through the mangrove. For a short distance mangroves, it is seen they do not influence flow. Mangroves have a negative influence on sedimentation when flow travels a distance varying between 500-1,000 m through them. Then, the influence of the mangroves is such that they export more sediment than a coast without mangroves. If flow travels more than 1,000 m through the mangrove causes more sedimentation within the forest.

Objective 3. The third objective was to investigate the possibilities and design considerations of a sediment nourishment. Several nourishment designs have been tested on a mangrove coast, to compare and analyse the behaviour. Design considerations identified are the obtained bed level with the nourishment, the slope of the original bed, and the location of the nourishment. The nourishment has been found not to influence the tipping point of the bed shape $d\beta/dx$. It is able to influence the sedimentation by increasing bed levels, thereby increasing bed shear stresses and sediment pick-up rates. The slope of the original bed largely determines the constructability of the nourishment. It limits the constructability by creating shallow water depths far away from the area of interest, as well as causing large volumes required for the nourishment. If the nourishment is placed too far offshore, then more sediment is transport offshore than onshore. A sediment nourishment should be used to increase bed levels in areas where the dominant transport direction is shorewards.

All in all, it is possible to use a sediment nourishment to rehabilitate mangroves. Sediment can be used to increase wave pick-up, by increasing bed levels. The obtained increase is small per spring-neap tidal cycle, i.e. 0.1-0.3 cm, but it is an increase in sedimentation nonetheless. The quantity of volume required, combined with the effort required to obtain increases in sedimentation, should be considered when analysing the economic feasibility of a mangrove rehabilitation project. However, if a sediment nourishment can be executed in combination with a maintenance dredging operation, then it proves to be a promising solution for the rehabilitation of mangroves.

Chapter 7

Recommendations

In this final chapter, recommendations for both the application of this research and future research are made. First, the application of this thesis is discussed in section 7.1. Section 7.2 covers the recommendations for future research.

7.1 Application

This thesis has shown that, under the right conditions, a sediment nourishment can be used to rehabilitate mangroves. A suppletion increases sedimentation within a mangrove forest, by increasing sediment pick-up rates. Exact sedimentation rates depend on the conditions present, as well as on the nourishment design. Obtaining a non-linear effect with the nourishment, has not been shown to be reasonable. To do so, the sediment would require placement up to the intertidal. Dredging vessels that suit the kind of project limit the placement of the sediment in the intertidal. Furthermore, possible negative side effects, i.e. the smothering of mangroves due to high sedimentation rates, should also be considered when placing the sediment in the intertidal.

The use of a nourishment to rehabilitate mangroves limits itself to increasing sediment pick-up, by increasing bed levels. Dredging projects, in the proximity of mangroves, should consider nourishing a mangrove coast, thereby re-using the dredged material. The sediment nourishment should obtain a balance between the constructability, possible negative effects on the environmental, and achieved results.

7.2 Future research

This thesis has shown the possibilities of a sediment nourishment on a mangrove coast. However, more research is required to understand behaviour of both mangrove coasts and sediment nourishments. Three suggestions for future research are made, in no particular order of importance.

7.2.1 Case location

It has been shown that a sediment suppletion can lead to more sedimentation on a mangrove coast. This was found using a schematised, one-dimensional model. Investigating a case loca-

tion allows for several 'improvements'. The first is that validation of the model, based on data of the case location, is possible. The second is that, by using a case location a 2DH model can be created based on local geometry. This allows for an investigation on long-shore processes, as well as the formation of tidal channels due to the outflow accelerations mangroves cause. The final improvement is that the hydrodynamic boundary conditions then match the bottom profile. That match allows for a morphostatic and morphodynamic process analysis, which enables research of feedback loops on mangrove coasts.

Another reason for finding a case location is to analyse multiple sediment nourishments on an equilibrium bottom profile. Then, nourishment strategies can be analysed in a 'real' situation, which allows investigation of the behaviour over time. Applying the nourishment on a case location will show sedimentation rates within the mangrove and erosion rates of the nourishment. Thereby allowing a more precise analysis of the effectiveness of varying nourishment strategies. Furthermore, more precise erosion rates of the nourishment and sedimentation rates in the mangrove can then be discovered.

7.2.2 Sea level rise and mangrove vegetation interaction

Mangrove habitat is above MSL, so with increasing sea levels, their habitat moves. However, in this research, this behaviour has not been included. Results show that when mangroves do not die, tidal asymmetry is enhanced by increasing flow resistance on a larger length of the flow. This increases sedimentation with increasing SLR rates. Including the movement of mangroves with SLR for both the growth and the disappearance of vegetation, by introducing equations for ecology habitat, allows for the investigation when the observed behaviour changes.

7.2.3 Extreme weather events behaviour

In this research, regular conditions have been assumed. However, during extreme weather events, the behaviour of mangrove coasts changes (Smith et al., 2009). During extreme weather, several processes happen. For example, increasing water depths change the tidal asymmetry, water set-up by the wind induces barotropic currents, and increasing wave height changes sedimentation behaviour. Understanding how extreme weather events change the behaviour of mangroves coasts, both with and without a sediment nourishment, can lead to a more effective approach on the rehabilitation of mangroves using sediment.

Bibliography

Albers, T., & Schmitt, K. (2015). Dyke design, floodplain restoration and mangrove co-management as parts of an area coastal protection strategy for the mud coasts of the mekong delta, vietnam. *Wetlands Ecology and Management*, *23*(6), 991–1004. doi: 10.1007/s11273-015-9441-3

Alvarez Cruz, N. (2008). *Avicennia marina (forssk.) vierh.* PROTA (Plant Resources of Tropical Africa / Ressources végétales de l'Afrique tropicale), Wageningen, The Netherlands. Retrieved from `http://www.prota4u.org/search.asp`

Athanasiou, P., Van Dongeren, A., Giardino, A., Vousdoukas, M., Gaytan-Aguilar, S., & Ranasinghe, R. (2019). Global distribution of nearshore slopes with implications for coastal retreat. *Earth system science data*, *11*(4), 1515–1529.

Bamber, J. L., Oppenheimer, M., Kopp, R. E., Aspinall, W. P., & Cooke, R. M. (2019). Ice sheet contributions to future sea-level rise from structured expert judgment. *Proceedings of the National Academy of Sciences*, *116*(23), 11195–11200.

Baptist, M. J., Gerkema, T., Van Prooijen, B., Van Maren, D., Van Regteren, M., Schulz, K., ... others (2019). Beneficial use of dredged sediment to enhance salt marsh development by applying a 'mud motor'. *Ecological Engineering*, *127*, 312–323.

Barbier, E. B., Hacker, S. D., Kennedy, C., Koch, E. W., Stier, A. C., & Silliman, B. R. (2011). The value of estuarine and coastal ecosystem services. *Ecological monographs*, *81*(2), 169–193.

Bosboom, J., & Stive, M. J. (2012). *Coastal dynamics I: lectures notes CIE4305*.

Bouma, T. J., Belzen, J. V., Balke, T., Zhu, Z., Airoldi, L., Blight, A. J., ... et al. (2014). Identifying knowledge gaps hampering application of intertidal habitats in coastal protection: Opportunities steps to take. *Coastal Engineering*, *87*, 147–157. doi: 10.1016/j.coastaleng.2013.11.014

Cahoon, D. R., Hensel, P., Rybczyk, J., McKee, K. L., Proffitt, C. E., & Perez, B. C. (2003). Mass tree mortality leads to mangrove peat collapse at bay islands, honduras after hurricane mitch. *Journal of ecology*, *91*(6), 1093–1105.

Dale, P., Knight, J., & Dwyer, P. (2014). Mangrove rehabilitation: a review focusing on ecological and institutional issues. *Wetlands ecology and management*, *22*(6), 587–604.

Deltares. (2021a). *Delft3d-flow user manual.* Deltares Delft, The Netherlands.

Deltares. (2021b). *Delft3d-wave user manual.* Deltares Delft, The Netherlands.

Dutch Dredging, B. (n.d.-a). *Maintenance dredging scheveningen harbour.* Retrieved from https://www.dutchdredging.nl/en/projects/maintenance-dredging/maintenance-dredging-scheveningen-harbour

Dutch Dredging, B. (n.d.-b). *Maintenance dredging waterways and harbors, province of zeeland.* Retrieved from https://www.dutchdredging.nl/en/projects/maintenance-dredging/maintenance-dredging-waterways-and-harbors-province-of-zeeland

Dwivedi, S., & Padmakumar, K. (1983). Ecology of a mangrove swamp near juhu beach, bombay with reference to sewage pollution. In *Biology and ecology of mangroves* (pp. 163–170). Springer.

Ellison, J. C. (1999). Impacts of sediment burial on mangroves. *Marine Pollution Bulletin*, *37*(8-12), 420–426.

Erftemeijer, P. L., & Lewis III, R. R. R. (2006). Environmental impacts of dredging on seagrasses: a review. *Marine pollution bulletin*, *52*(12), 1553–1572.

Etminan, V., Ghisalberti, M., & Lowe, R. J. (2018). Predicting bed shear stresses in vegetated channels. *Water Resources Research*, *54*(11), 9187–9206.

Friedrichs, C. (2012). *Tidal flat morphodynamics: A synthesis. treatise on estuarine and coastal science, volume 3 estuarine and coastal geology and geomorphology.* Academic Press.

Friess, D. A., Rogers, K., Lovelock, C. E., Krauss, K. W., Hamilton, S. E., Lee, S. Y., ... et al. (2019). The state of the worlds mangrove forests: Past, present, and future. *Annual Review of Environment and Resources*, *44*(1), 89–115. doi: 10.1146/annurev-environ-101718-033302

Furukawa, K., Wolanski, E., & Mueller, H. (1997). Currents and sediment transport in mangrove forests. *Estuarine, Coastal and Shelf Science*, *44*(3), 301–310.

Guo, L., Brand, M., Sanders, B. F., Foufoula-Georgiou, E., & Stein, E. D. (2018). Tidal asymmetry and residual sediment transport in a short tidal basin under sea level rise. *Advances in water resources*, *121*, 1–8.

Horstman, E. M., Bryan, K. R., Mullarney, J. C., Pilditch, C. A., & Eager, C. A. (2018). Are flow-vegetation interactions well represented by mimics? a case study of mangrove pneumatophores. *Advances in water resources*, *111*, 360–371.

Horstman, E. M., Lundquist, C. J., Bryan, K. R., Bulmer, R. H., Mullarney, J. C., & Stokes, D. J. (2018). The dynamics of expanding mangroves in new zealand. In *Threats to mangrove forests* (pp. 23–51). Springer.

Huisman, B., Wijsman, J., Arens, S., Vertegaal, C., van der Valk, L., van Donk, S., ... Taal, M. (2021). *Evaluatie van 10 jaar zandmotor: Bevindingen uit het monitoring-en evaluatie programma (mep) voor de periode 2011 tot 2021* (Tech. Rep.). Deltares.

IADC. (2014). INTERNATIONAL ASSOCIATION OF DREDGING COMPANIES. Retrieved from https://www-iadc-dredging-com.tudelft.idm.oclc.org/wp-content/uploads/2016/07/facts-about-trailing-suction-hopper-dredgers.pdf

Janssen-Stelder, B., Augustinus, P., & Santen, W. V. (2002). Sedimentation in a coastal mangrove system, red river delta, vietnam. *Fine Sediment Dynamics in the Marine Environment Proceedings in Marine Science*, 455–467. doi: 10.1016/s1568-2692(02)80033-x

Kodikara, K. A. S., Mukherjee, N., Jayatissa, L. P., Dahdouh-Guebas, F., & Koedam, N. (2017). Have mangrove restoration projects worked? an in-depth study in sri lanka. *Restoration Ecology*, *25*(5), 705–716.

Kranck, K. (1973). Flocculation of suspended sediment in the sea. *Nature*, *246*(5432), 348–350.

Krauss, K. W., Lovelock, C. E., McKee, K. L., López-Hoffman, L., Ewe, S. M., & Sousa, W. P. (2008). Environmental drivers in mangrove establishment and early development: a review. *Aquatic botany*, *89*(2), 105–127.

Krauss, K. W., McKee, K. L., Lovelock, C. E., Cahoon, D. R., Saintilan, N., Reef, R., & Chen, L. (2014). How mangrove forests adjust to rising sea level. *New Phytologist*, *202*(1), 19–34.

Laboyrie, P., Van Koningsveld, M., Aarninkhof, S., Van Parys, M., Lee, M., Jensen, A., ... Kolman, R. (2018). *Dredging for sustainable infrastructure*. CEDA/IADC The Hague, The Netherlands.

Lambers, H., & Poorter, H. (1992). Inherent variation in growth rate between higher plants: a search for physiological causes and ecological consequences. *Advances in ecological research*, *23*, 187–261.

Le Bars, D., Drijfhout, S., & de Vries, H. (2017). A high-end sea level rise probabilistic projection including rapid antarctic ice sheet mass loss. *Environmental Research Letters*, *12*(4), 044013.

Le Hir, P., Roberts, W., Cazaillet, O., Christie, M., Bassoullet, P., & Bacher, C. (2000). Characterization of intertidal flat hydrodynamics. *Continental shelf research*, *20*(12-13), 1433–1459.

Lewis, R. (2009). Methods and criteria for successful mangrove forest restoration. *Coastal Wetlands: An integrated ecosystem approach*, 787–800.

Lewis III, R. R., Brown, B. M., & Flynn, L. L. (2019). Methods and criteria for successful mangrove forest rehabilitation. In *Coastal wetlands* (pp. 863–887). Elsevier.

Lewis III, R. R., Milbrandt, E. C., Brown, B., Krauss, K. W., Rovai, A. S., Beever III, J. W., & Flynn, L. L. (2016). Stress in mangrove forests: Early detection and preemptive rehabilitation are essential for future successful worldwide mangrove forest management. *Marine Pollution Bulletin*, *109*(2), 764–771.

Lovelock, C. E., Adame, M. F., Bennion, V., Hayes, M., Reef, R., Santini, N., & Cahoon, D. R. (2015). Sea level and turbidity controls on mangrove soil surface elevation change. *Estuarine, Coastal and Shelf Science*, *153*, 1–9.

Lovelock, C. E., & Brown, B. M. (2019). Land tenure considerations are key to successful mangrove restoration. *Nature ecology & evolution*, *3*(8), 1135–1135.

Lovelock, C. E., Cahoon, D. R., Friess, D. A., Guntenspergen, G. R., Krauss, K. W., Reef, R., ... others (2015). The vulnerability of indo-pacific mangrove forests to sea-level rise. *Nature*, *526*(7574), 559–563.

Lugo, A. E., Medina, E., & McGinley, K. (2014). Issues and challenges of mangrove conservation in the anthropocene. *Madera y bosques*, *20*(SPE), 11–38.

Maan, D., Van Prooijen, B., Wang, Z., & De Vriend, H. (2015). Do intertidal flats ever reach equilibrium? *Journal of Geophysical Research: Earth Surface*, *120*(11), 2406–2436.

Martín-Díaz, M. L., Blasco, J., Sales, D., & DelValls, T. (2008). Field validation of a battery of biomarkers to assess sediment quality in spanish ports. *Environmental Pollution*, *151*(3), 631–640.

Mazda, Y., Kanazawa, N., & Wolanski, E. (1995). Tidal asymmetry in mangrove creeks. *Hydrobiologia*, *295*(1), 51–58.

Mazda, Y., Magi, M., Kogo, M., & Hong, P. N. (1997). Mangroves as a coastal protection from waves in the tong king delta, vietnam. *Mangroves and Salt marshes*, *1*(2), 127–135.

McIvor, A. L., Spencer, T., Möller, I., & Spalding, M. (2013). The response of mangrove soil surface elevation to sea level rise. *Natural Coastal Protection Series: Report 3. Cambridge Coastal Research Unit Working Paper 42. ISSN 2050-7941.*.

Michel, J. (2000). Assessment and recommendations for the oil spill cleanup of guanabara bay, brazil. *Spill Science & Technology Bulletin*, *6*(1), 89–96.

Moy, C. M., Seltzer, G. O., Rodbell, D. T., & Anderson, D. M. (2002). Variability of el niño/southern oscillation activity at millennial timescales during the holocene epoch. *Nature*, *420*(6912), 162–165.

Nardin, W., Woodcock, C. E., & Fagherazzi, S. (2016). Bottom sediments affect sonneratia mangrove forests in the prograding mekong delta, vietnam. *Estuarine, Coastal and Shelf Science*, *177*, 60–70.

Nienhuis, P., & Smaal, A. (1994). The oosterschelde estuary, a case-study of a changing ecosystem: an introduction. *Hydrobiologia*, *282*(1), 1–14.

NOAA. (2006, Feb). *Global forecast system (gfs) [0.5 deg.].* NOAA National Centers for Environmental Information (NCEI). Retrieved from `https://www.ncei.noaa.gov/access/metadata/landing-page/bin/iso?id=gov.noaa.ncdc:C00634`

Norris, B. K., Mullarney, J. C., Bryan, K. R., & Henderson, S. M. (2017). The effect of pneumatophore density on turbulence: a field study in a sonneratia-dominated mangrove forest, vietnam. *Continental Shelf Research*, *147*, 114–127.

Oh, R., Friess, D., & Brown, B. (2017). The role of surface elevation in the rehabilitation of abandoned aquaculture ponds to mangrove forests, sulawesi, indonesia. *Ecological Engineering*, *100*, 325–334.

Oppenheimer, M., & Hinkel, J. (2019). Sea level rise and implications for low lying islands, coasts and communities supplementary material.

Polidoro, B. A., Carpenter, K. E., Collins, L., Duke, N. C., Ellison, A. M., Ellison, J. C., ... others (2010). The loss of species: mangrove extinction risk and geographic areas of global concern. *PloS one*, *5*(4), e10095.

Primavera, J. H., & Esteban, J. M. A. (2008). A review of mangrove rehabilitation in the philippines: successes, failures and future prospects. *Wetlands Ecology and Management*, *16*(5), 345–358.

Ray, R. D., & Center., G. S. F. (1999). *A global ocean tide model from topex/poseidon altimetry [microform] : Got99.2 / richard d. ray* [Book, Microform]. National Aeronautics and Space Administration, Goddard Space Flight Center ; National Technical Information Service, distributor Greenbelt, Md. : [Springfield, Va.

Ricklefs, R. E., & Latham, R. E. (1993). Global patterns of diversity in mangrove floras. In *Species diversity in ecological communities: Historical and geographical perspectives.* University of Chicago Press.

Salmon, J., Holthuijsen, L., Zijlema, M., van Vledder, G. P., & Pietrzak, J. (2015). Scaling depth-induced wave-breaking in two-dimensional spectral wave models. *Ocean Modelling*, *87*, 30–47.

Sidik, F., Neil, D., & Lovelock, C. E. (2016). Effect of high sedimentation rates on surface sediment dynamics and mangrove growth in the porong river, indonesia. *Marine Pollution Bulletin*, *107*(1), 355–363.

Smith, T. J., Anderson, G. H., Balentine, K., Tiling, G., Ward, G. A., & Whelan, K. R. (2009). Cumulative impacts of hurricanes on florida mangrove ecosystems: sediment deposition, storm surges and vegetation. *Wetlands*, *29*(1), 24–34.

Spada, G. (2017). Glacial isostatic adjustment and contemporary sea level rise: An overview. *Integrative Study of the Mean Sea Level and Its Components*, 155–187.

Spalding, M., Kainuma, M., & Collins, L. (2010). *World atlas of mangroves*. Earthscan.

Terrados, J., Thampanya, U., Srichai, N., Kheowvongsri, P., Geertz-Hansen, O., Boromthanarath, S., ... Duarte, C. (1997). The effect of increased sediment accretion on the survival and growth of rhizophora apiculata seedlings. *Estuarine, Coastal and Shelf Science*, *45*(5), 697–701.

Thomas, N., Lucas, R., Bunting, P., Hardy, A., Rosenqvist, A., & Simard, M. (2017). Distribution and drivers of global mangrove forest change, 1996–2010. *PloS one*, *12*(6), e0179302.

Toffolon, M., Vignoli, G., & Tubino, M. (2006, 10). Relevant parameters and finite amplitude effects in estuarine hydrodynamics. *Copyright J. Geophys. Res*, *111*. doi: 10.1029/2005JC003104

Torfs, H., Mitchener, H., Huysentruyt, H., & Toorman, E. (1996). Settling and consolidation of mud/sand mixtures. *Coastal Engineering*, *29*(1-2), 27–45.

Van Maren, D. (n.d.). An introduction to cohesive sediment transport modelling. *OSS Deltares*.

Van Maren, D., & Winterwerp, J. (2013). The role of flow asymmetry and mud properties on tidal flat sedimentation. *Continental Shelf Research*, *60*, S71–S84.

Van Nes, E. H., Arani, B. M., Staal, A., van der Bolt, B., Flores, B. M., Bathiany, S., & Scheffer, M. (2016). What do you mean,'tipping point'? *Trends in ecology & evolution*, *31*(12), 902–904.

Van Rijn, L. C. (2020). Erodibility of mud–sand bed mixtures. *Journal of Hydraulic Engineering*, *146*(1), 04019050.

Van Santen, P., Augustinus, P., Janssen-Stelder, B., Quartel, S., & Tri, N. (2007). Sedimentation in an estuarine mangrove system. *Journal of Asian Earth Sciences*, *29*(4), 566–575.

Volvaiker, S. S., Vethamony, P., Bhaskaran, P. K., Pednekar, P., Jishad, M., & James, A. (2018). Wave energy dissipation in the mangrove vegetation off mumbai, india. *Ocean Science Discussions*, 1–18.

Winterwerp, J. (2002). On the flocculation and settling velocity of estuarine mud. *Continental shelf research*, *22*(9), 1339–1360.

Winterwerp, J., Albers, T., Anthony, E., Friess, D., Mancheño, A., Moseley, K., ... others (2020). Managing erosion of mangrove-mud coasts with permeable dams–lessons learned. *Ecological Engineering*, *158*, 106078.

Winterwerp, J., Erftemeijer, P., Suryadiputra, N., Van Eijk, P., & Zhang, L. (2013). Defining eco-morphodynamic requirements for rehabilitating eroding mangrove-mud coasts. *Wetlands*, *33*(3), 515–526.

Appendix A

Plots of sensitivity analysis

This appendix presents the plots for the sensitivity analysis, as described in chapter 2. The sensitivity analysis has been performed on a linear slope, with a tidal range of 0.8-1.5 m and waves with significant wave height 0.6 m. First, the quantitative simulations are presented in the form of cross-shore overviews. Afterwards, qualitative runs are presented, in the form of flow velocity and bed shear stress signals over time at MSL +0.0 m.

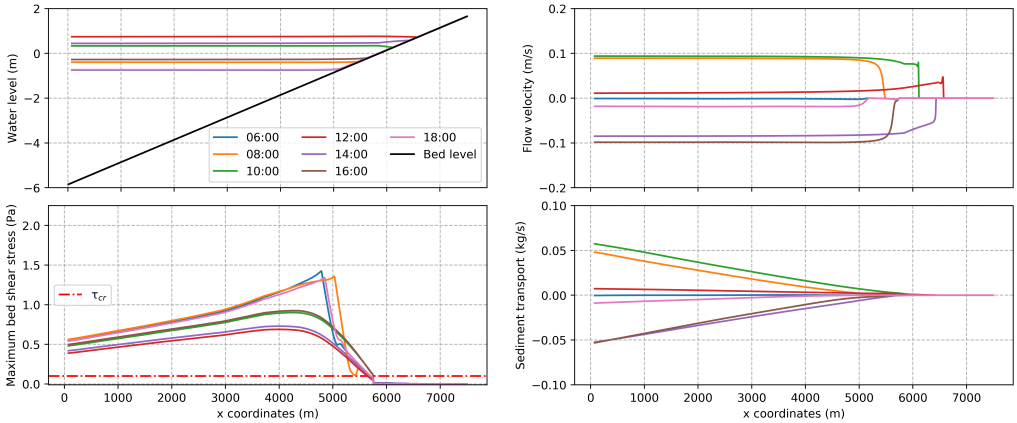

Figure A.1: Cross-shore overview of the model run using the parameters as used in this research. Tidal range of 0.8-1.5 m, significant wave height of 0.6 m, on a linear slope

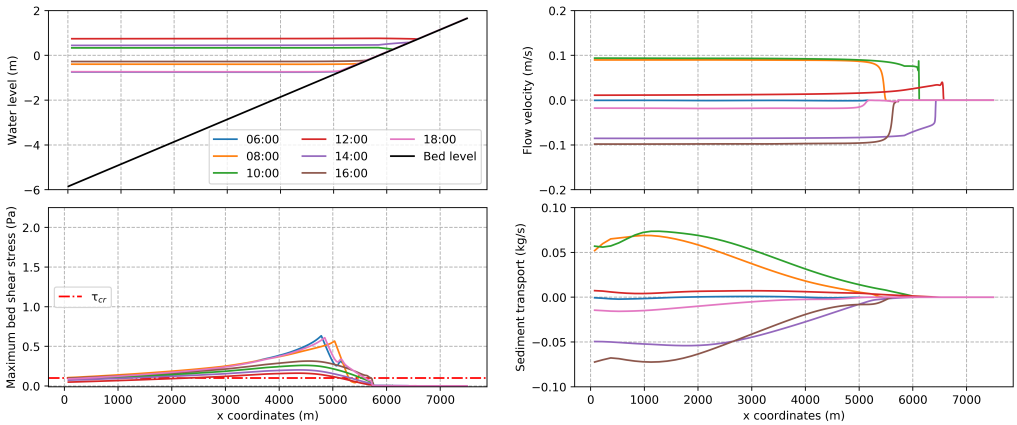

Figure A.2: Cross-shore overview of the model run using Chézy parameter of 90 $m^1/2/s$. Tidal range of 0.8-1.5 m, significant wave height of 0.6 m, on a linear slope

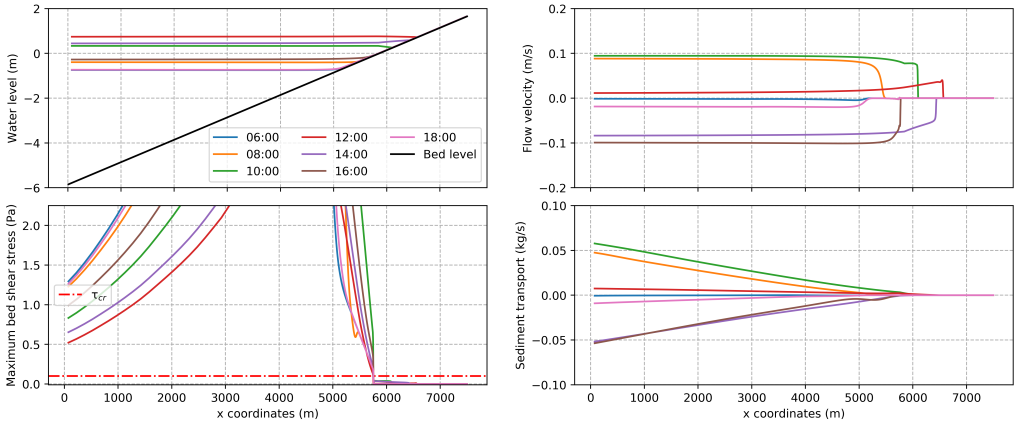

Figure A.3: Cross-shore overview of the model run using Chézy parameter of 40 $m^1/2/s$. Tidal range of 0.8-1.5 m, significant wave height of 0.6 m, on a linear slope

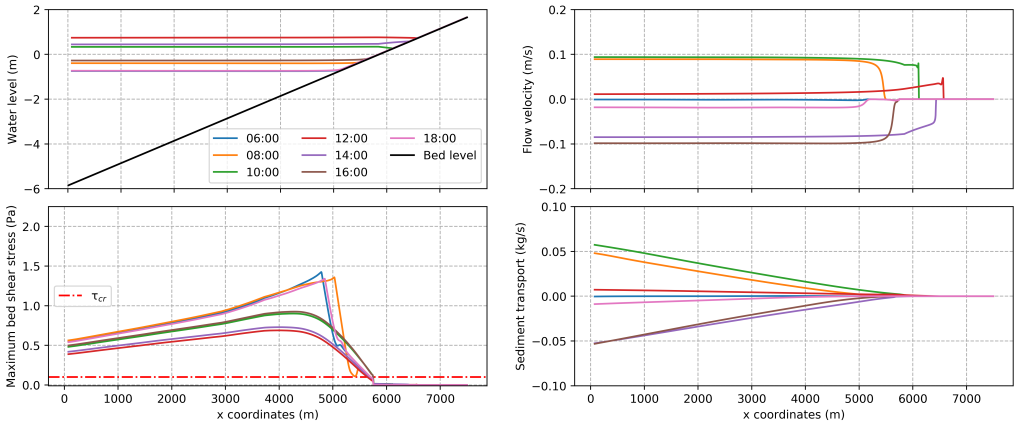

Figure A.4: Cross-shore overview of the model run using erosion parameter of 0.1 $kg/m^2/s$. Tidal range of 0.8-1.5 m, significant wave height of 0.6 m, on a linear slope

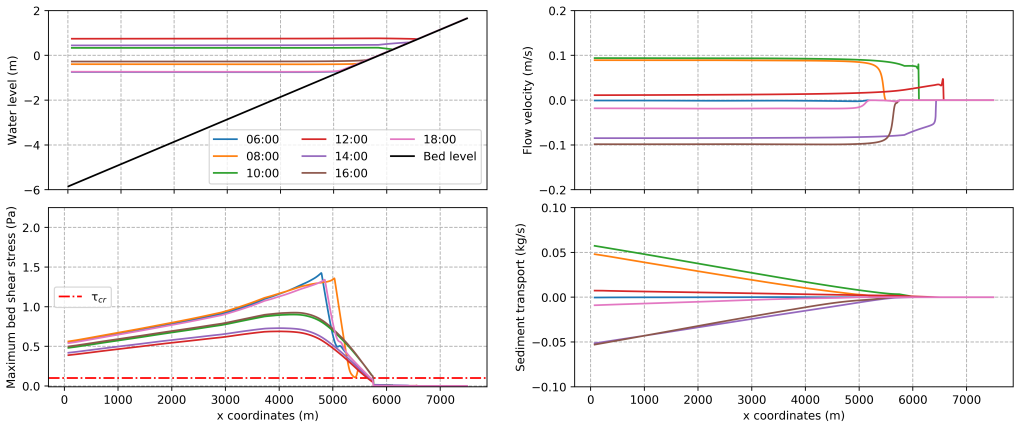

Figure A.5: Cross-shore overview of the model run using erosion parameter of 0.001 kg/m^2/s. Tidal range of 0.8-1.5 m, significant wave height of 0.6 m, on a linear slope

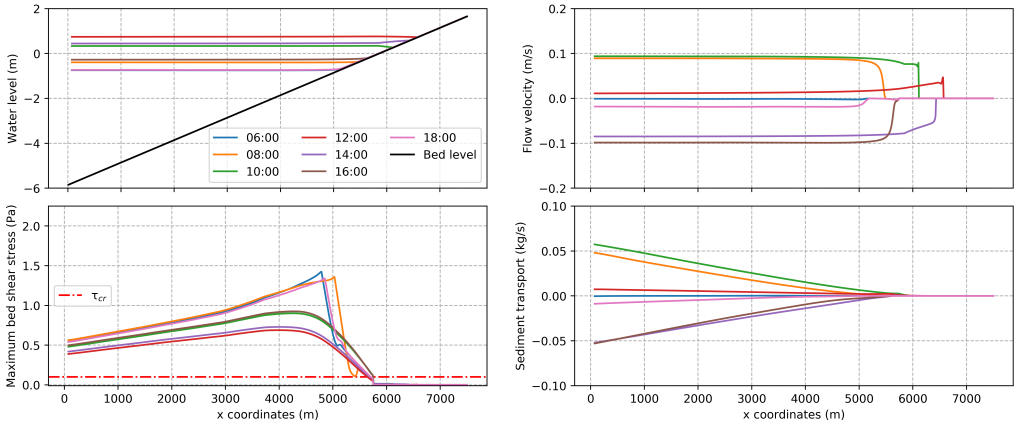

Figure A.6: Cross-shore overview of the model run using erosion parameter of 0.5 mm/s. Tidal range of 0.8-1.5 m, significant wave height of 0.6 m, on a linear slope

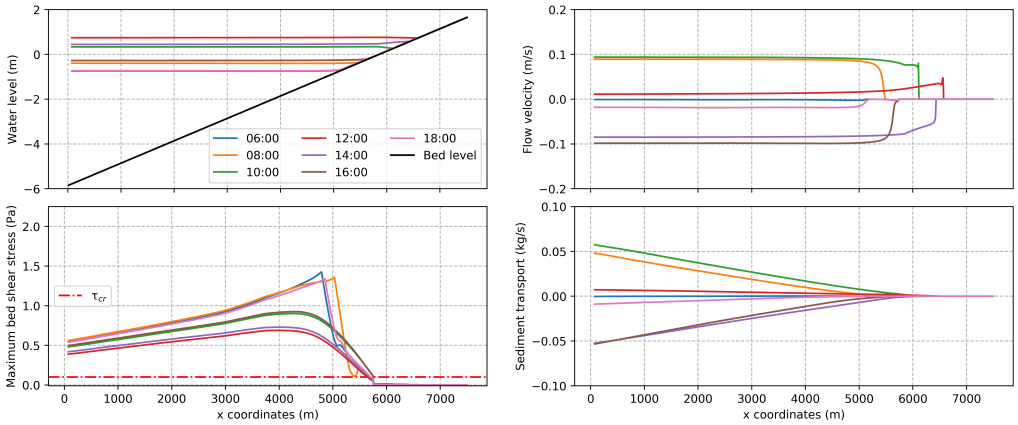

Figure A.7: Cross-shore overview of the model run using erosion parameter of 0.05 mm/s. Tidal range of 0.8-1.5 m, significant wave height of 0.6 m, on a linear slope

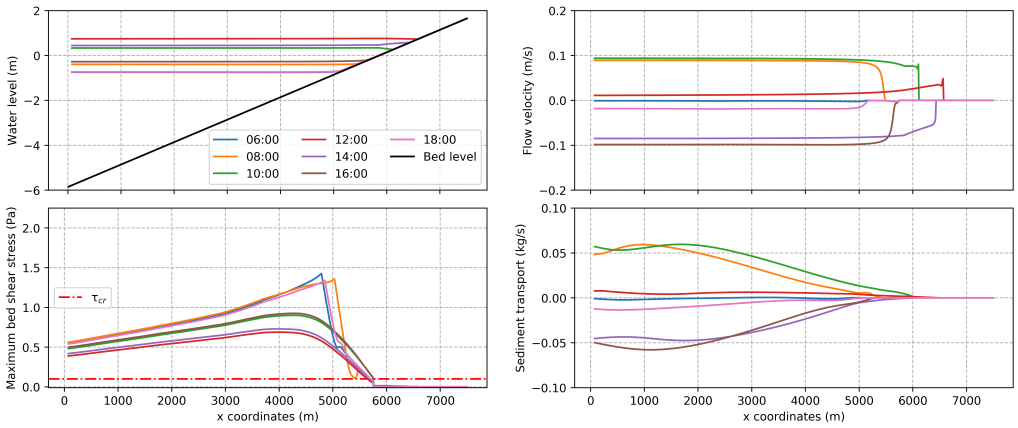

Figure A.8: Cross-shore overview of the model run using a critical bed shear stress of 0.5 Pa. Tidal range of 0.8-1.5 m, significant wave height of 0.6 m, on a linear slope

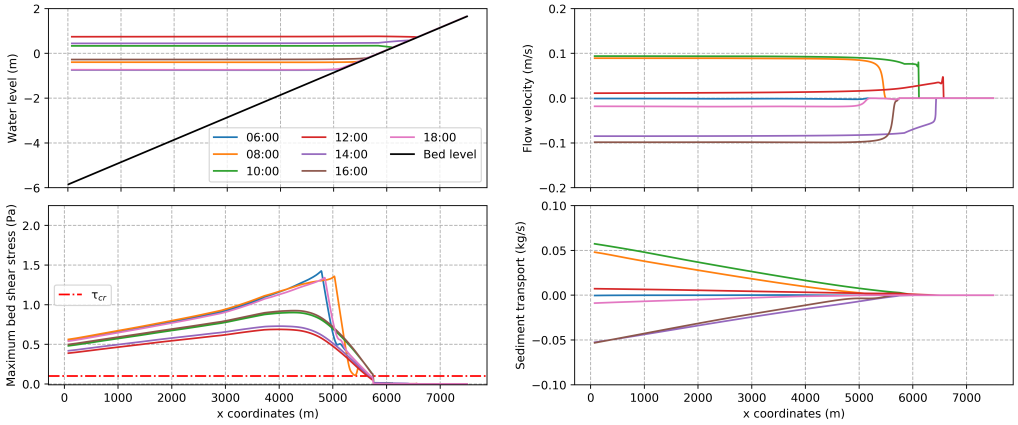

Figure A.9: Cross-shore overview of the model run using a critical bed shear stress of 0.05 Pa. Tidal range of 0.8-1.5 m, significant wave height of 0.6 m, on a linear slope

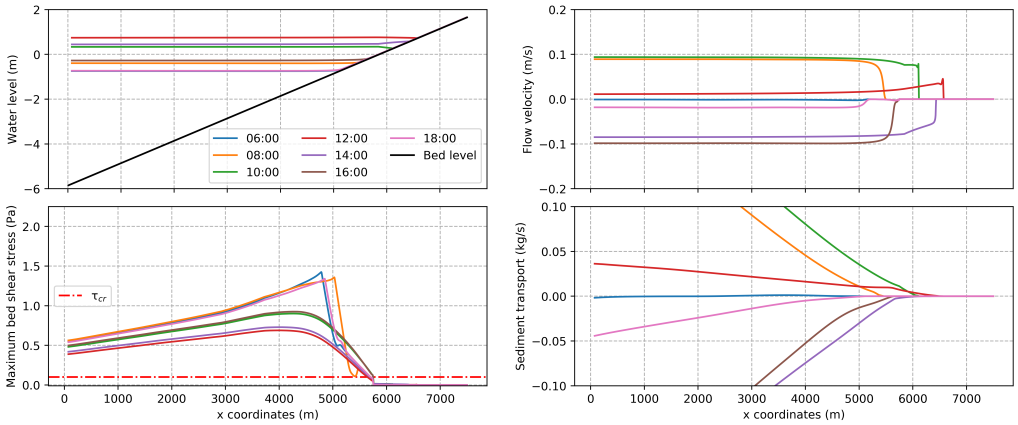

Figure A.10: Cross-shore overview of the model run using a sediment boundary concentration of 0.5 kg/m^3. Tidal range of 0.8-1.5 m, significant wave height of 0.6 m, on a linear slope

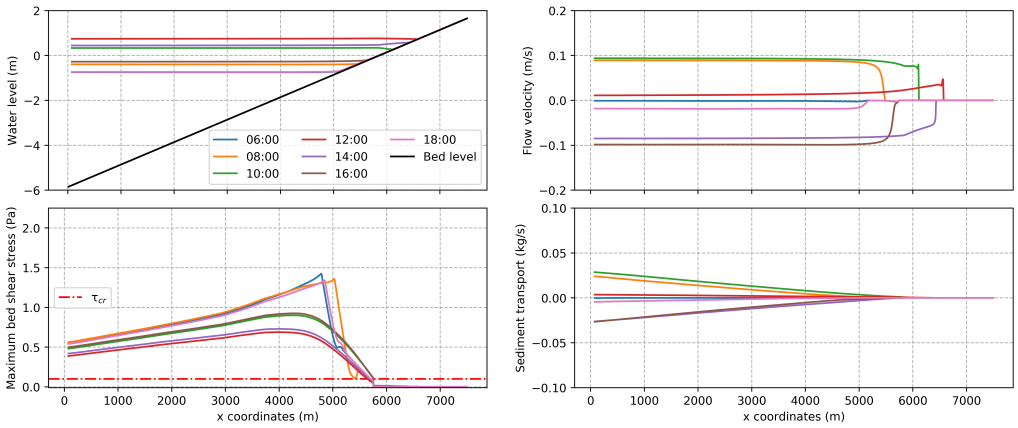

Figure A.11: Cross-shore overview of the model run using a sediment boundary concentration of 0.05 kg/m^3. Tidal range of 0.8-1.5 m, significant wave height of 0.6 m, on a linear slope

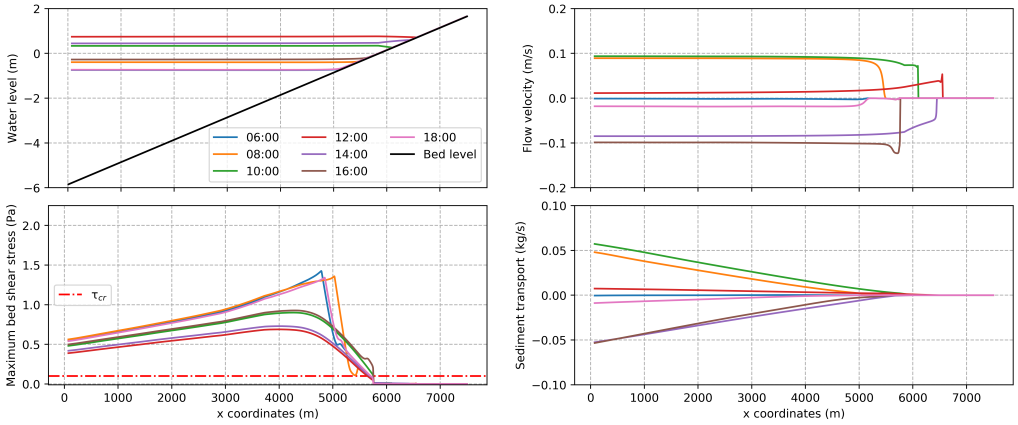

Figure A.12: Cross-shore overview of the model run using a root drag coefficient of 0.9. Tidal range of 0.8-1.5 m, significant wave height of 0.6 m, on a linear slope

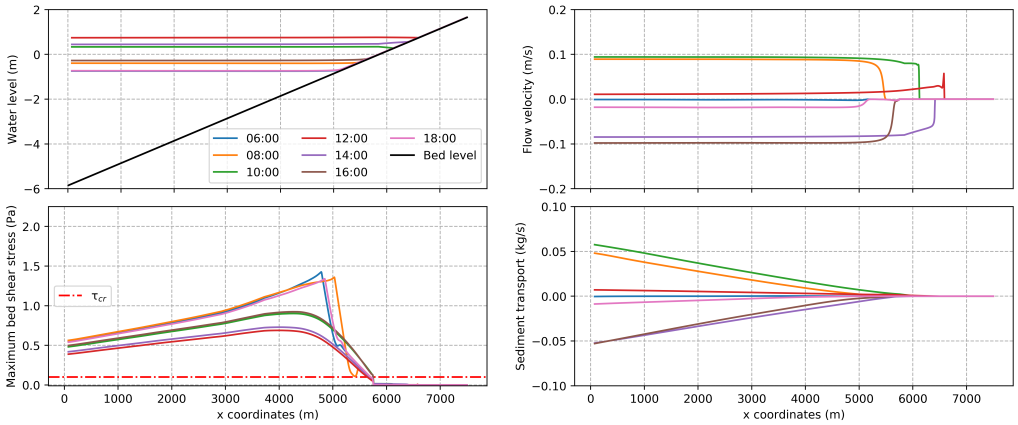

Figure A.13: Cross-shore overview of the model run using a root drag coefficient of 0.5. Tidal range of 0.8-1.5 m, significant wave height of 0.6 m, on a linear slope

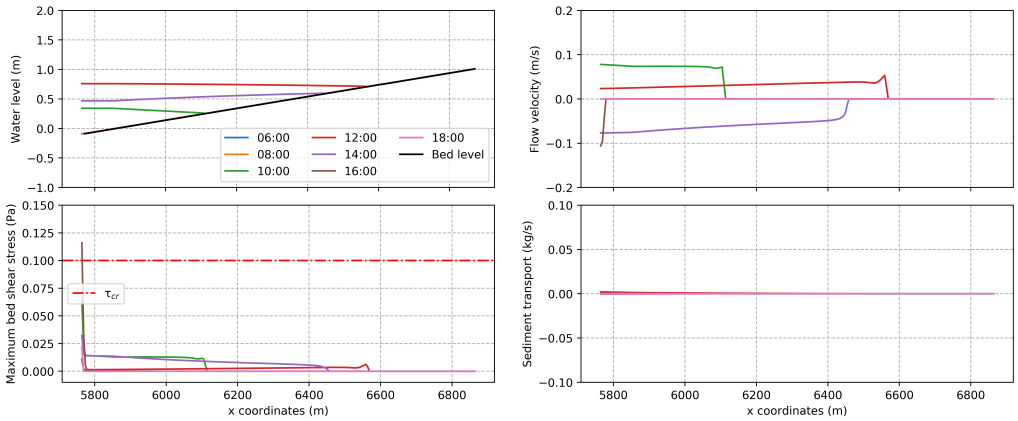

Figure A.14: Cross-shore overview, zoomed within the intertidal, of the model run using a root drag coefficient of 0.9. Tidal range of 0.8-1.5 m, significant wave height of 0.6 m, on a linear slope

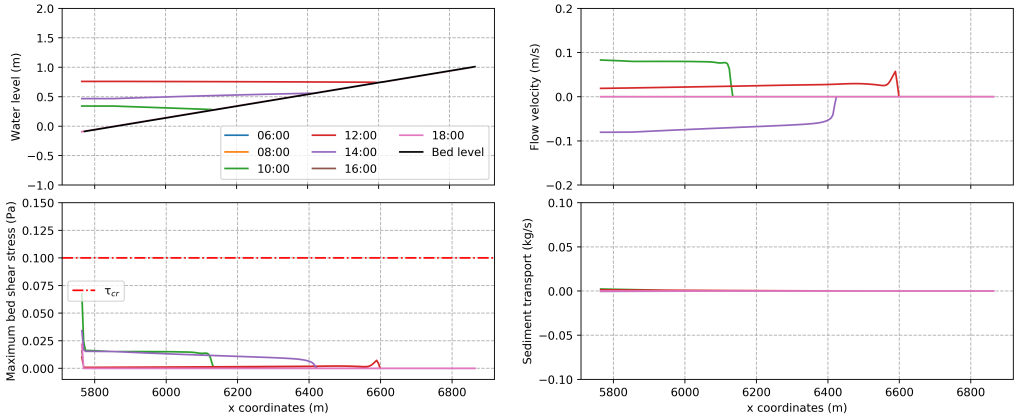

Figure A.15: Cross-shore overview, zoomed within the intertidal, of the model run using a root drag coefficient of 0.5. Tidal range of 0.8-1.5 m, significant wave height of 0.6 m, on a linear slope

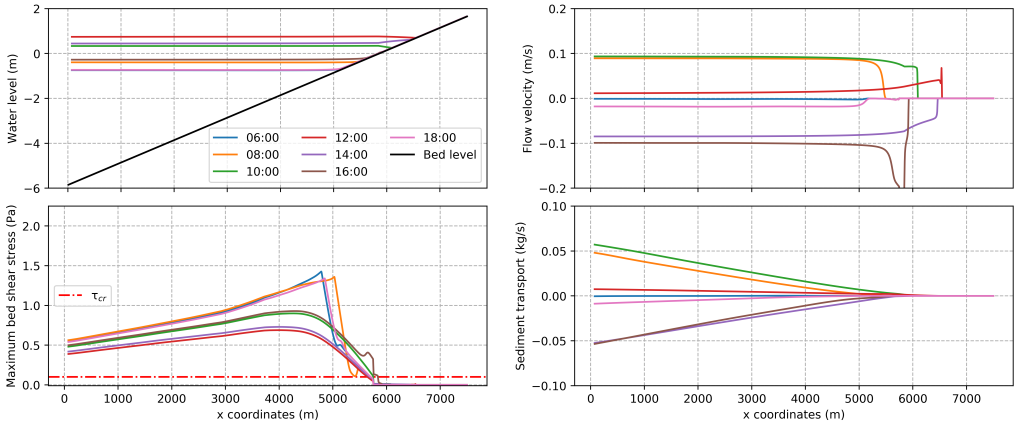

Figure A.16: Cross-shore overview of the model run using a root density of 200 roots/m^2. Tidal range of 0.8-1.5 m, significant wave height of 0.6 m, on a linear slope

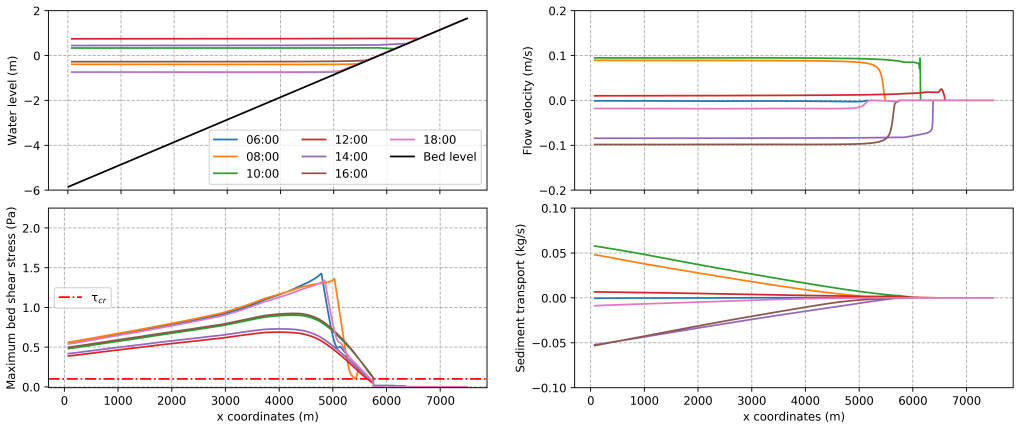

Figure A.17: Cross-shore overview of the model run using a root density of 50 roots/m^2. Tidal range of 0.8-1.5 m, significant wave height of 0.6 m, on a linear slope

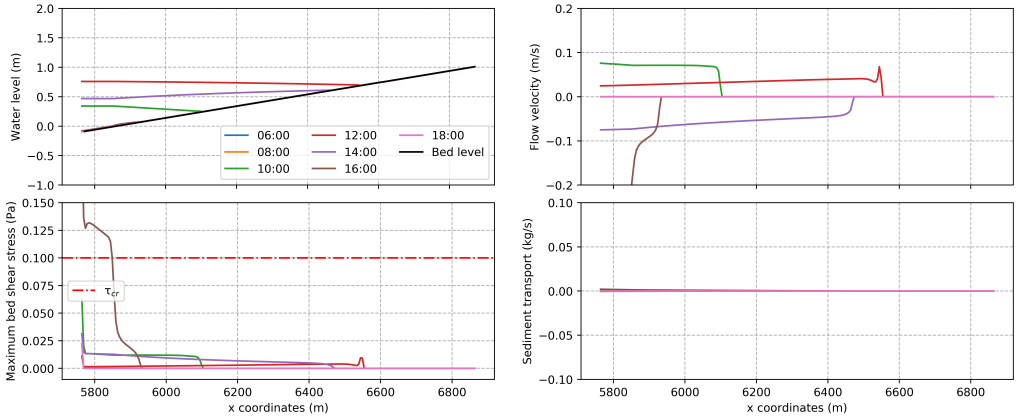

Figure A.18: Cross-shore overview, zoomed in the intertidal, of the model run using a root density of 200 roots/m^2. Tidal range of 0.8-1.5 m, significant wave height of 0.6 m, on a linear slope

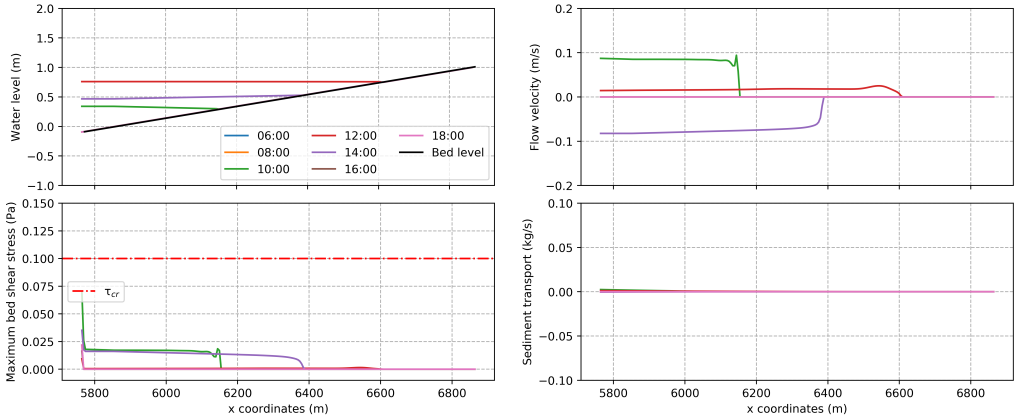

Figure A.19: Cross-shore overview, zoomed in the intertidal, of the model run using a root density of 50 roots/m^2. Tidal range of 0.8-1.5 m, significant wave height of 0.6 m, on a linear slope

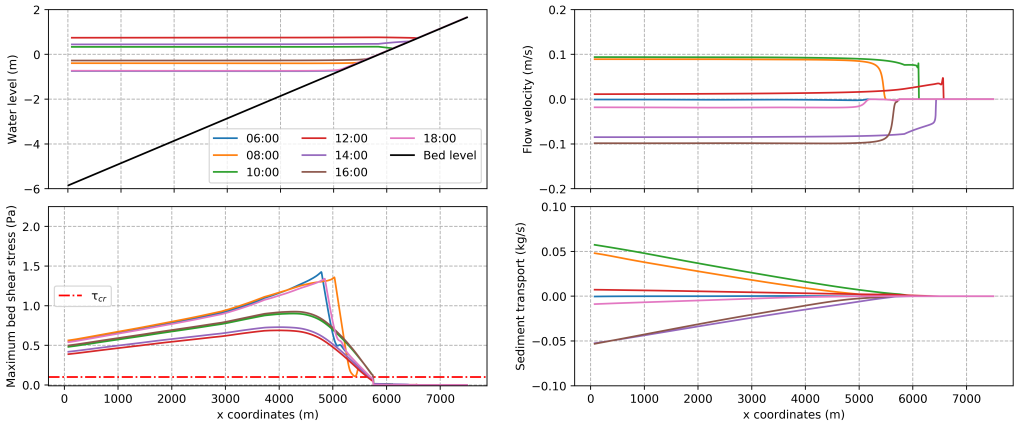

Figure A.20: Cross-shore overview of the model run using a stem density of 1.0 stem/m^2. Tidal range of 0.8-1.5 m, significant wave height of 0.6 m, on a linear slope

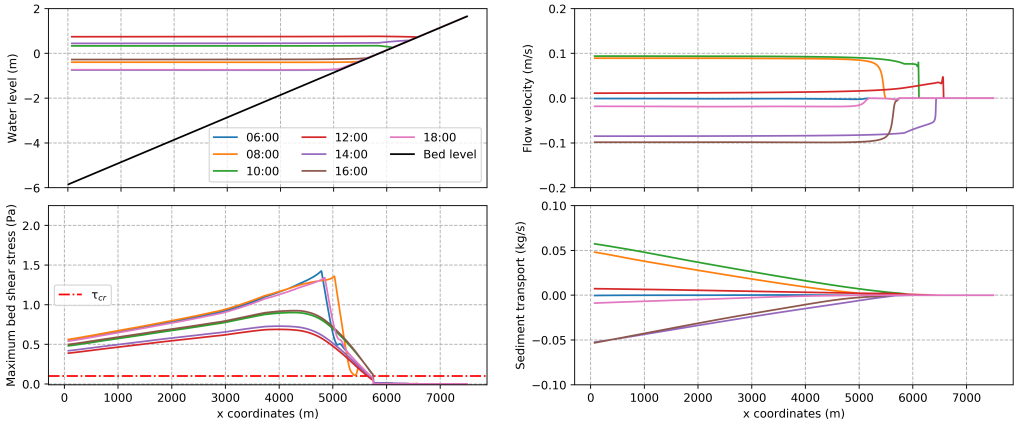

Figure A.21: Cross-shore overview of the model run using a stem density of 0.33 stem/m^2. Tidal range of 0.8-1.5 m, significant wave height of 0.6 m, on a linear slope

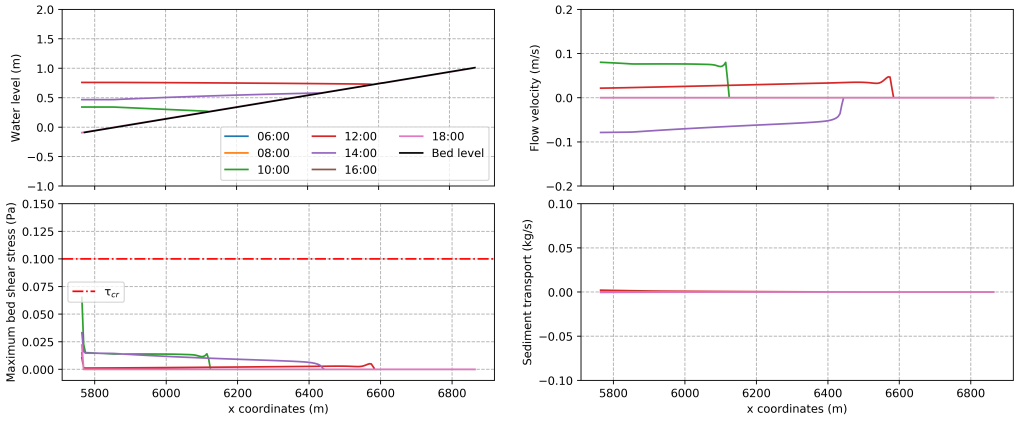

Figure A.22: Cross-shore overview, zoomed in the intertidal, of the model run using a stem density of 1.0 stem/m^2. Tidal range of 0.8-1.5 m, significant wave height of 0.6 m, on a linear slope

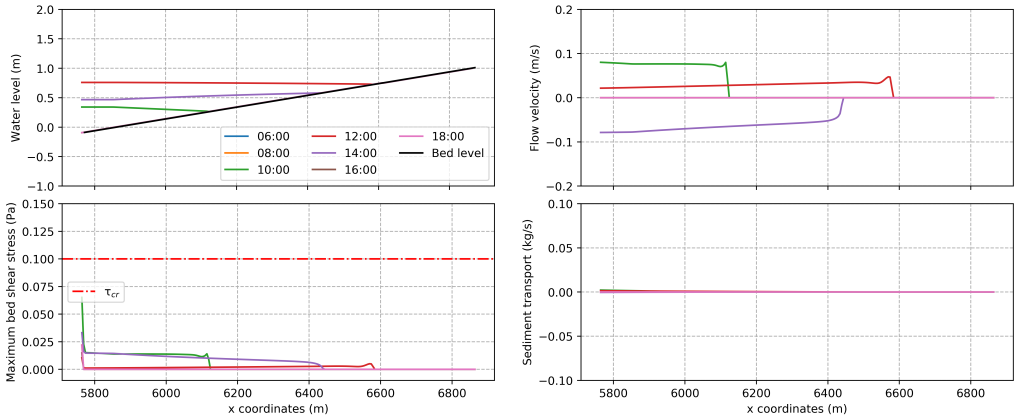

Figure A.23: Cross-shore overview, zoomed in the intertidal, of the model run using a stem density of 0.33 stem/m^2. Tidal range of 0.8-1.5 m, significant wave height of 0.6 m, on a linear slope

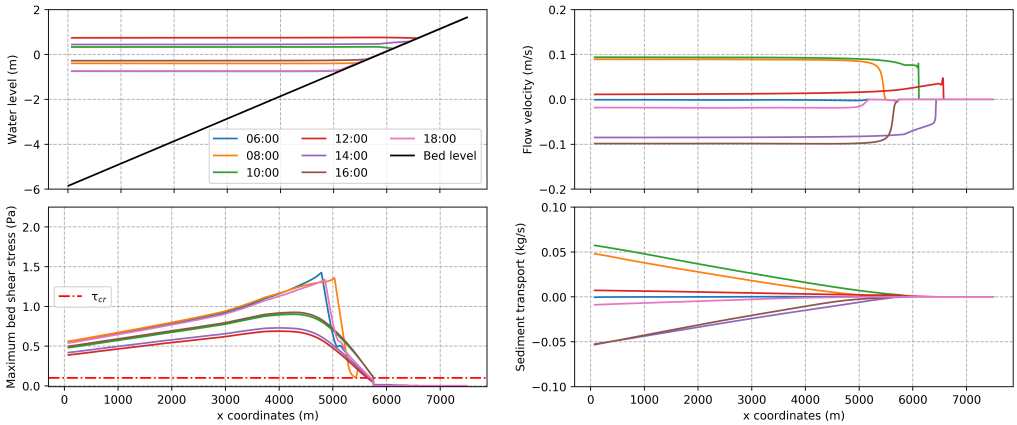

Figure A.24: Cross-shore overview of the model run using a stem drag coefficient of 1.2. Tidal range of 0.8-1.5 m, significant wave height of 0.6 m, on a linear slope

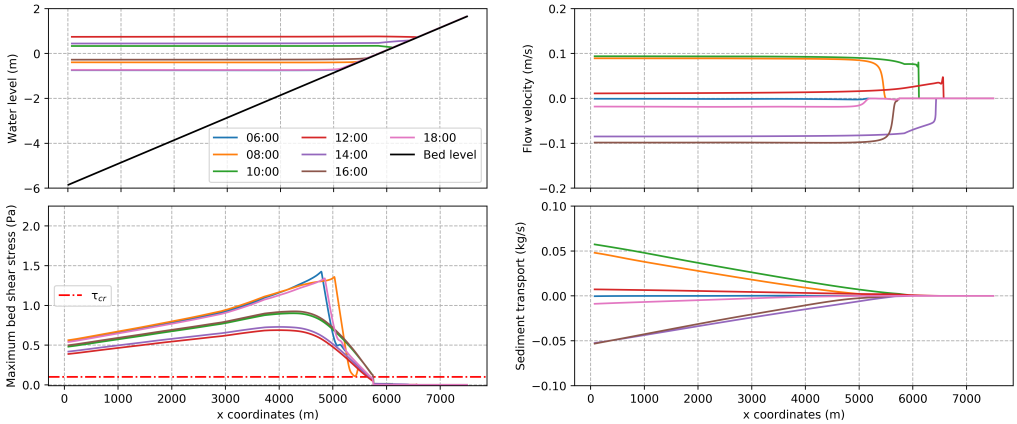

Figure A.25: Cross-shore overview of the model run using a stem drag coefficient of 0.8. Tidal range of 0.8-1.5 m, significant wave height of 0.6 m, on a linear slope

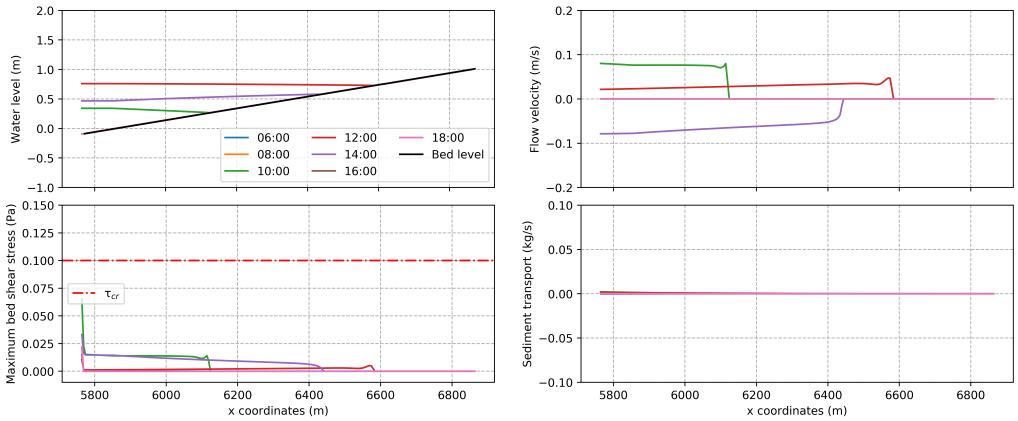

Figure A.26: Cross-shore overview, zoomed in the intertidal, of the model run using a stem drag coefficient of 1.2. Tidal range of 0.8-1.5 m, significant wave height of 0.6 m, on a linear slope

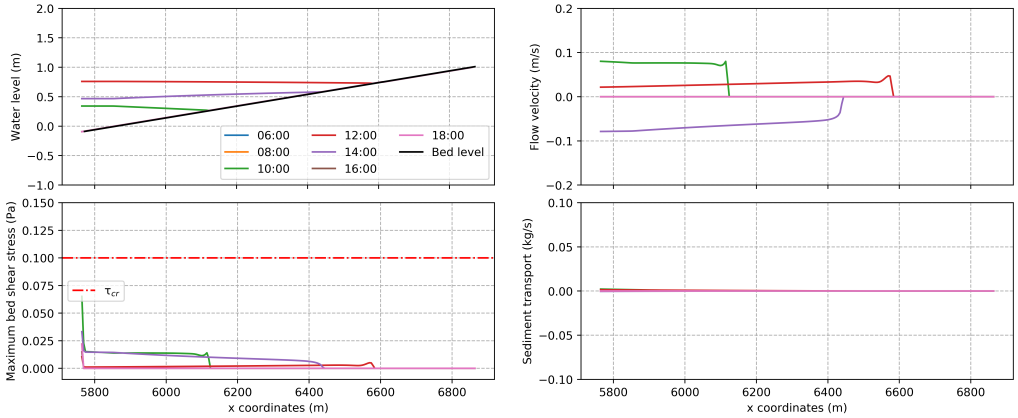

Figure A.27: Cross-shore overview, zoomed in the intertidal, of the model run using a stem drag coefficient of 0.8. Tidal range of 0.8-1.5 m, significant wave height of 0.6 m, on a linear slope

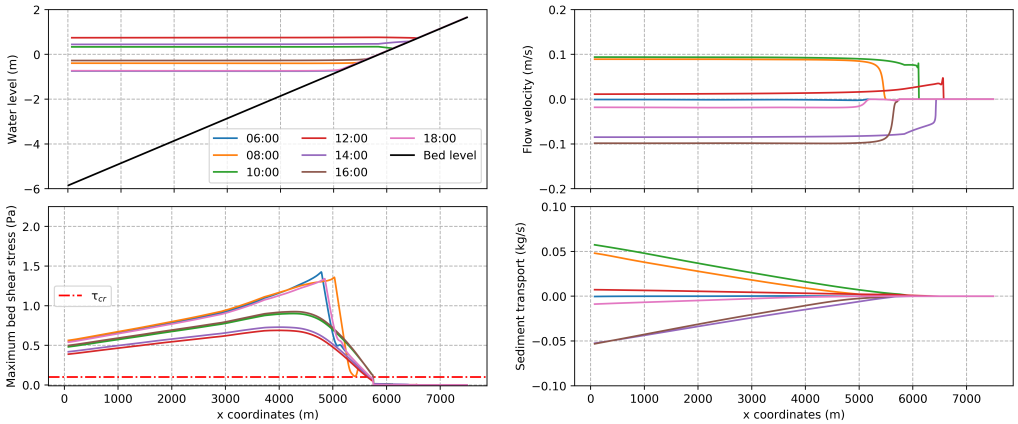

Figure A.28: Cross-shore overview of the model run using a stem diameter of 0.4 m. Tidal range of 0.8-1.5 m, significant wave height of 0.6 m, on a linear slope

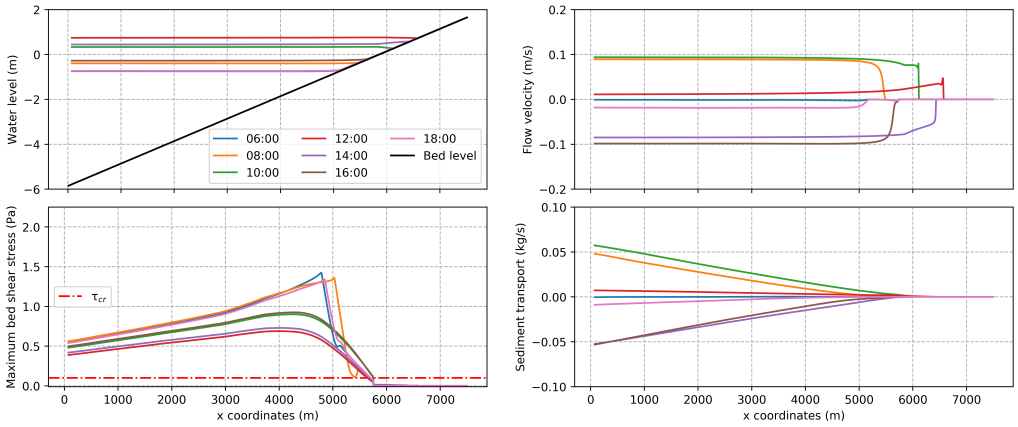

Figure A.29: Cross-shore overview of the model run using a stem diameter of 0.1 m. Tidal range of 0.8-1.5 m, significant wave height of 0.6 m, on a linear slope

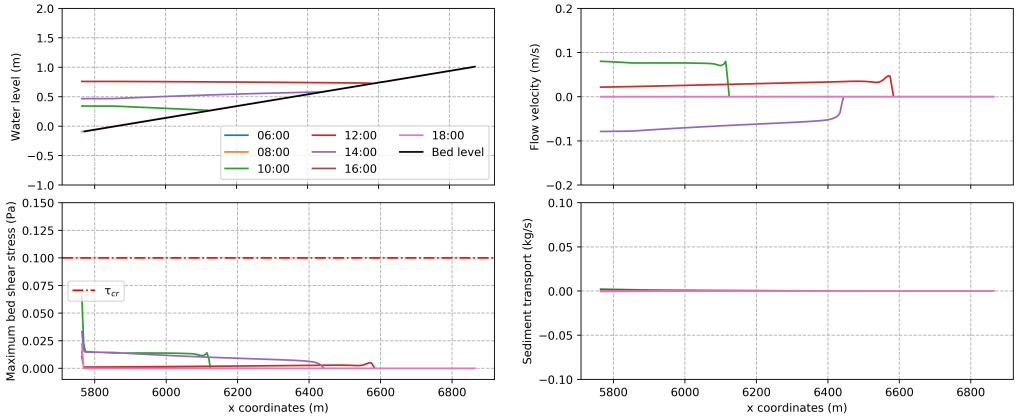

Figure A.30: Cross-shore overview, zoomed in the intertidal, of the model run using a stem diameter of 0.4 m. Tidal range of 0.8-1.5 m, significant wave height of 0.6 m, on a linear slope

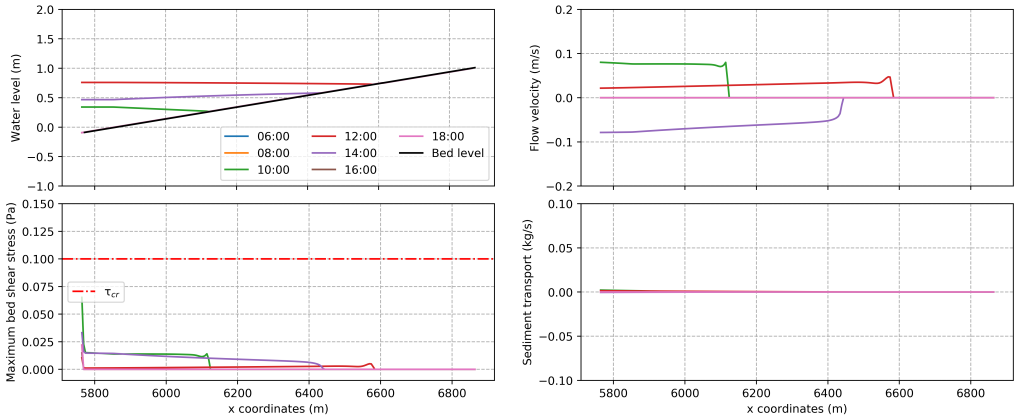

Figure A.31: Cross-shore overview, zoomed in the intertidal, of the model run using a stem diameter of 0.1 m. Tidal range of 0.8-1.5 m, significant wave height of 0.6 m, on a linear slope

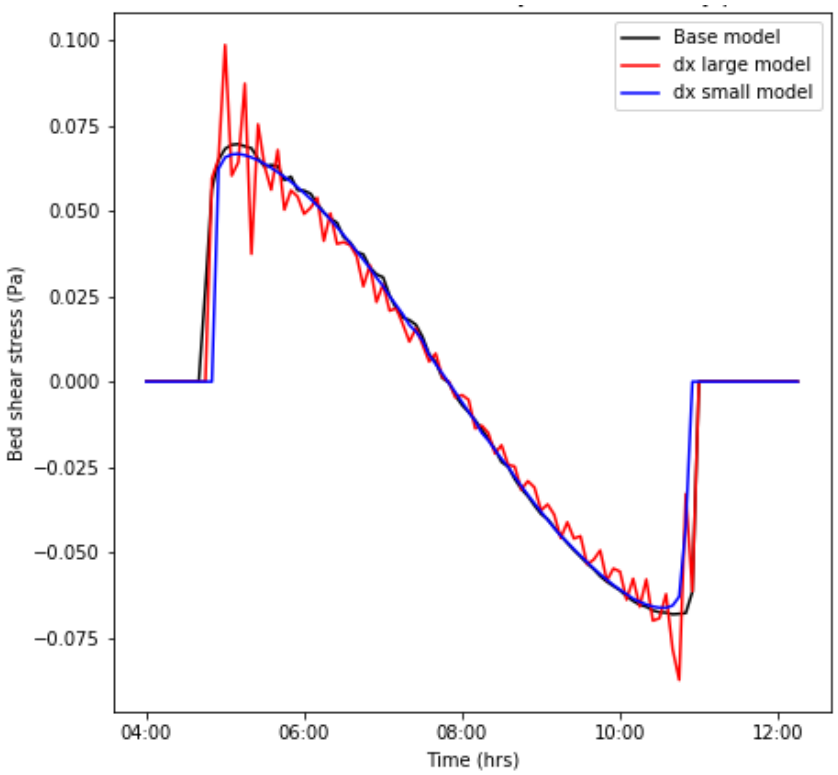

Figure A.32: Flow velocity signal at +0.0 m, for varying grid dimension in the x-direction

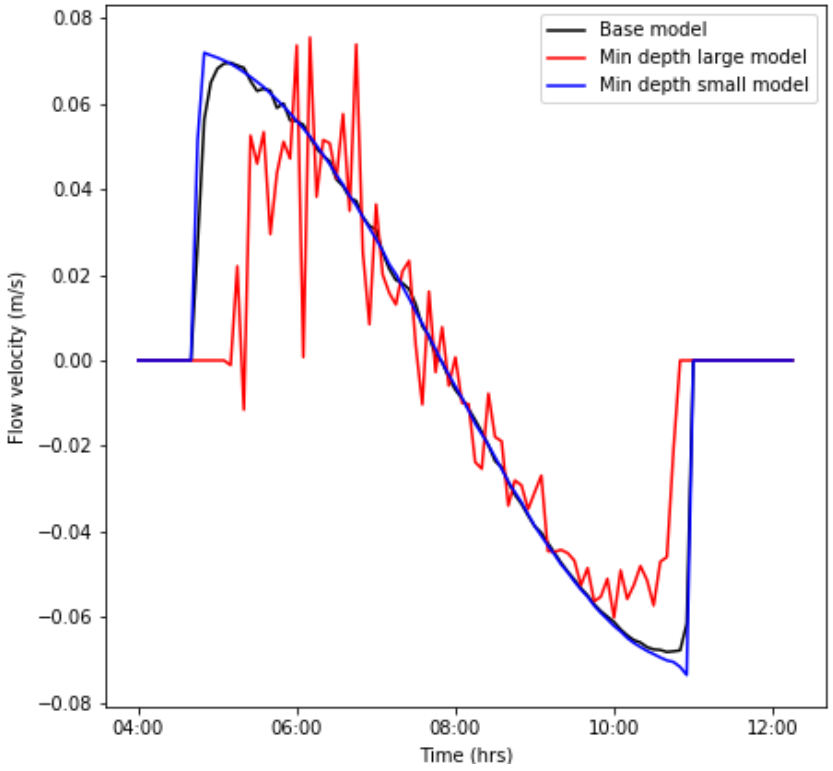

Figure A.33: Flow velocity signal at +0.0 m, for varying minimum depths for flow calculations

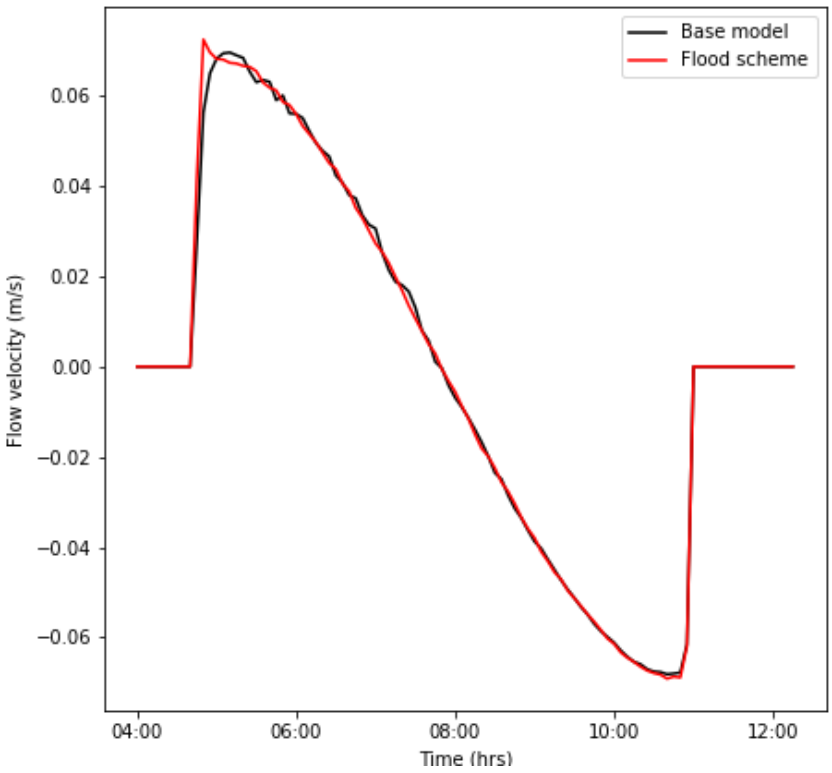

Figure A.34: Flow velocity signal at +0.0 m, for flow and cyclic advection schemes

Appendix B

Plots of process analysis model simulations

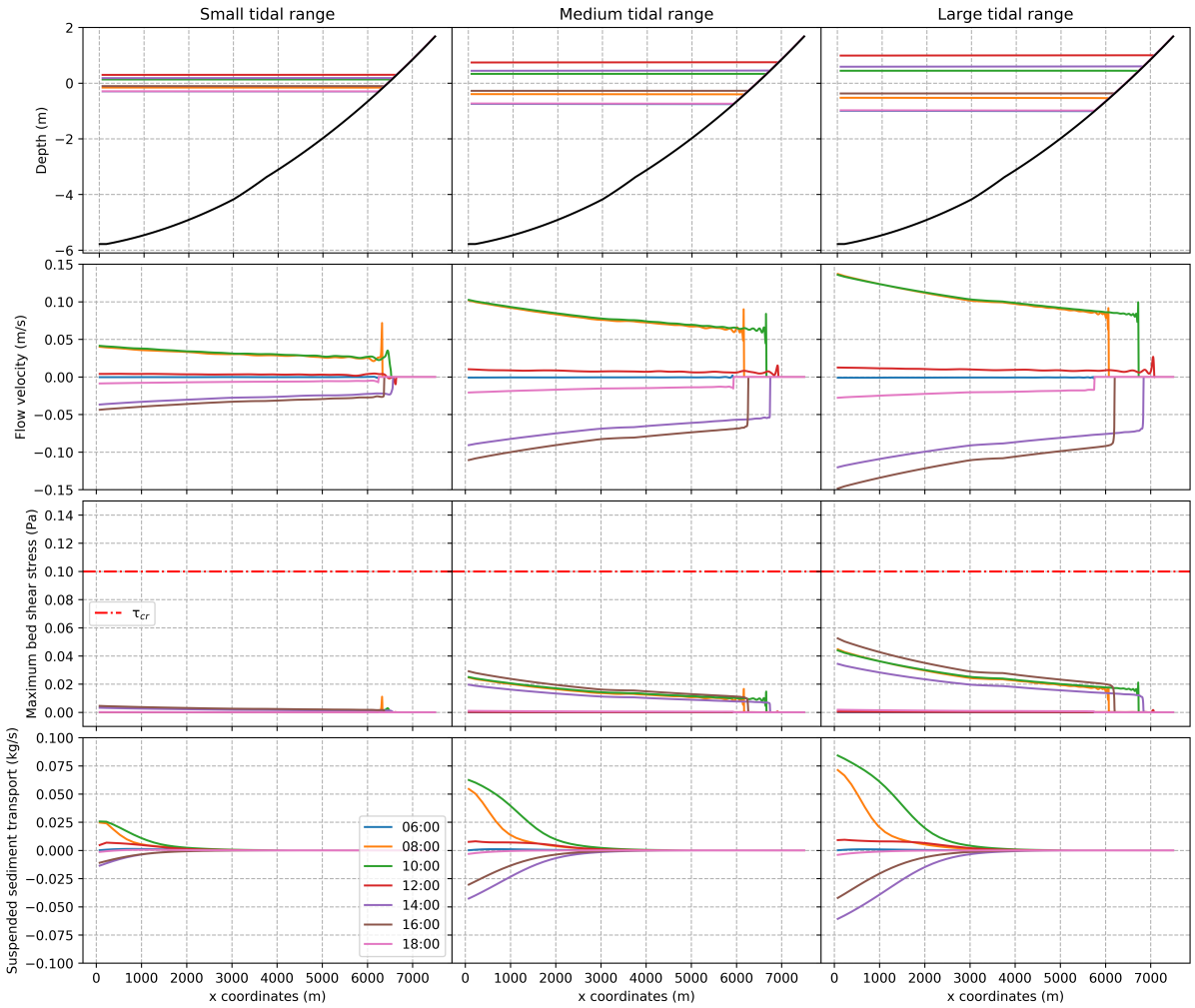

Figure B.1: Cross-shore overview of concave bottom profile, with all tidal ranges, snapshots in time during spring tide. No waves, nor mangroves.

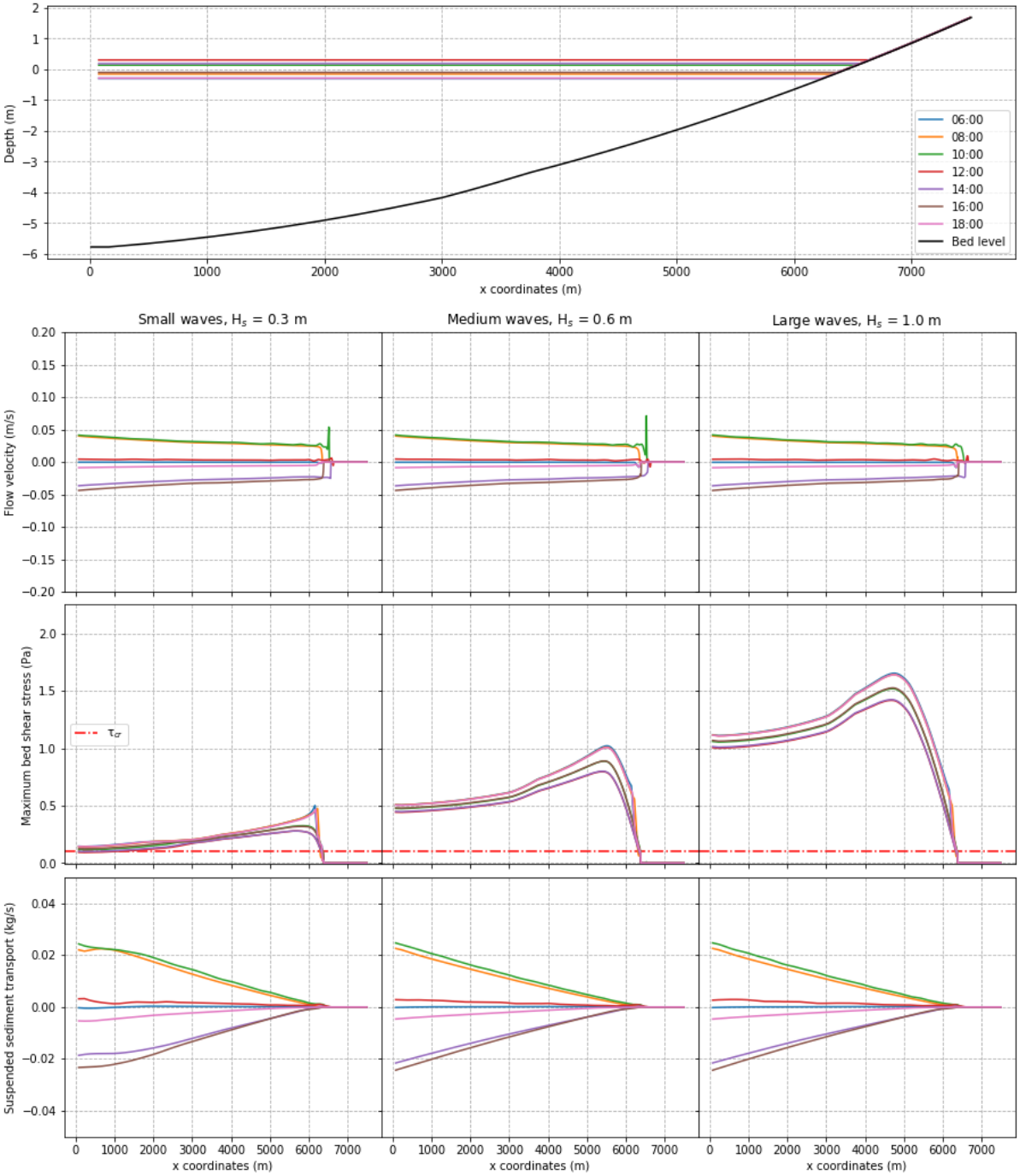

Figure B.2: Cross-shore overview of tide and wave simulation, tidal range 0.4-0.6 m. Concave bottom profile, snapshots in time during spring tide.

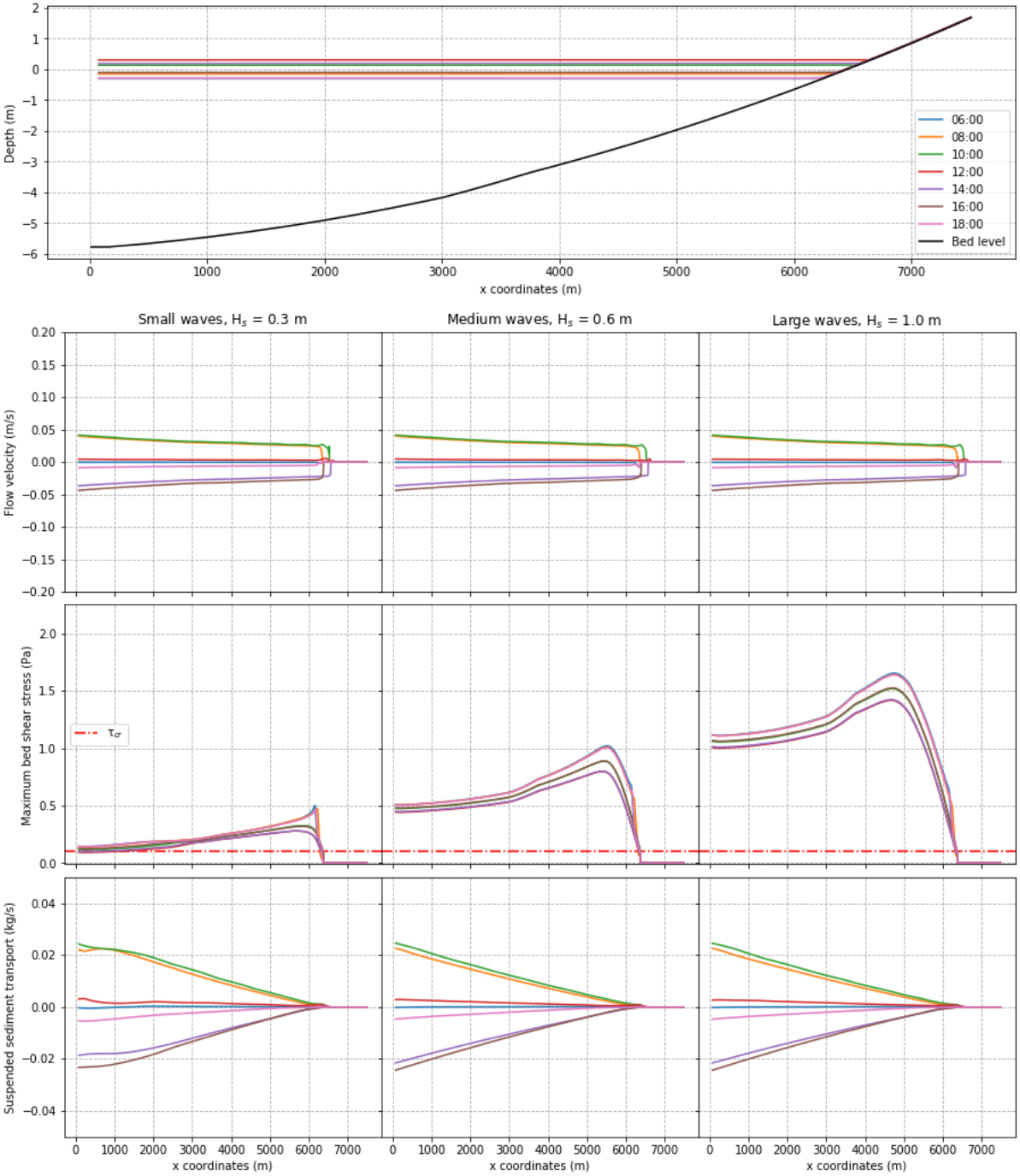

Figure B.3: Cross-shore overview of mangroves simulation, tidal range 0.4-0.6 m. Concave bottom profile, snapshots in time during spring tide.

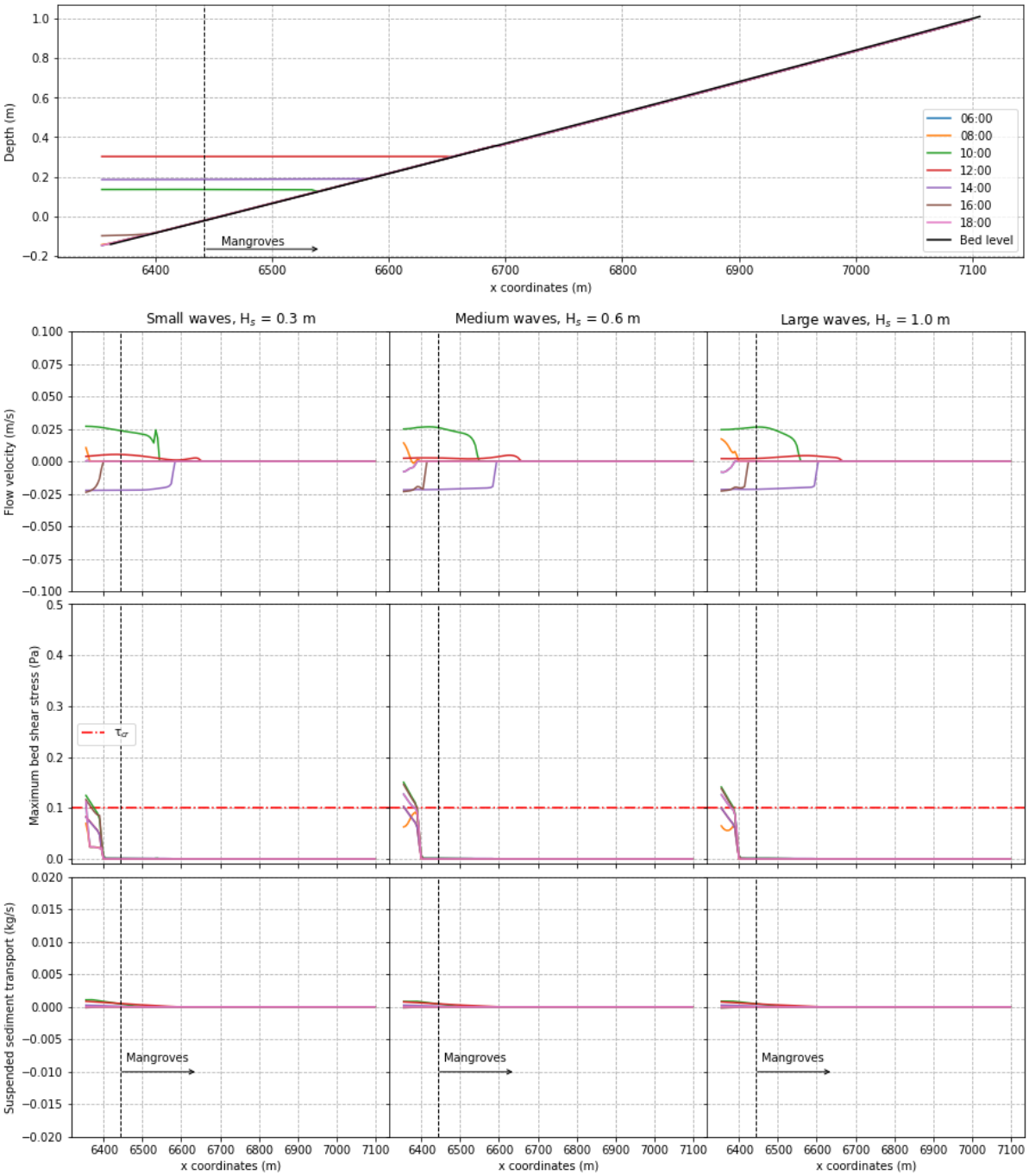

Figure B.4: Cross-shore overview of mangroves simulation, tidal range 0.4-0.6 m. Concave bottom profile, snapshots in time during spring tide, zoomed in on the intertidal

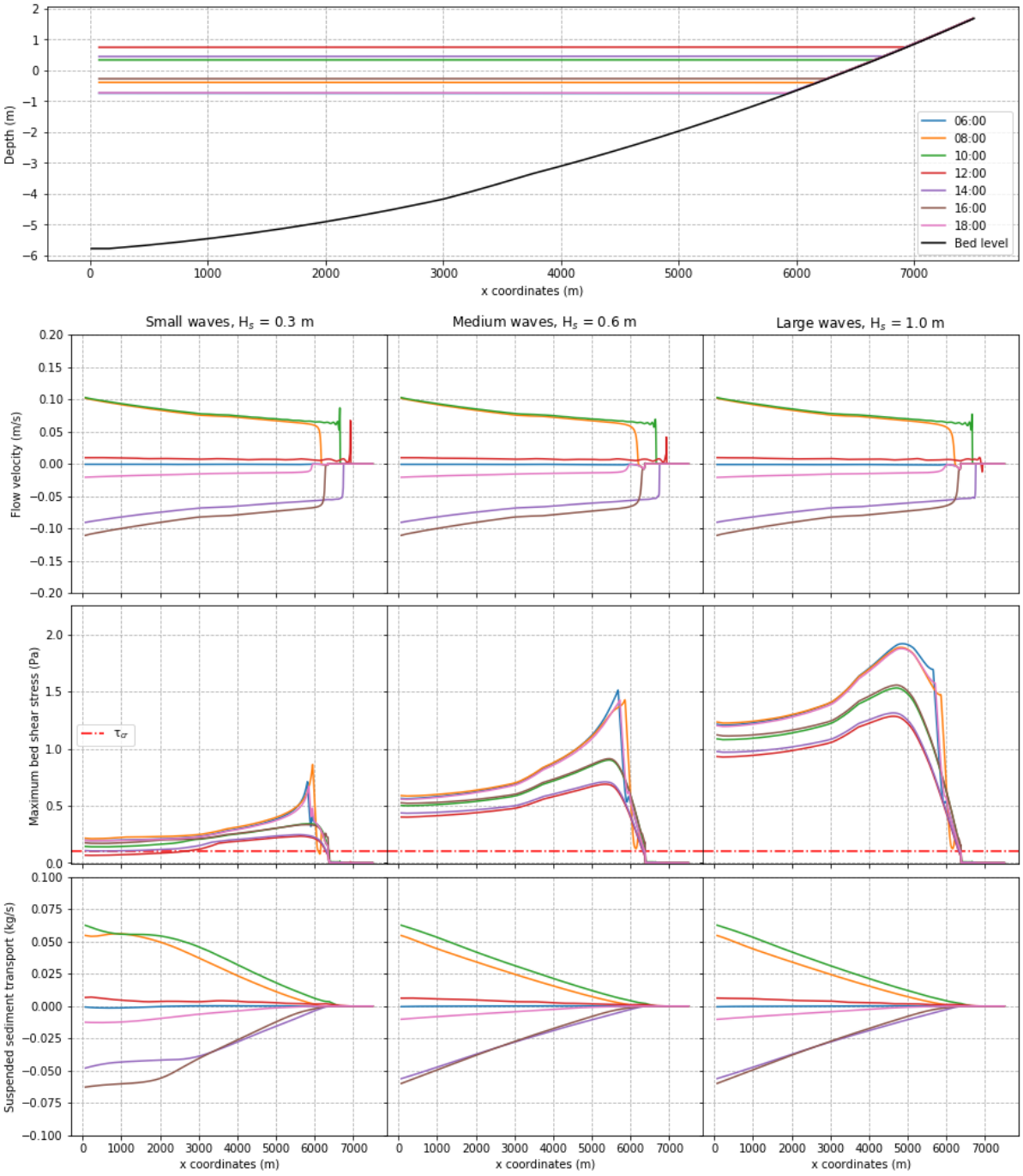

Figure B.5: Cross-shore overview of tide and wave simulation, tidal range 0.8-1.5 m. Concave bottom profile, snapshots in time during spring tide.

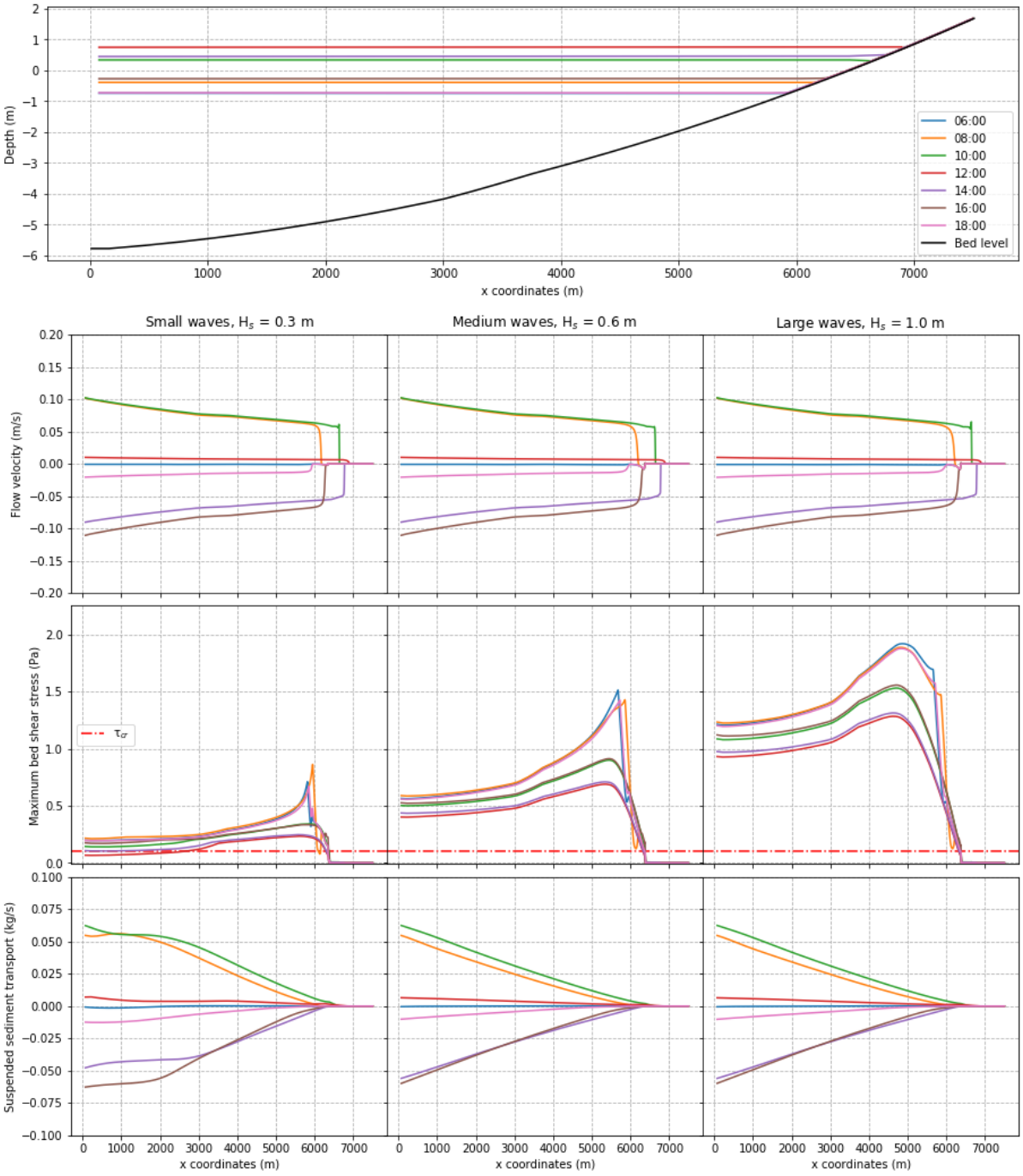

Figure B.6: Cross-shore overview of mangroves simulation, tidal range 0.8-1.5 m. Concave bottom profile, snapshots in time during spring tide.

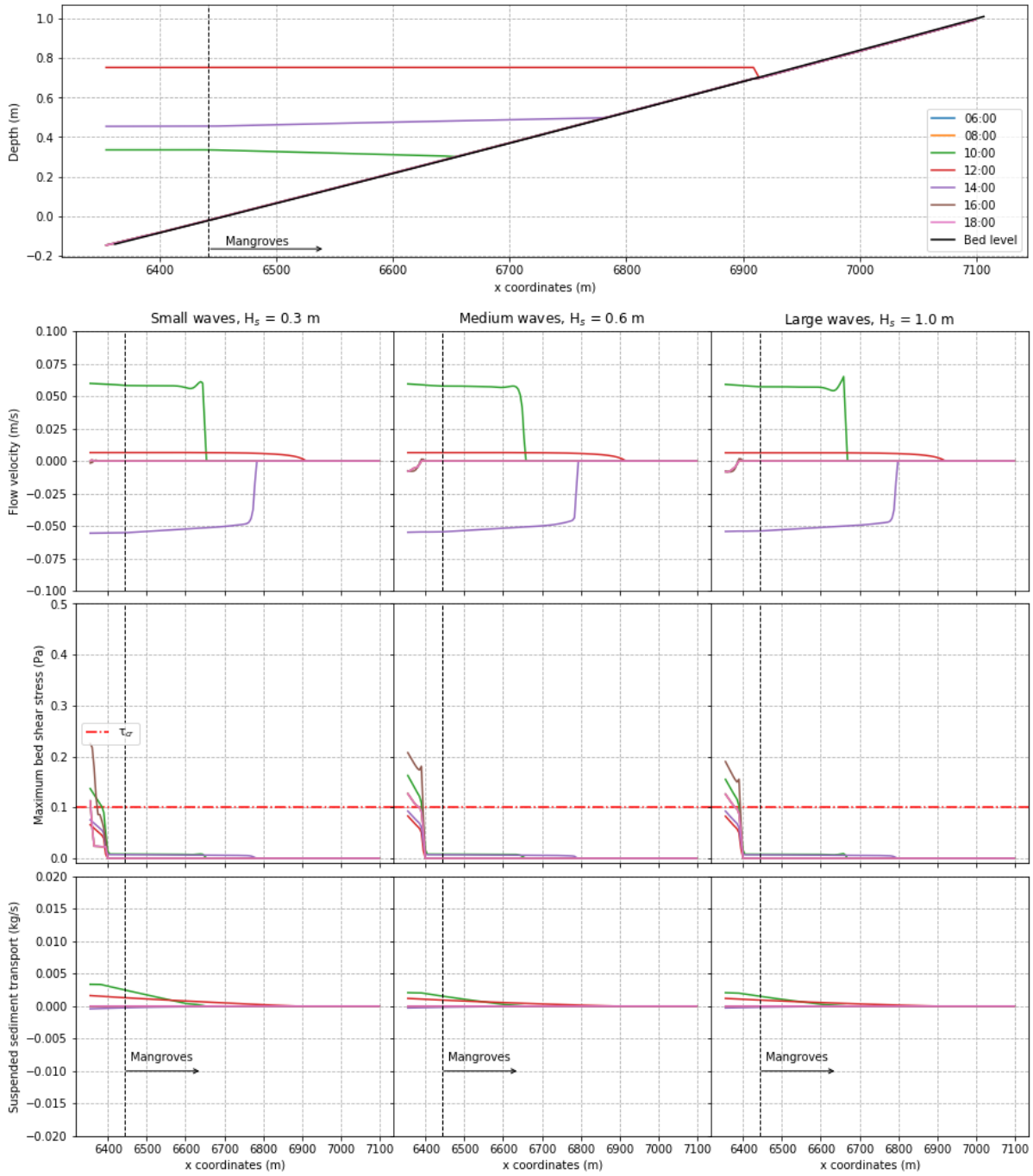

Figure B.7: Cross-shore overview of mangroves simulation, tidal range 0.8-1.5 m. Concave bottom profile, snapshots in time during spring tide, zoomed in on the intertidal

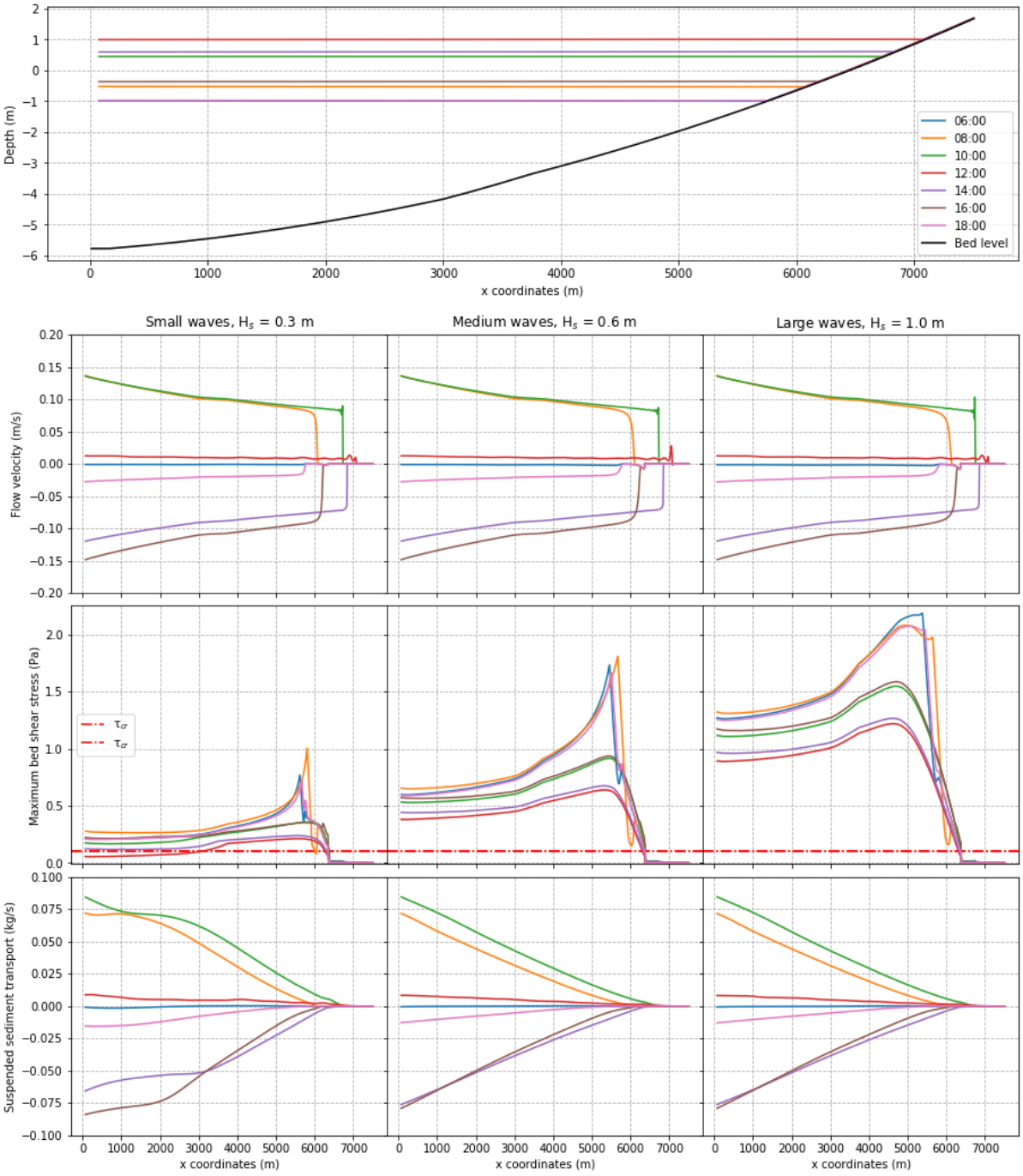

Figure B.8: Cross-shore overview of tide and wave simulation, tidal range 1.0-2.0 m. Concave bottom profile, snapshots in time during spring tide.

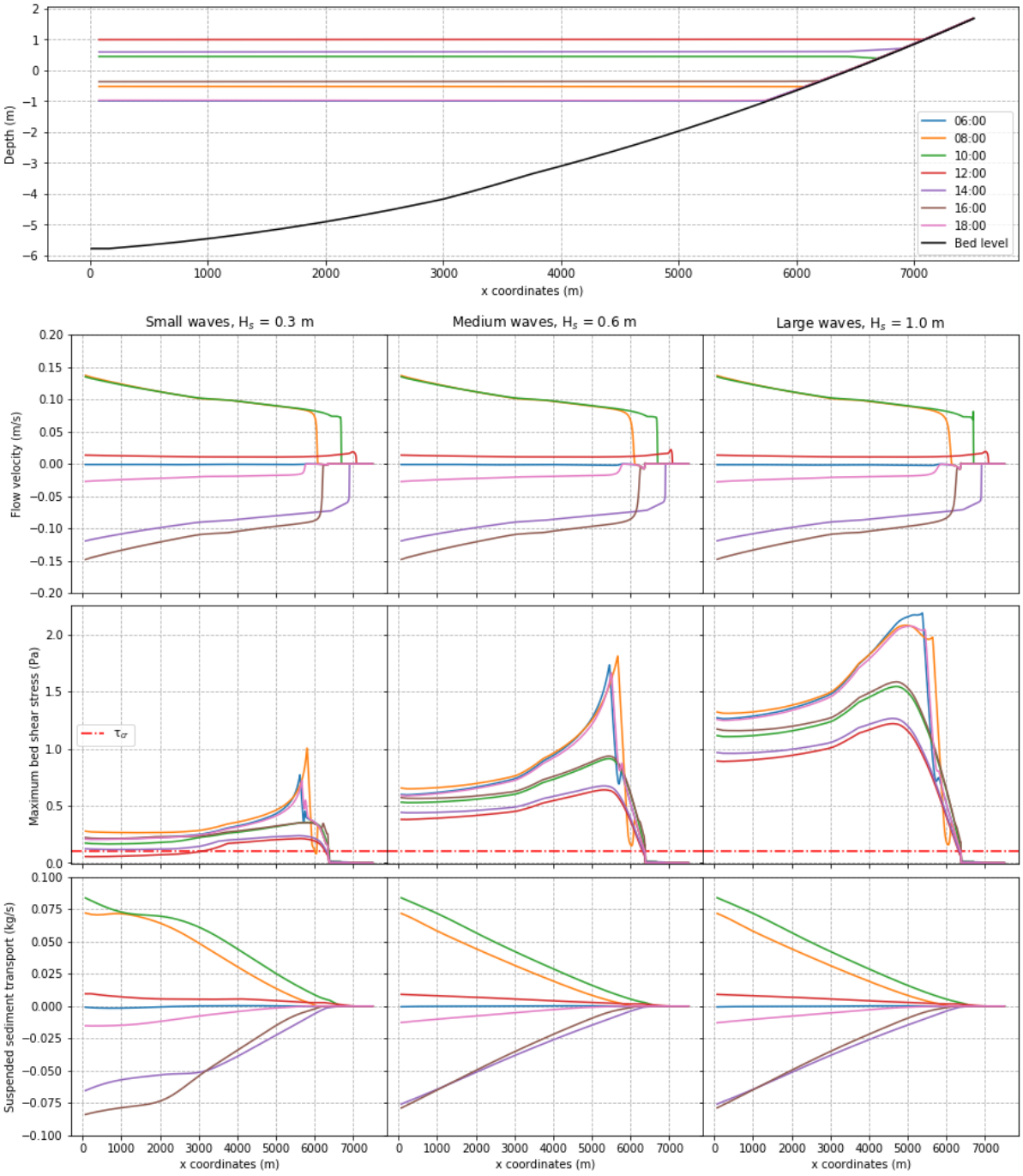

Figure B.9: Cross-shore overview of mangroves simulation, tidal range 1.0-2.0 m. Concave bottom profile, snapshots in time during spring tide.

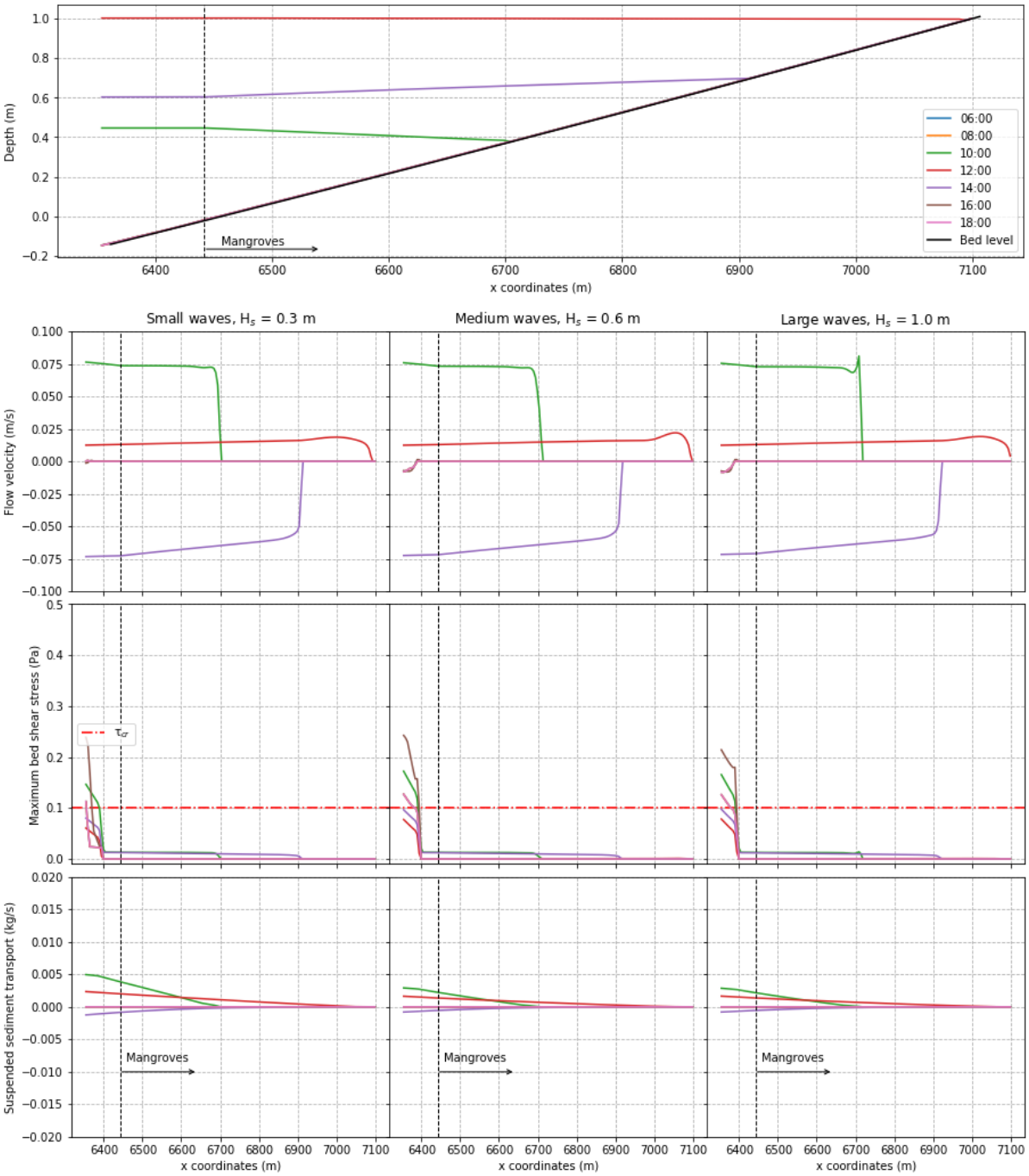

Figure B.10: Cross-shore overview of mangroves simulation, tidal range 1.0-2.0 m. Concave bottom profile, snapshots in time during spring tide, zoomed in on the intertidal

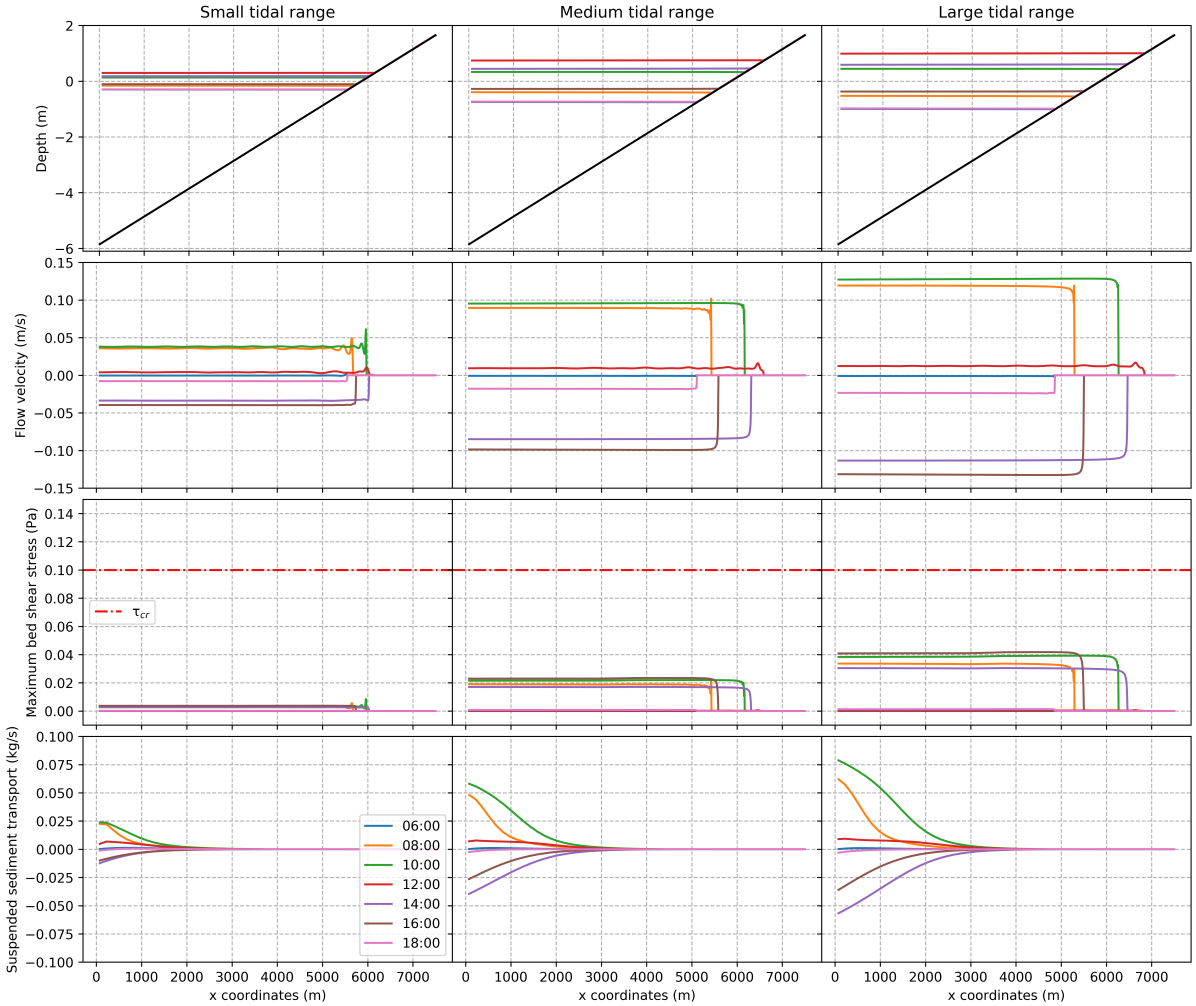

Figure B.11: Cross-shore overview of linear bottom profile, with all tidal ranges, snapshots in time during spring tide. No waves, nor mangroves.

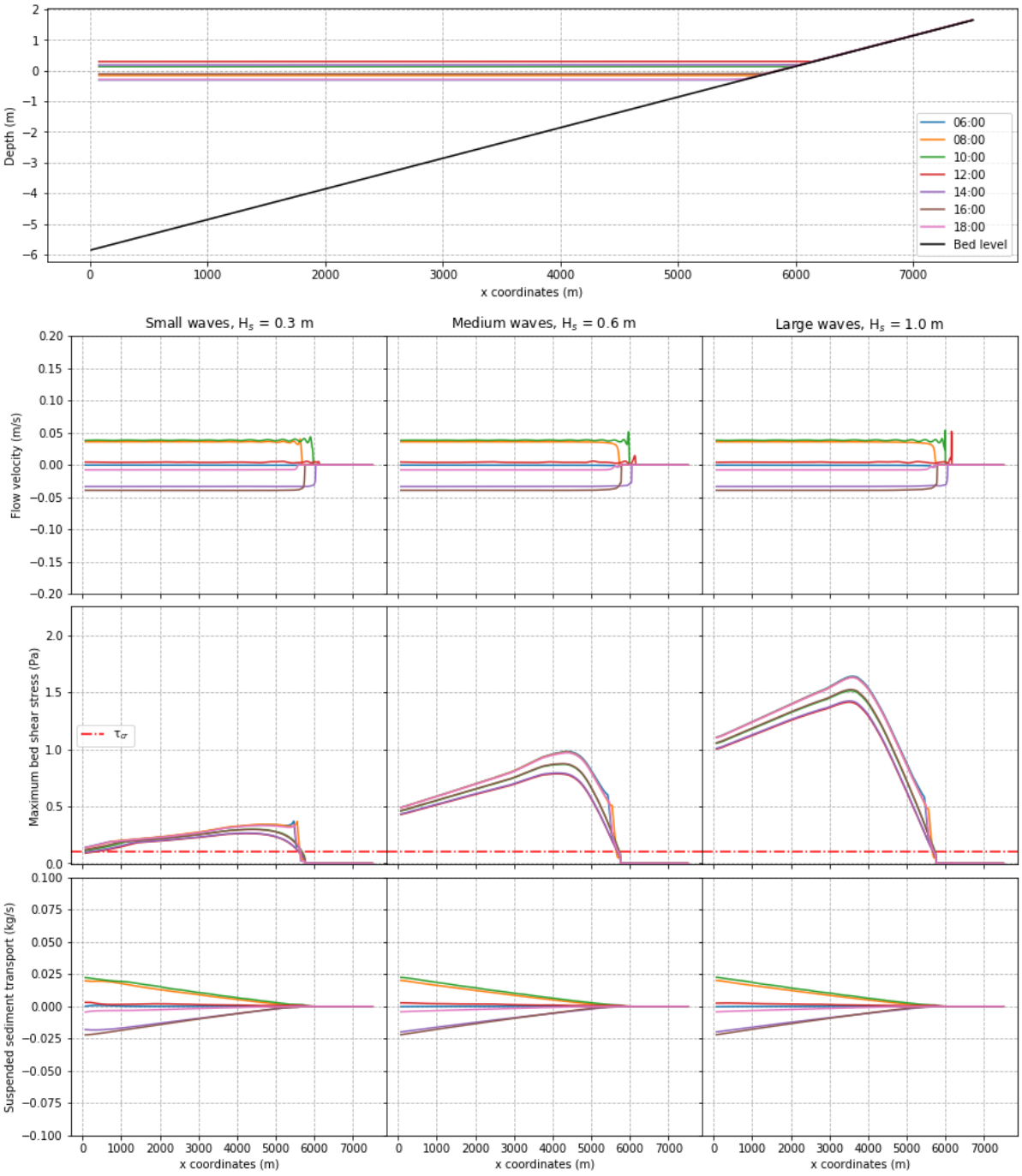

Figure B.12: Cross-shore overview of tide and wave simulation, tidal range 0.4-0.6 m. Linear bottom profile, snapshots in time during spring tide.

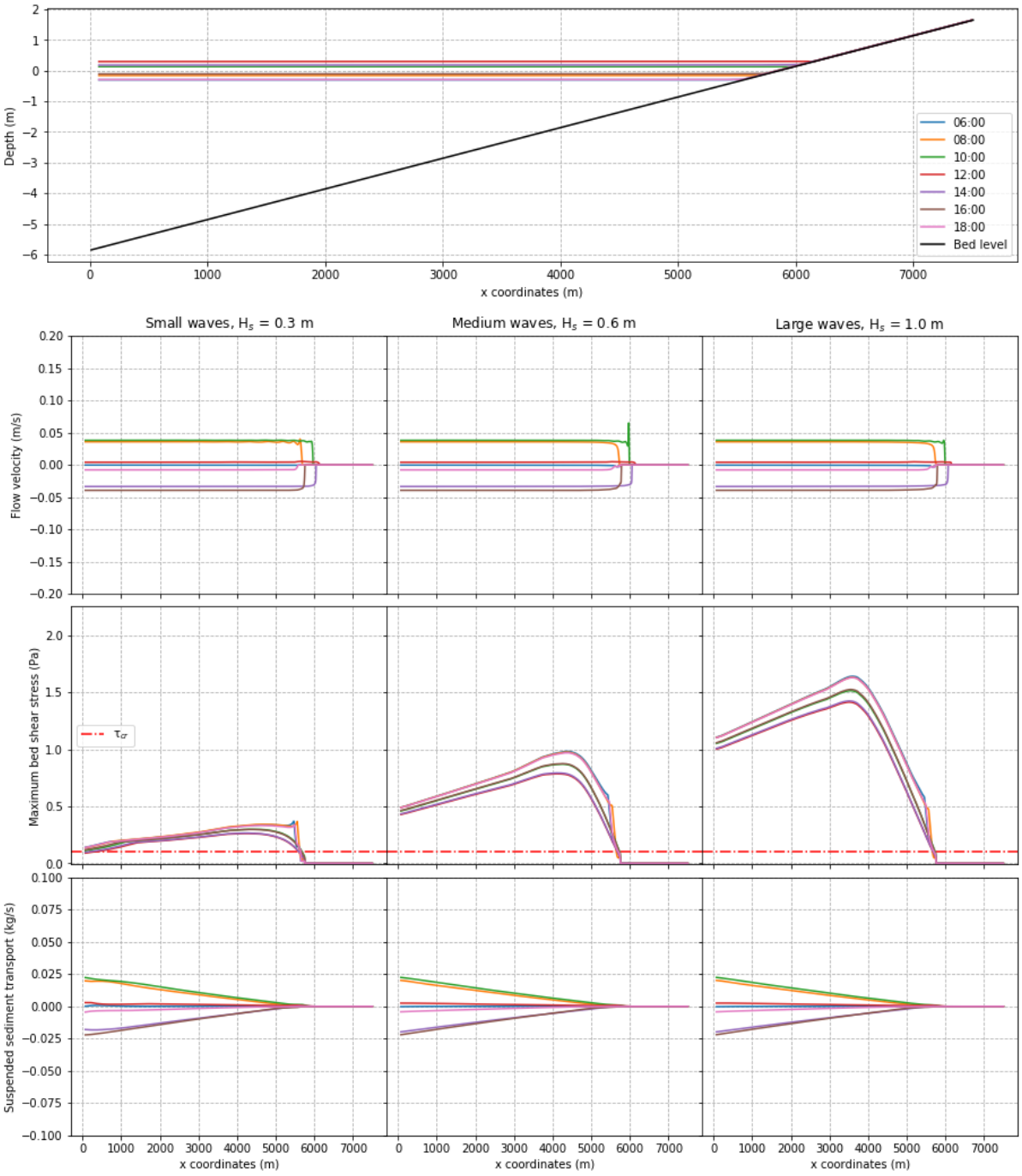

Figure B.13: Cross-shore overview of mangroves simulation, tidal range 0.4-0.6 m. Linear bottom profile, snapshots in time during spring tide.

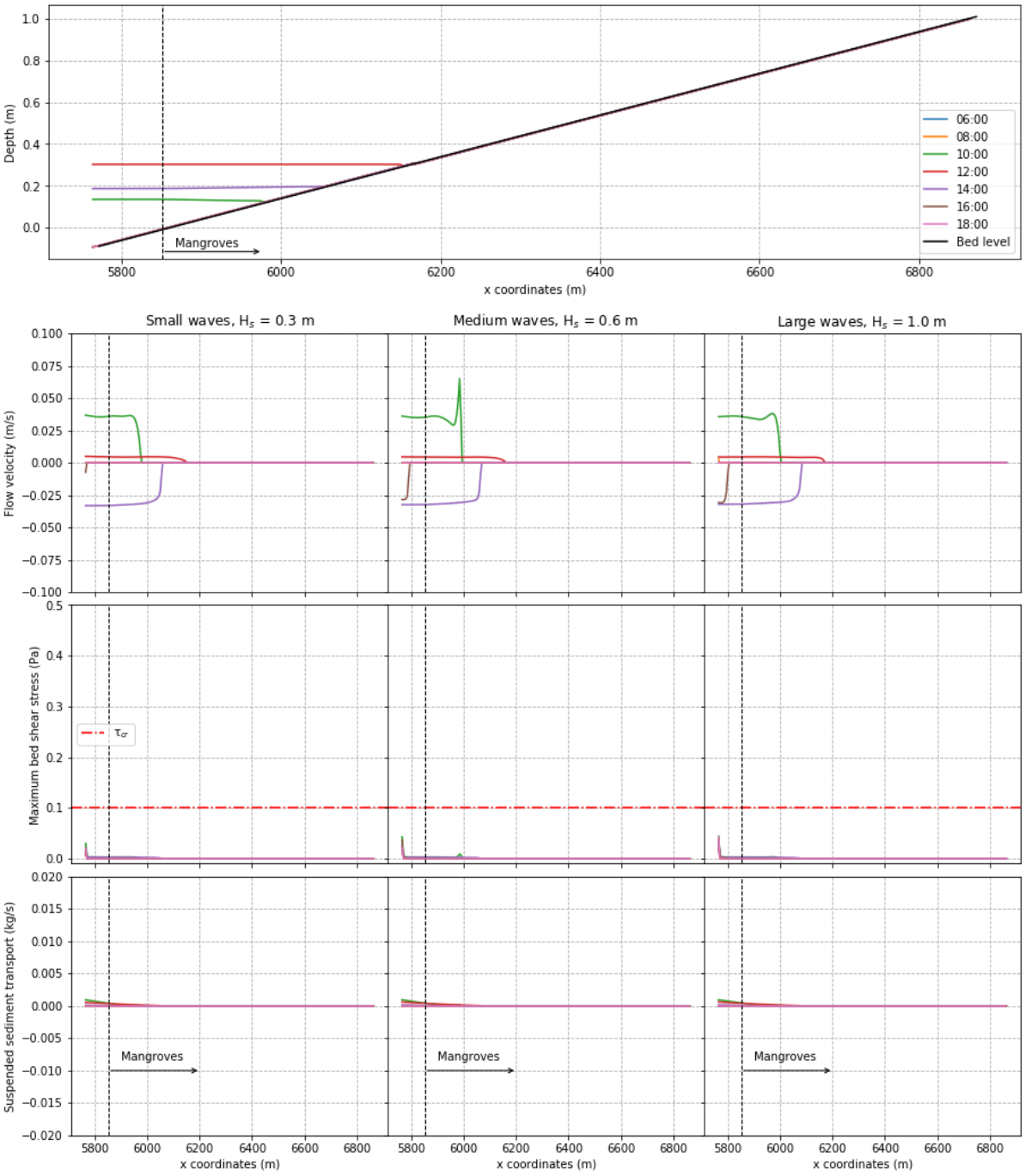

Figure B.14: Cross-shore overview of mangroves simulation, tidal range 0.4-0.6 m. Linear bottom profile, snapshots in time during spring tide, zoomed in on the intertidal

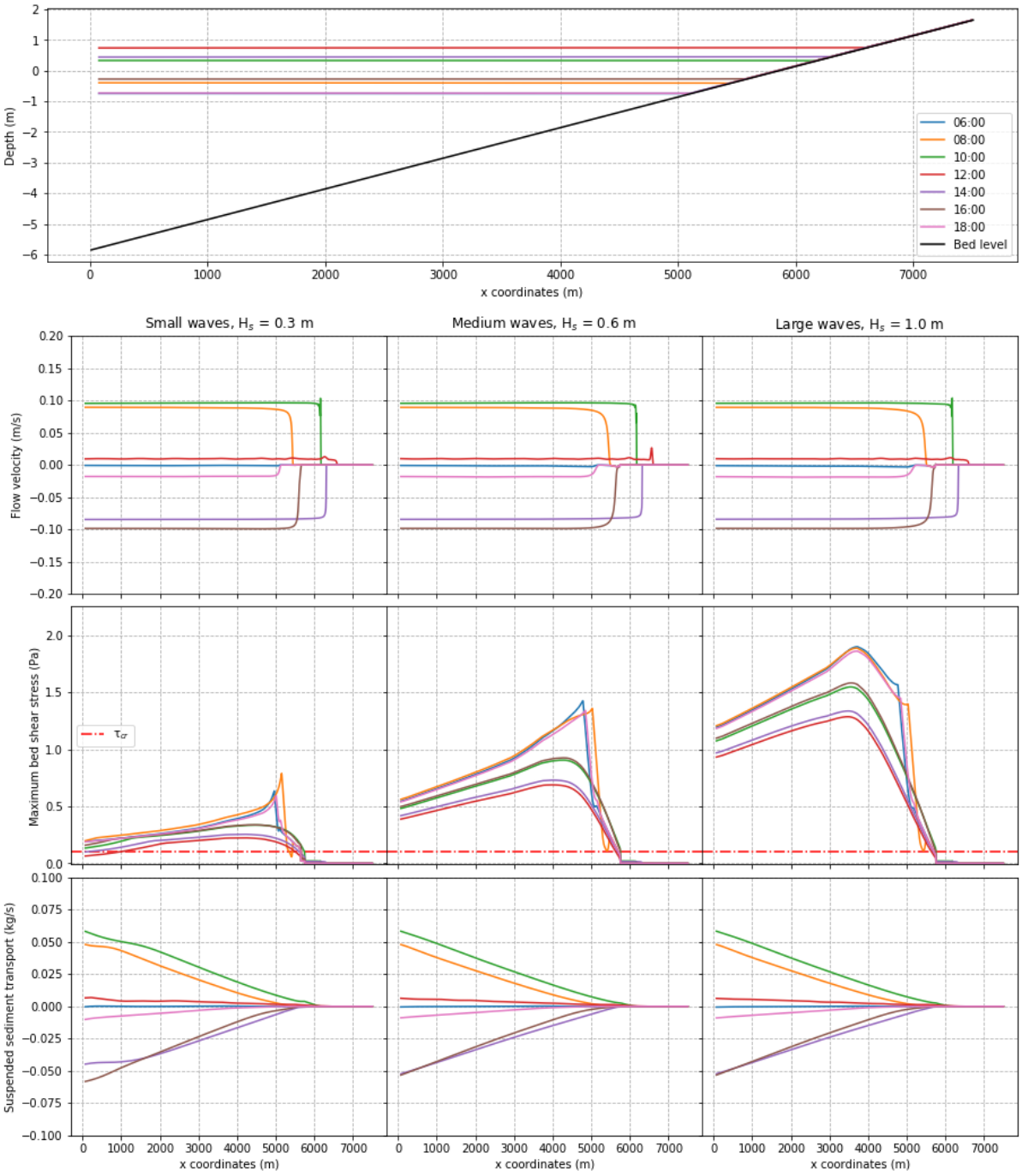

Figure B.15: Cross-shore overview of tide and wave simulation, tidal range 0.8-1.5 m. Linear bottom profile, snapshots in time during spring tide.

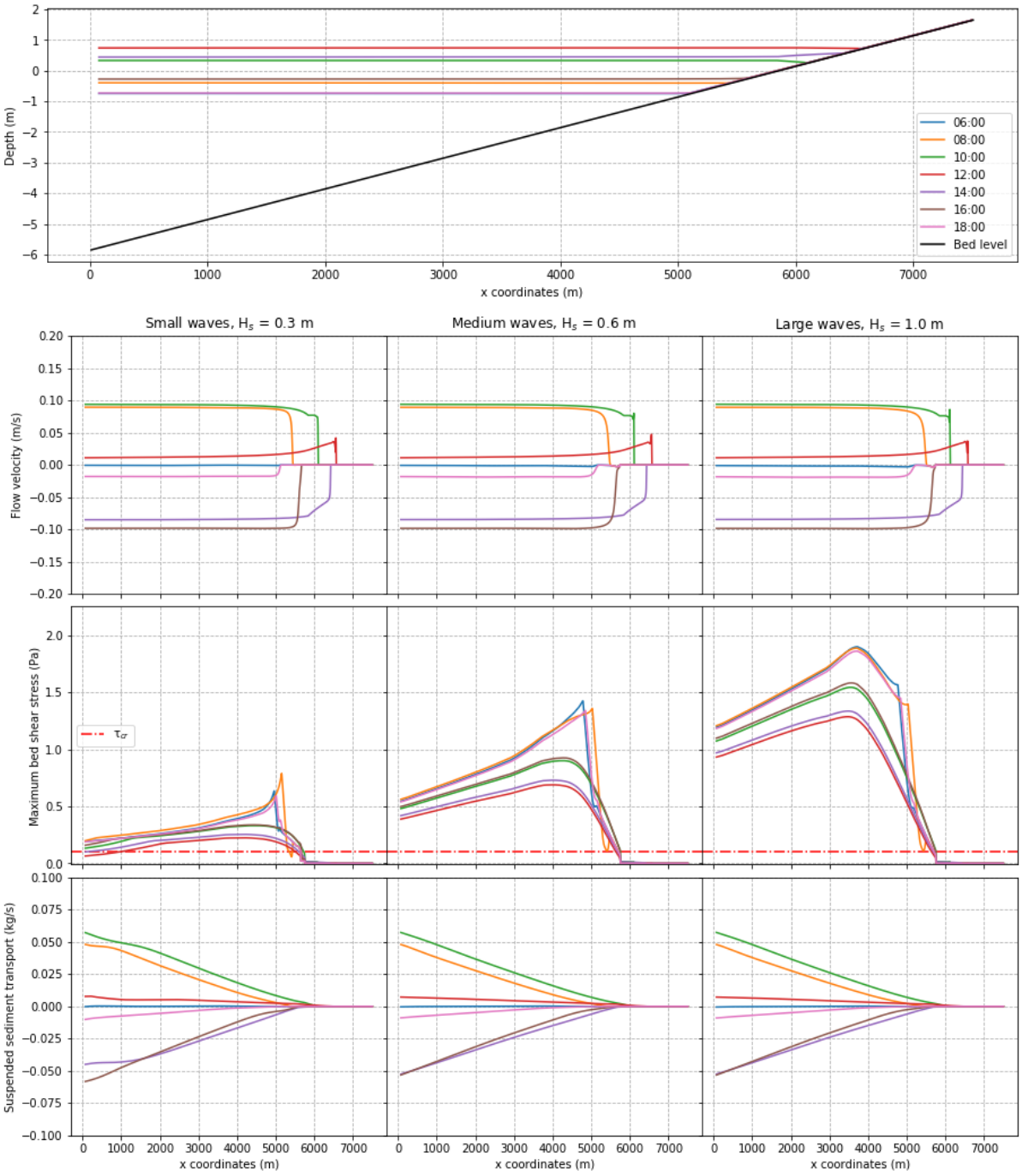

Figure B.16: Cross-shore overview of mangroves simulation, tidal range 0.8-1.5 m. Linear bottom profile, snapshots in time during spring tide.

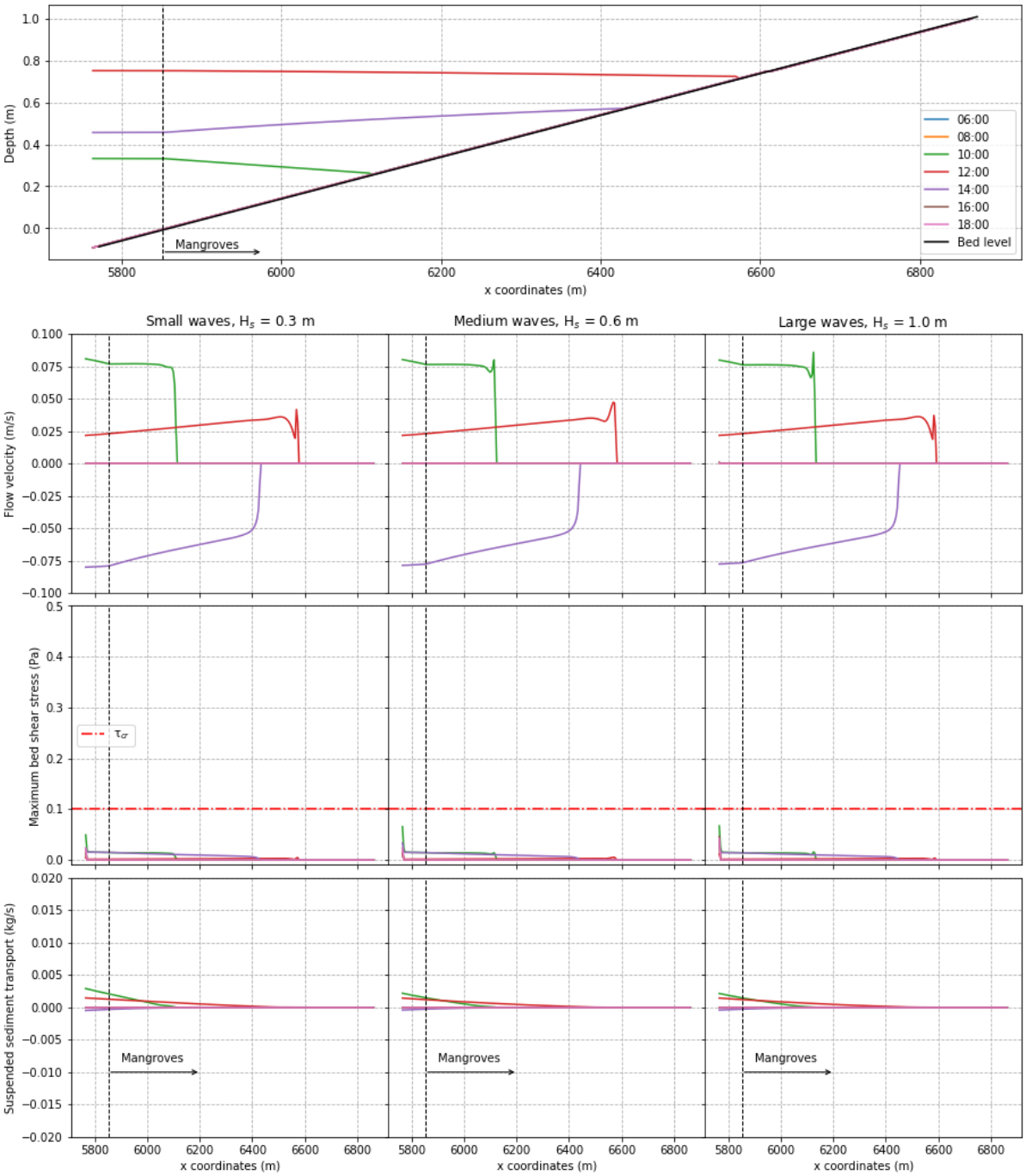

Figure B.17: Cross-shore overview of mangroves simulation, tidal range 0.8-1.5 m. Linear bottom profile, snapshots in time during spring tide, zoomed in on the intertidal

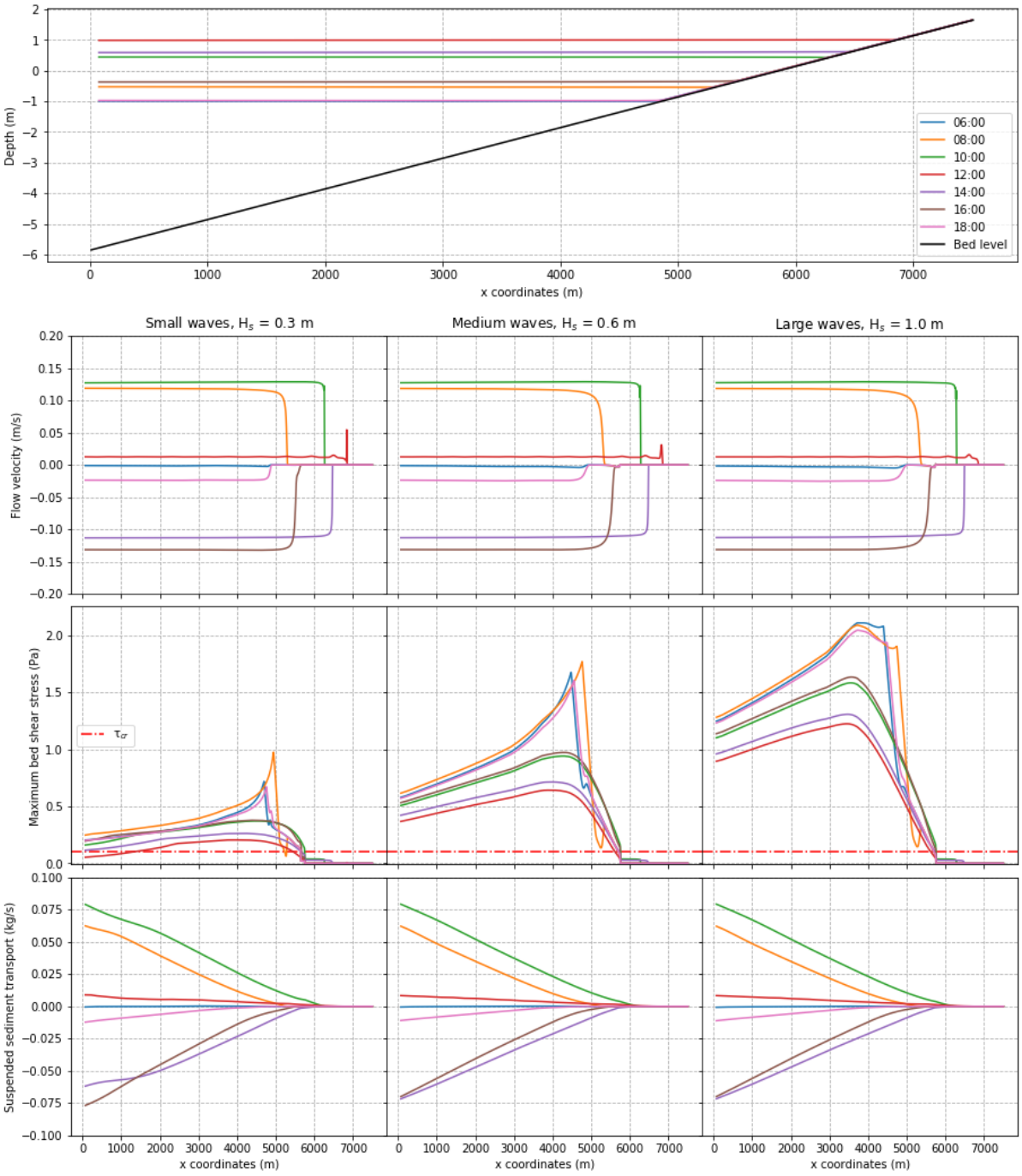

Figure B.18: Cross-shore overview of tide and wave simulation, tidal range 1.0-2.0 m. Linear bottom profile, snapshots in time during spring tide.

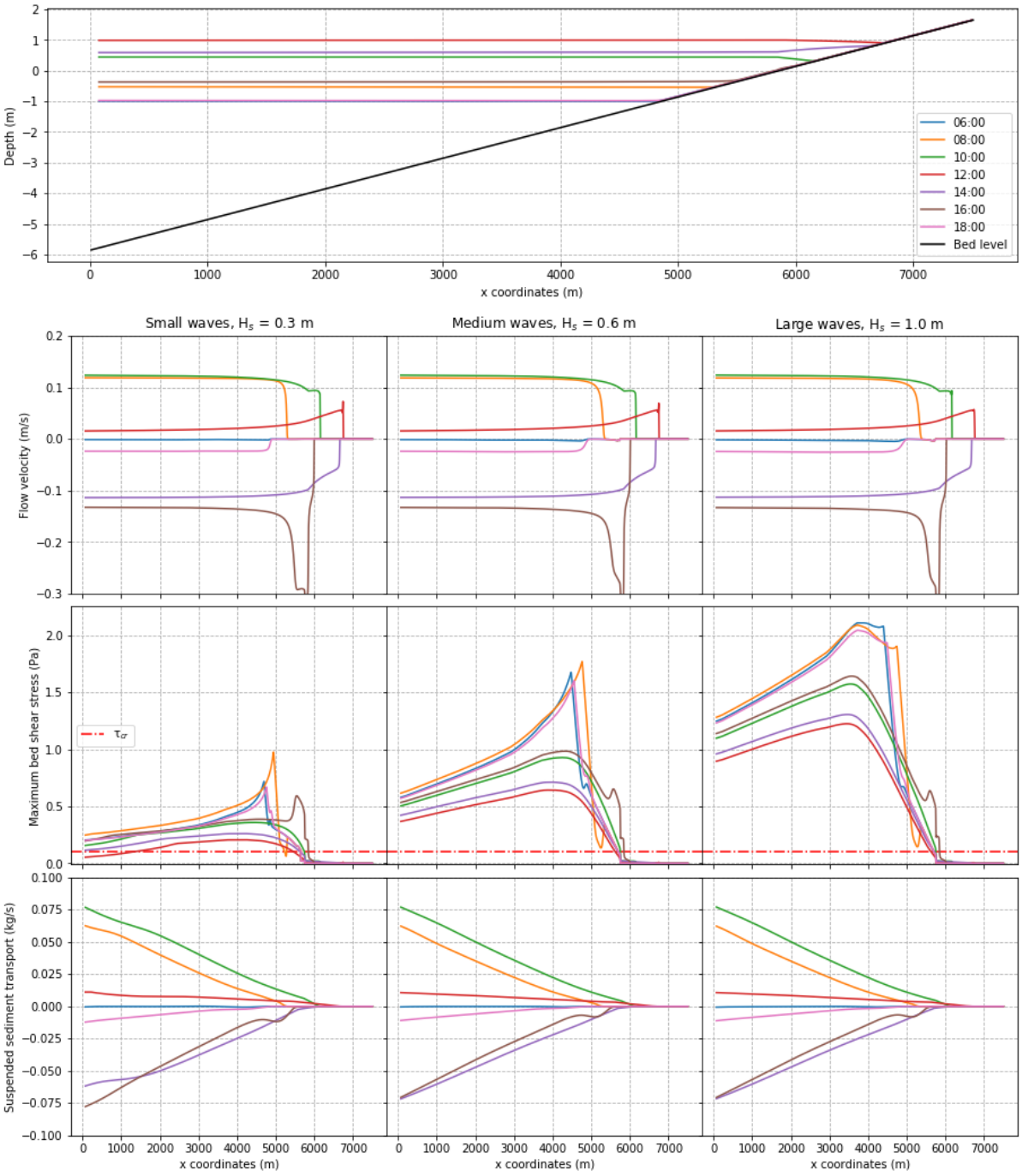

Figure B.19: Cross-shore overview of mangroves simulation, tidal range 1.0-2.0 m. Linear bottom profile, snapshots in time during spring tide.

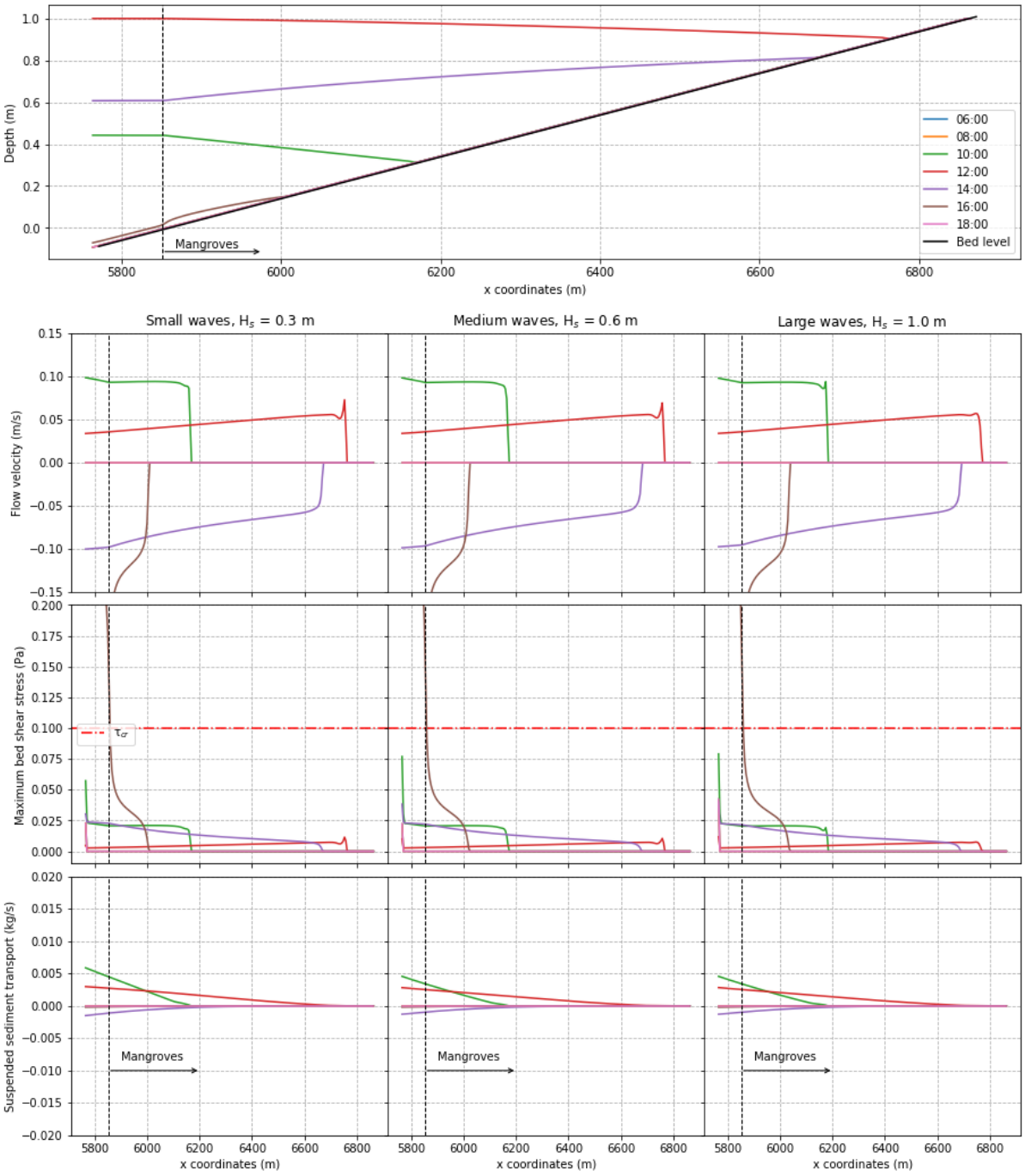

Figure B.20: Cross-shore overview of mangroves simulation, tidal range 1.0-2.0 m. Linear bottom profile, snapshots in time during spring tide, zoomed in on the intertidal

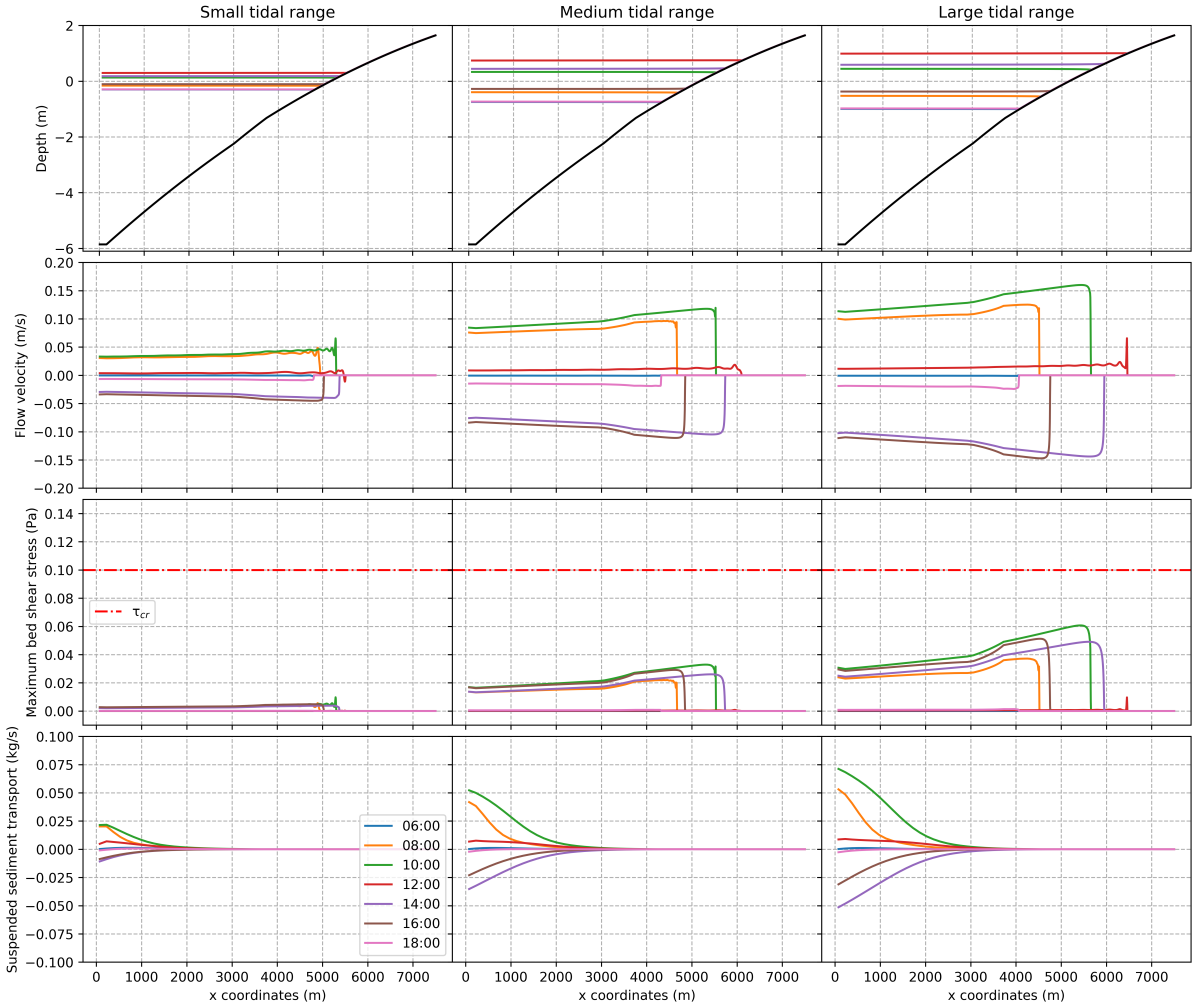

Figure B.21: Cross-shore overview of convex bottom profile, with all tidal ranges, snapshots in time during spring tide. No waves, nor mangroves.

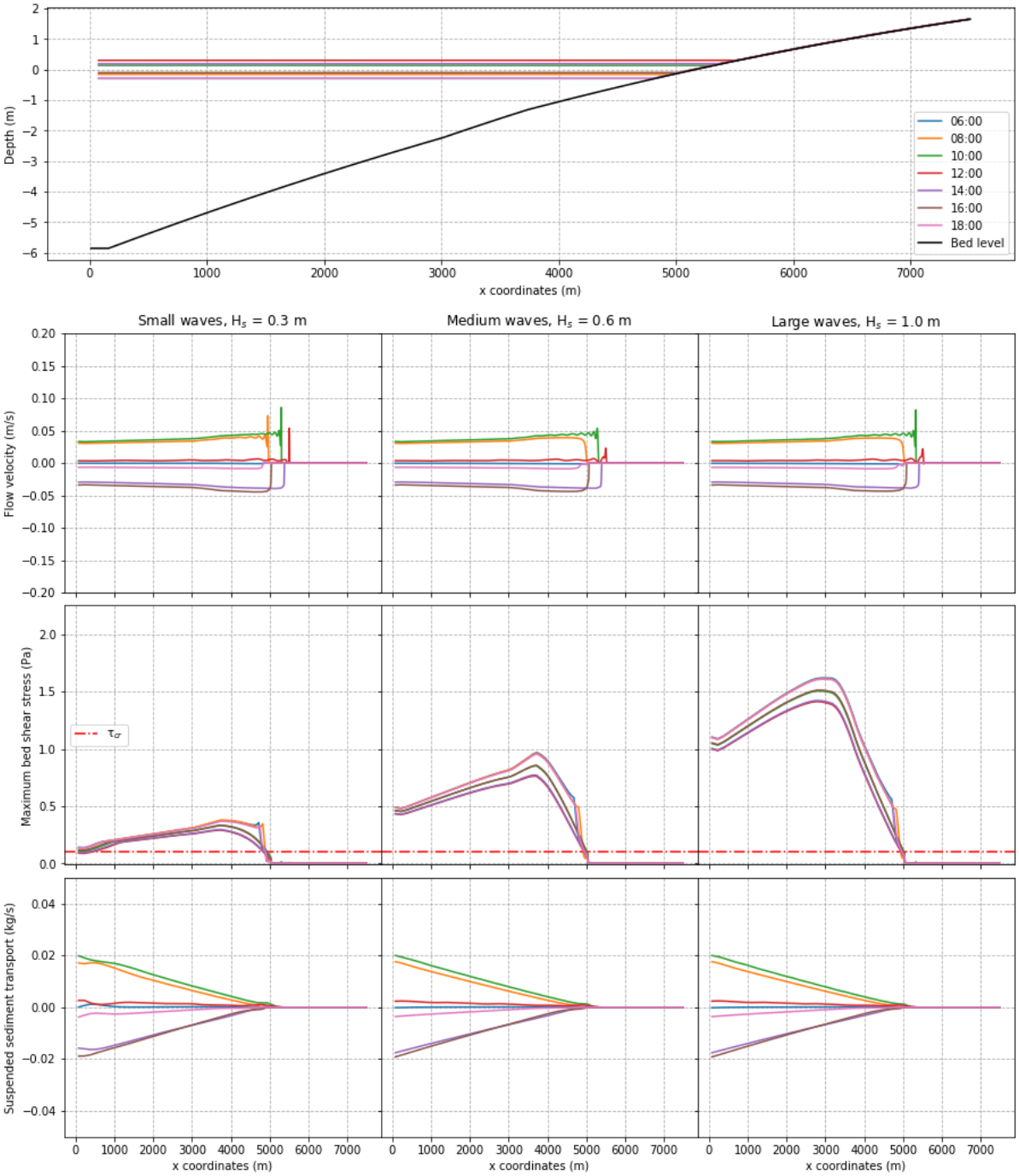

Figure B.22: Cross-shore overview of tide and wave simulation, tidal range 0.4-0.6 m. Convex bottom profile, snapshots in time during spring tide.

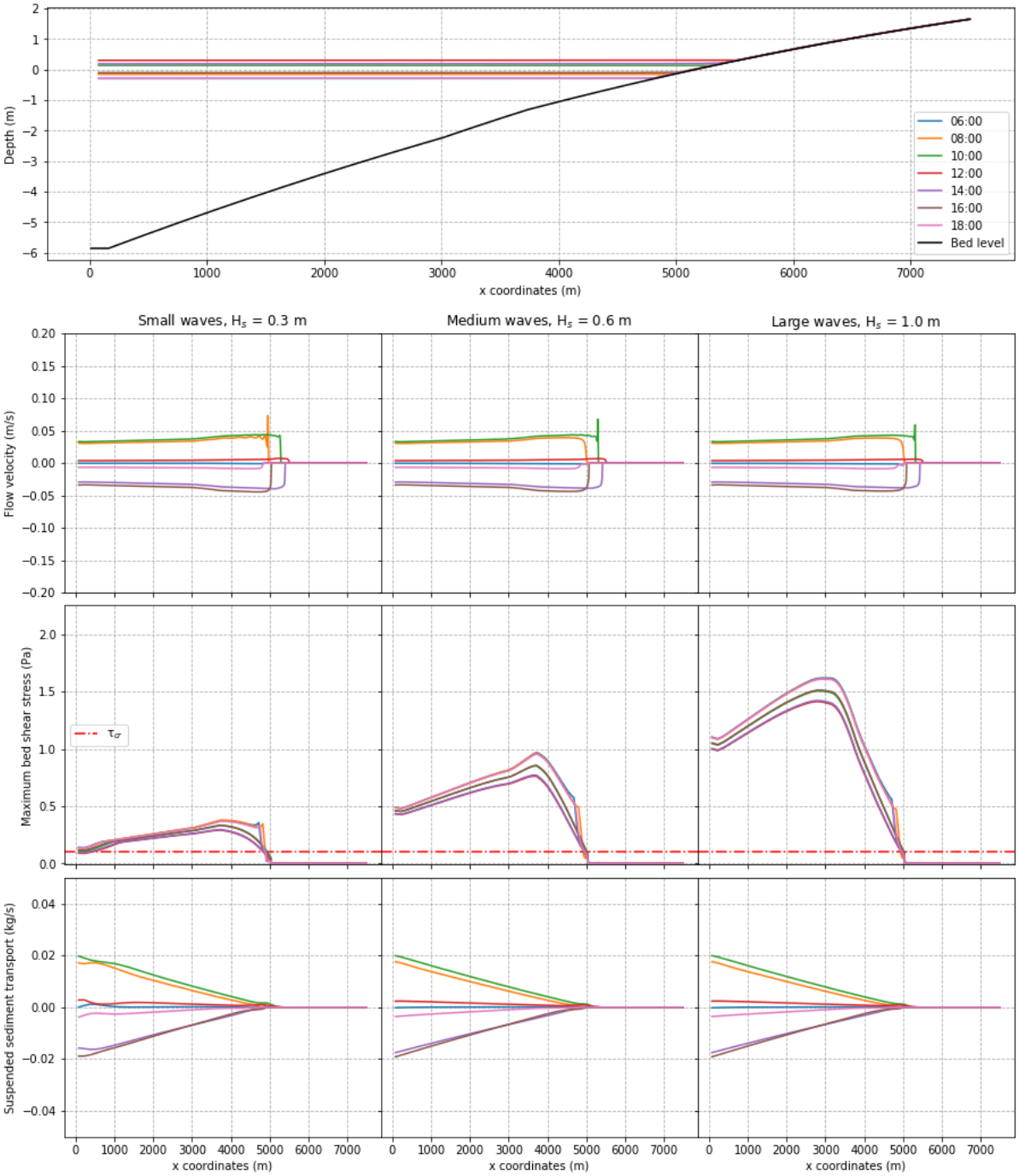

Figure B.23: Cross-shore overview of mangroves simulation, tidal range 0.4-0.6 m. Convex bottom profile, snapshots in time during spring tide.

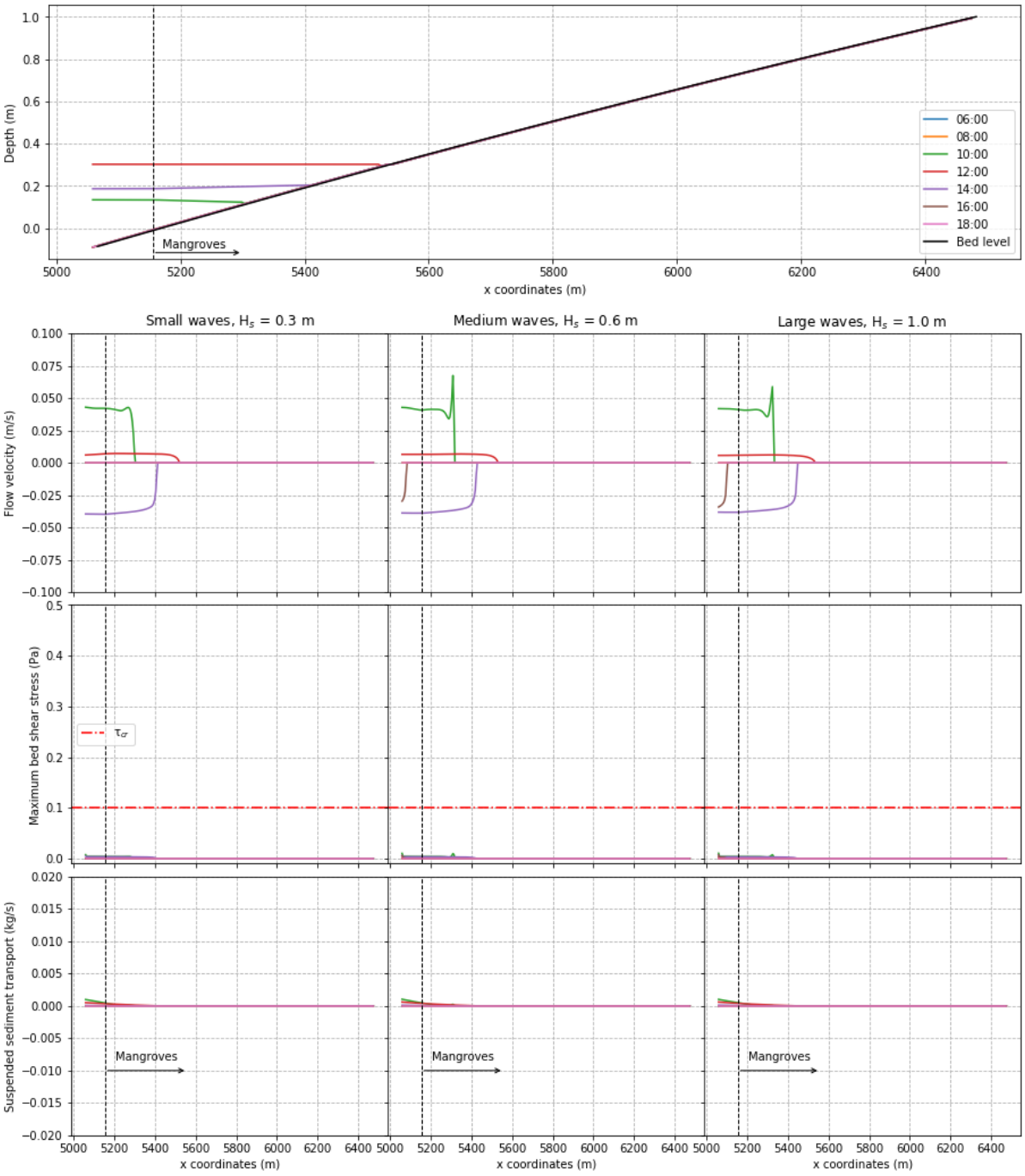

Figure B.24: Cross-shore overview of mangroves simulation, tidal range 0.4-0.6 m. Convex bottom profile, snapshots in time during spring tide, zoomed in on the intertidal

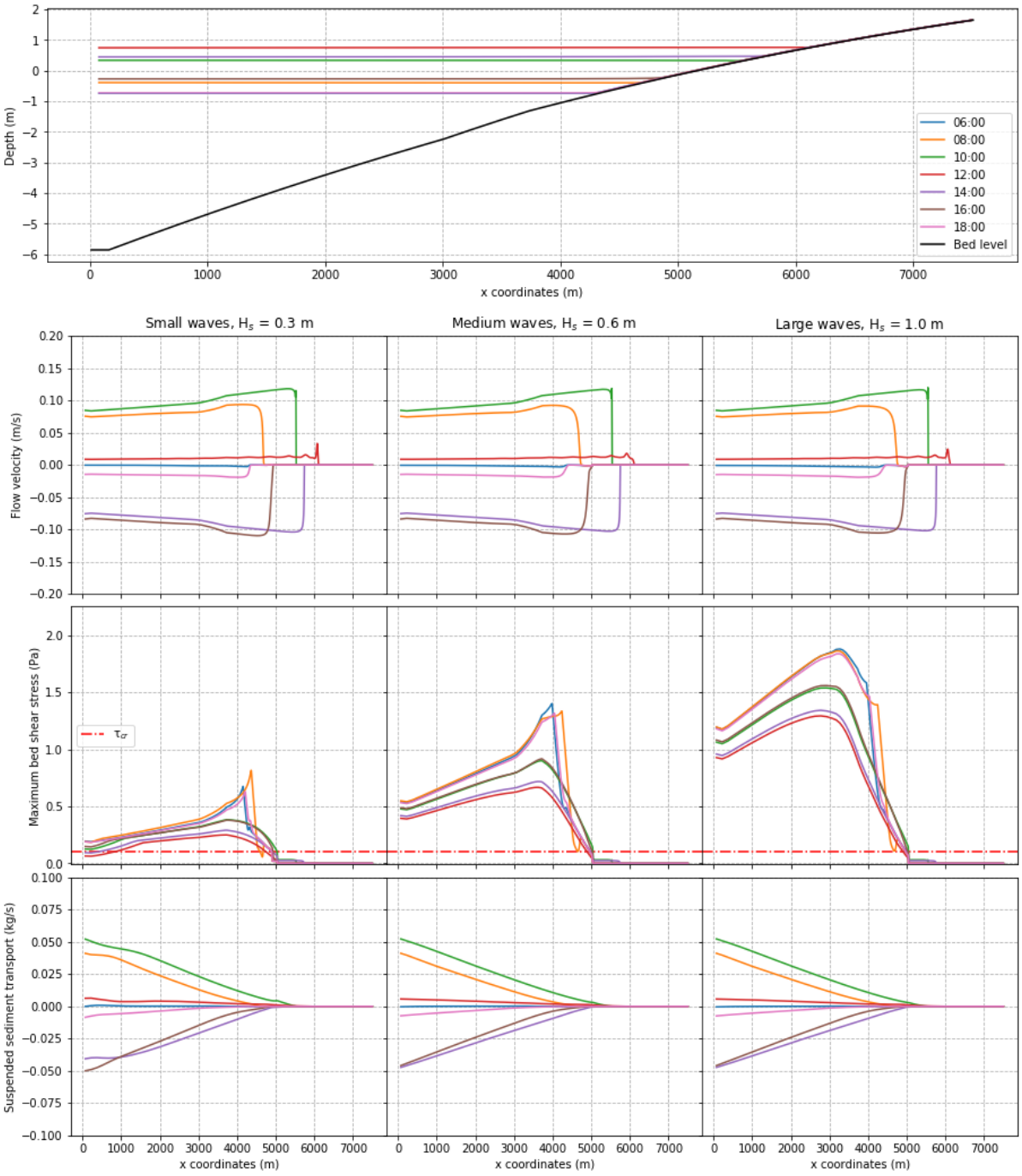

Figure B.25: Cross-shore overview of tide and wave simulation, tidal range 0.8-1.5 m. Convex bottom profile, snapshots in time during spring tide.

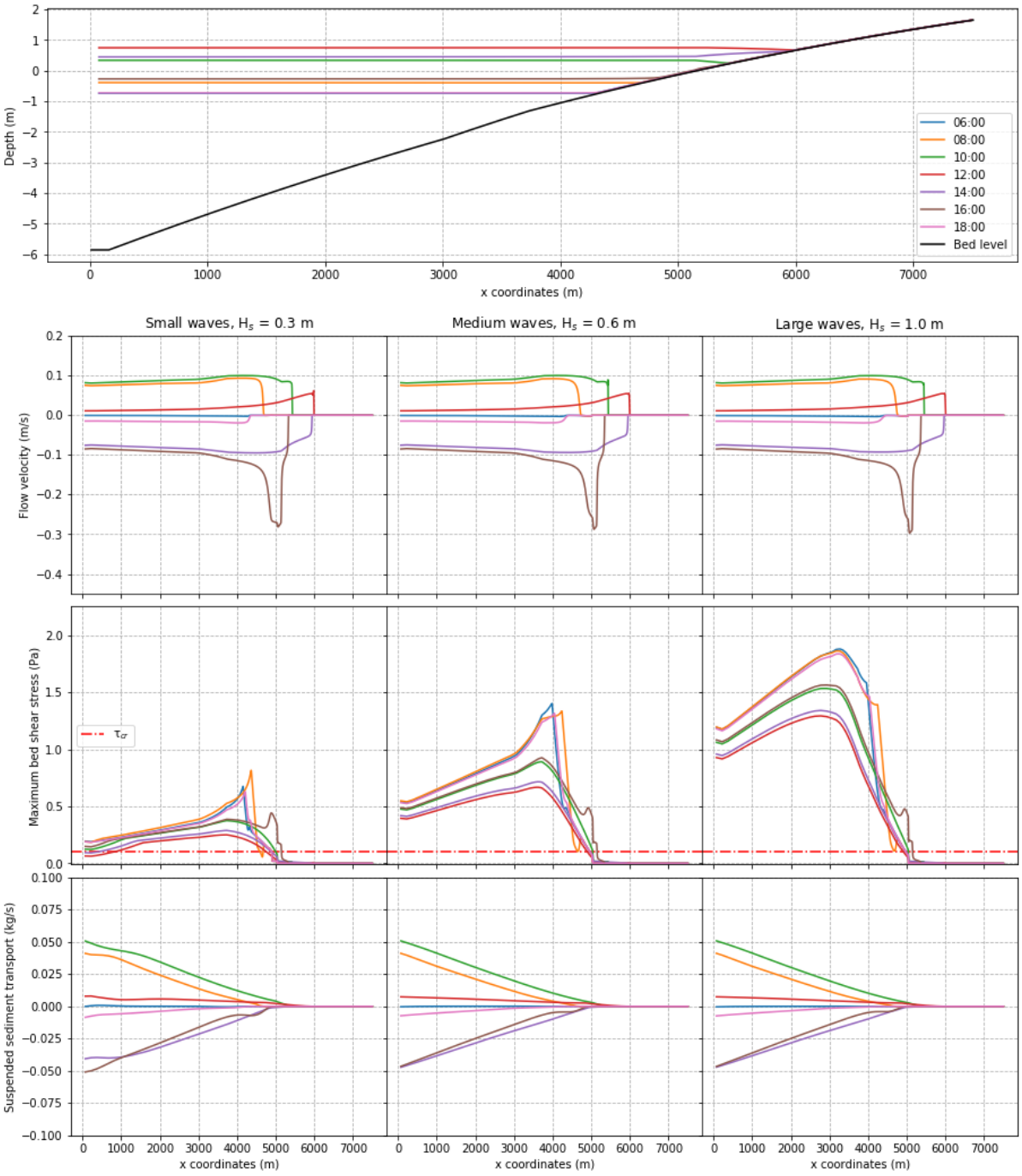

Figure B.26: Cross-shore overview of mangroves simulation, tidal range 0.8-1.5 m. Convex bottom profile, snapshots in time during spring tide.

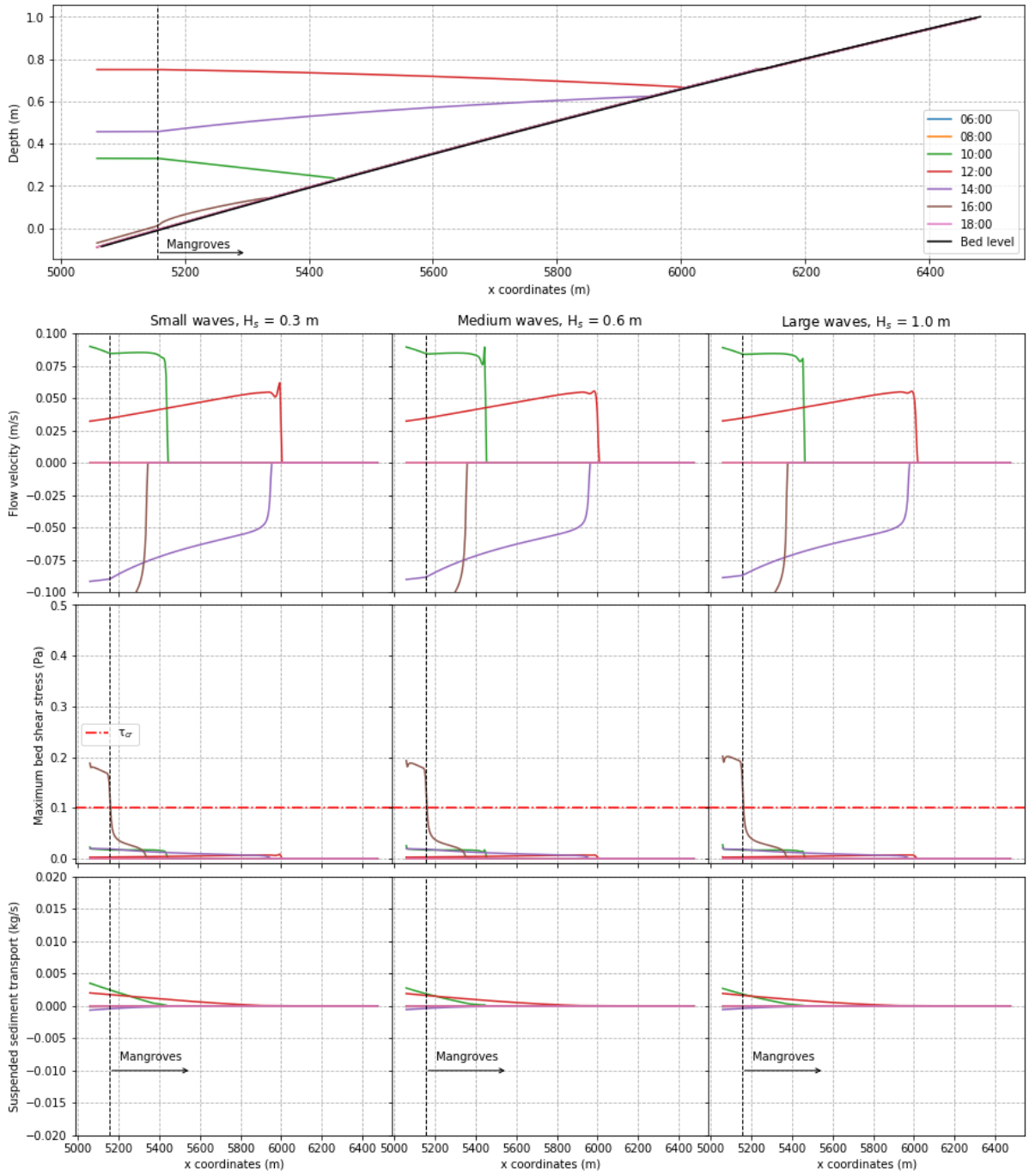

Figure B.27: Cross-shore overview of mangroves simulation, tidal range 0.8-1.5 m. Convex bottom profile, snapshots in time during spring tide, zoomed in on the intertidal

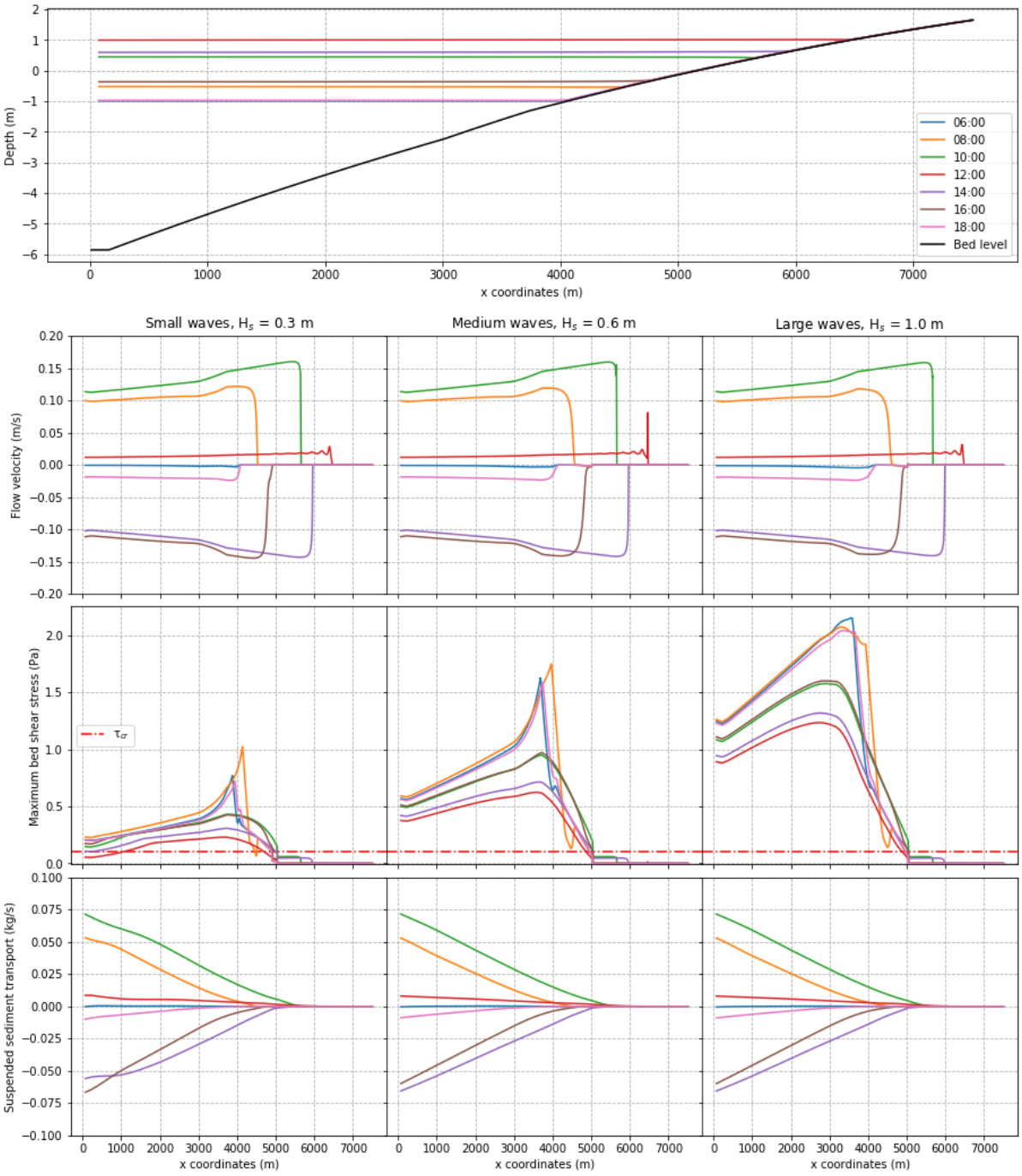

Figure B.28: Cross-shore overview of tide and wave simulation, tidal range 1.0-2.0 m. Convex bottom profile, snapshots in time during spring tide.

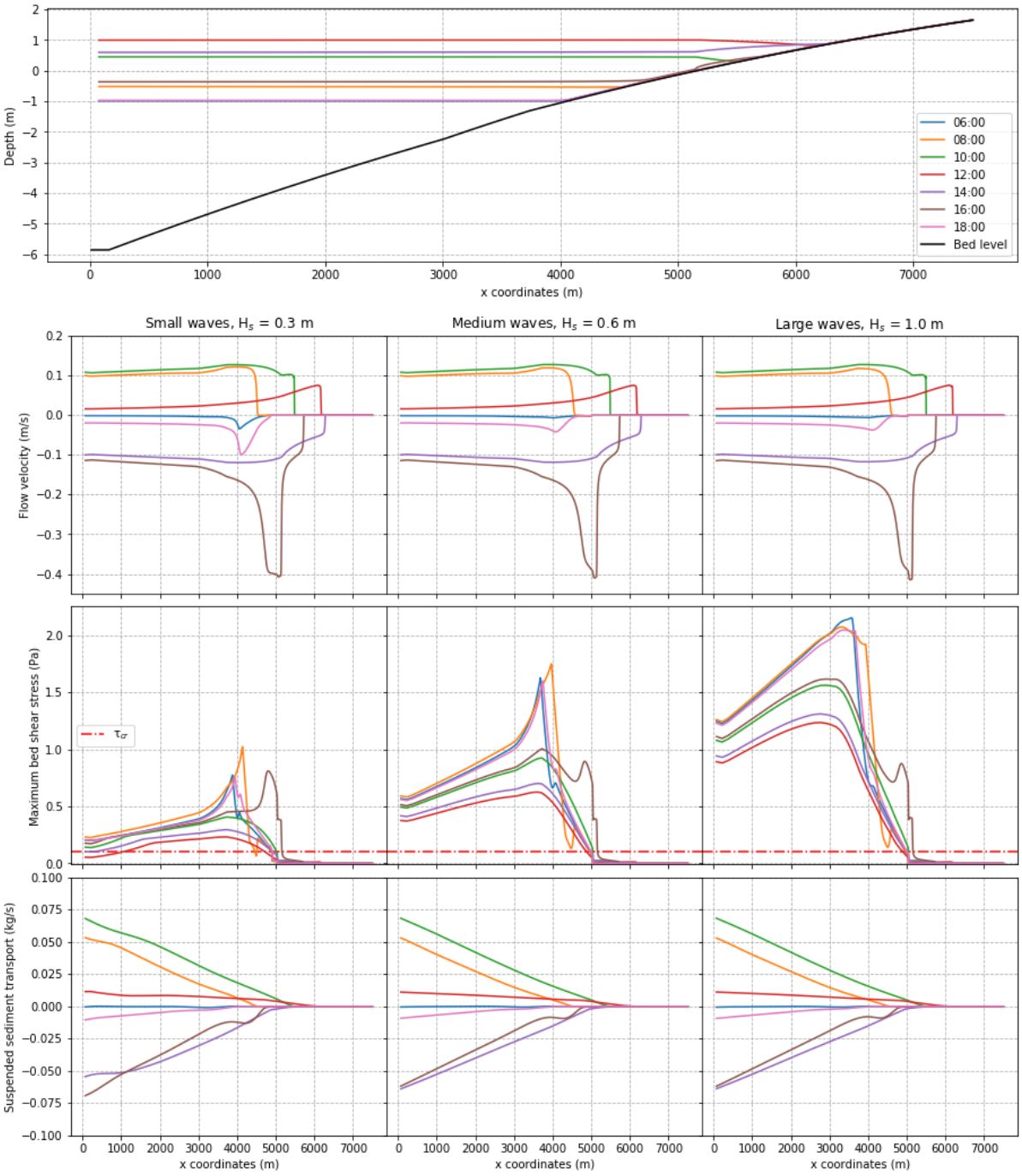

Figure B.29: Cross-shore overview of mangroves simulation, tidal range 1.0-2.0 m. Convex bottom profile, snapshots in time during spring tide.

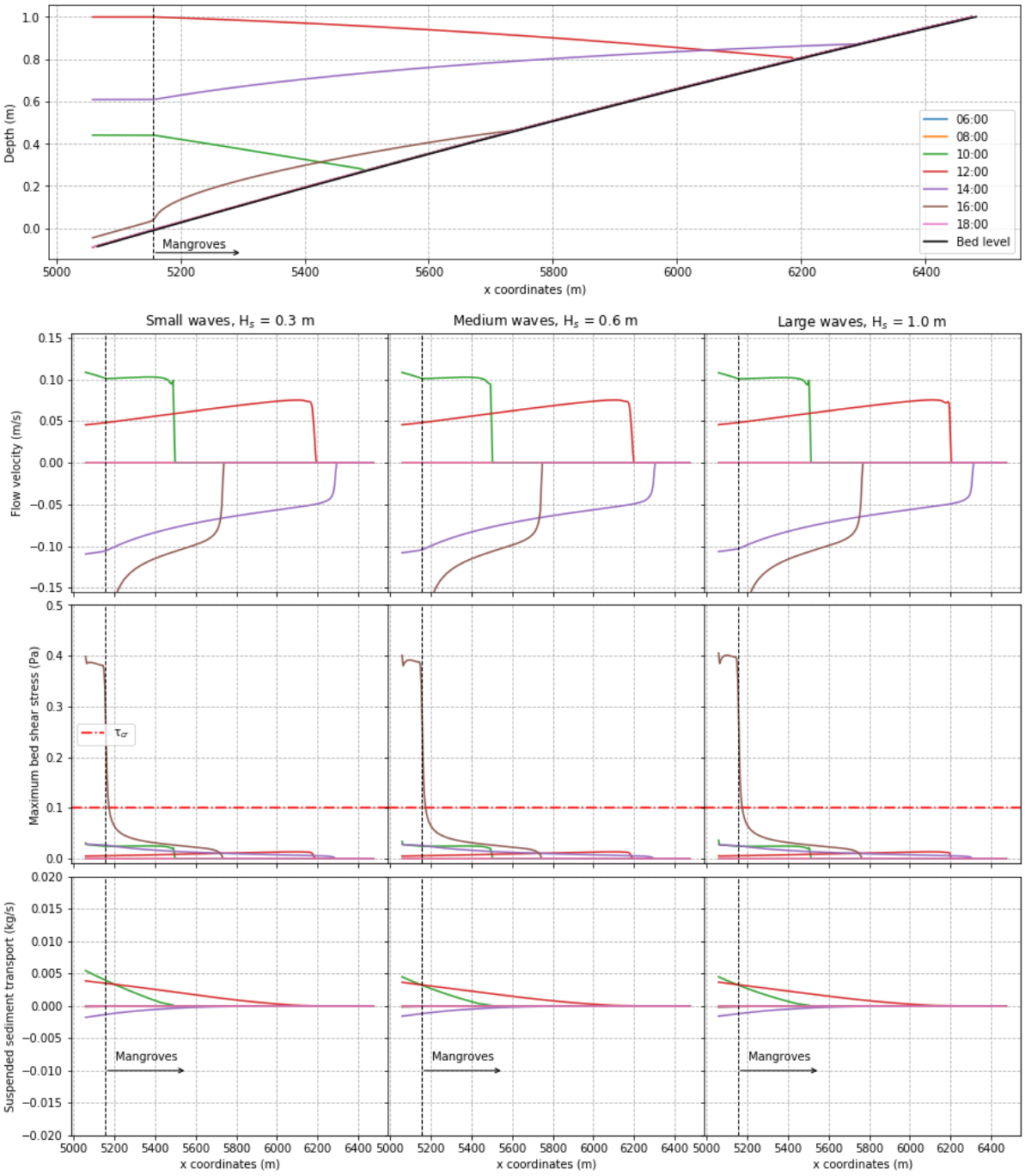

Figure B.30: Cross-shore overview of mangroves simulation, tidal range 1.0-2.0 m. Convex bottom profile, snapshots in time during spring tide, zoomed in on the intertidal

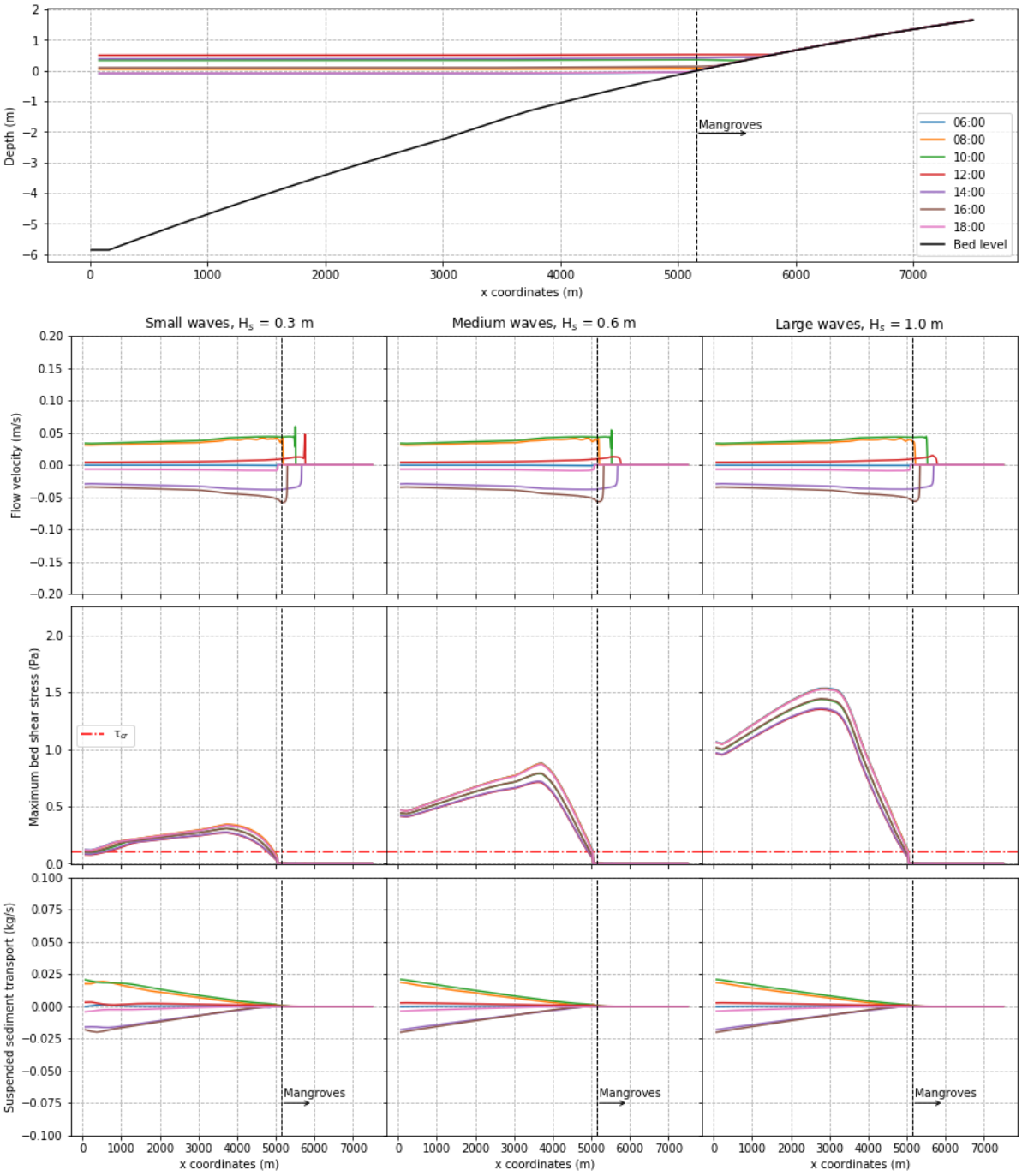

Figure B.31: Cross-shore overview of sea level rise simulation, 0.2 m SLR. Tidal range 0.4-0.6 m. Convex bottom profile, snapshots in time during spring tide.

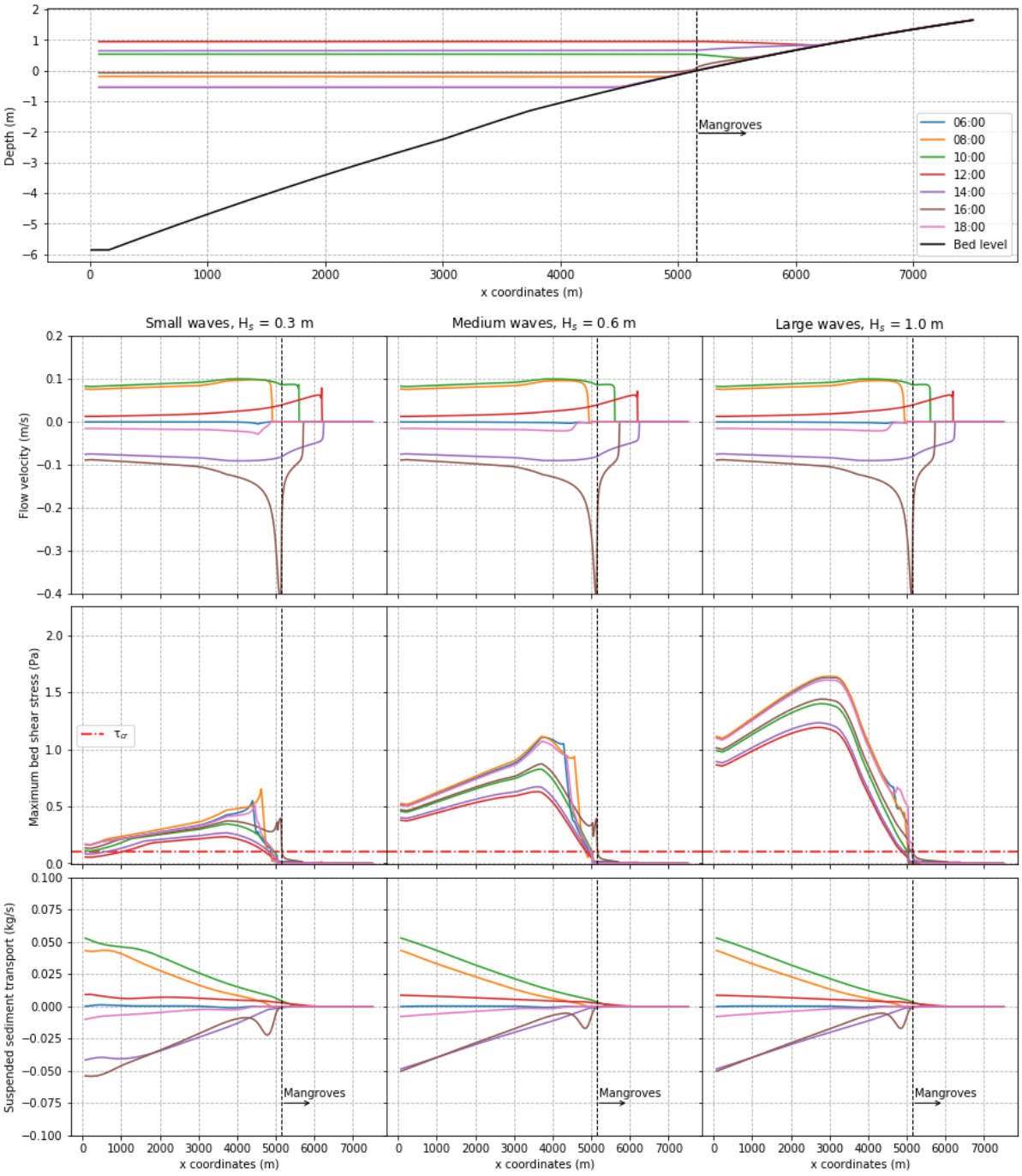

Figure B.32: Cross-shore overview of sea level rise simulation, 0.2 m SLR. Tidal range 0.8-1.5 m. Convex bottom profile, snapshots in time during spring tide.

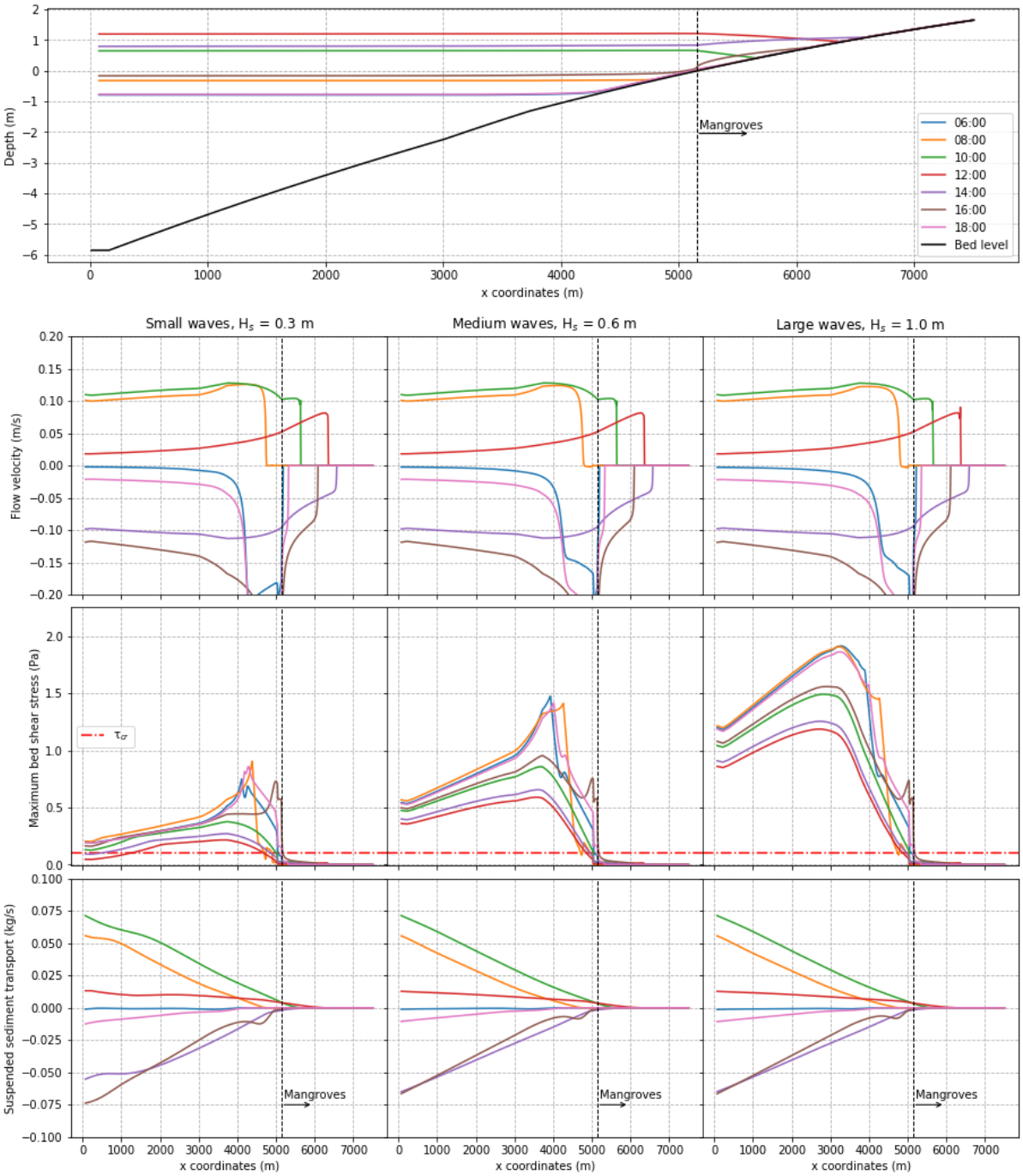

Figure B.33: Cross-shore overview of sea level rise simulation, 0.2 m SLR. Tidal range 1.0-2.0 m. Convex bottom profile, snapshots in time during spring tide.

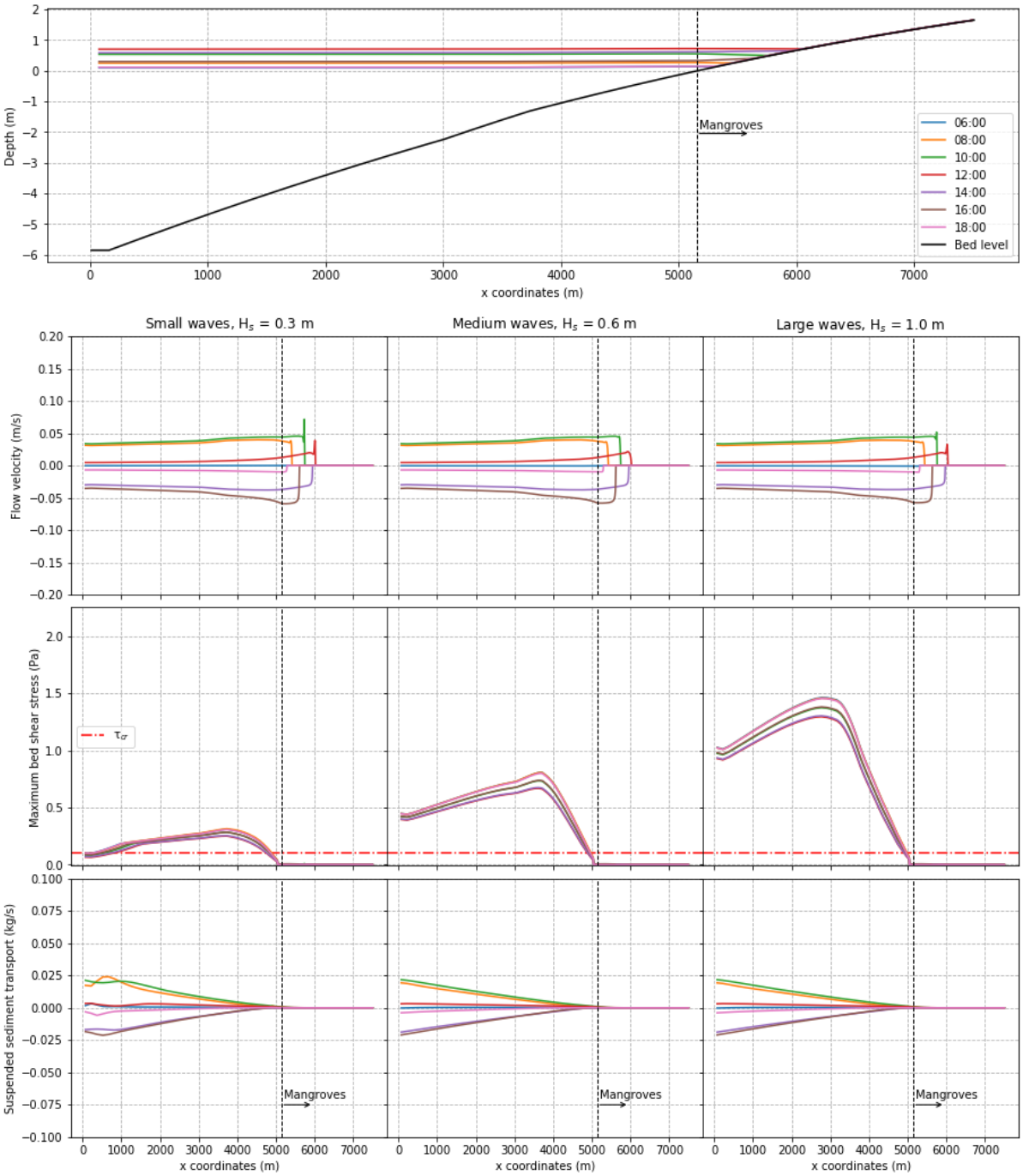

Figure B.34: Cross-shore overview of sea level rise simulation, 0.4 m SLR. Tidal range 0.4-0.6 m. Convex bottom profile, snapshots in time during spring tide.

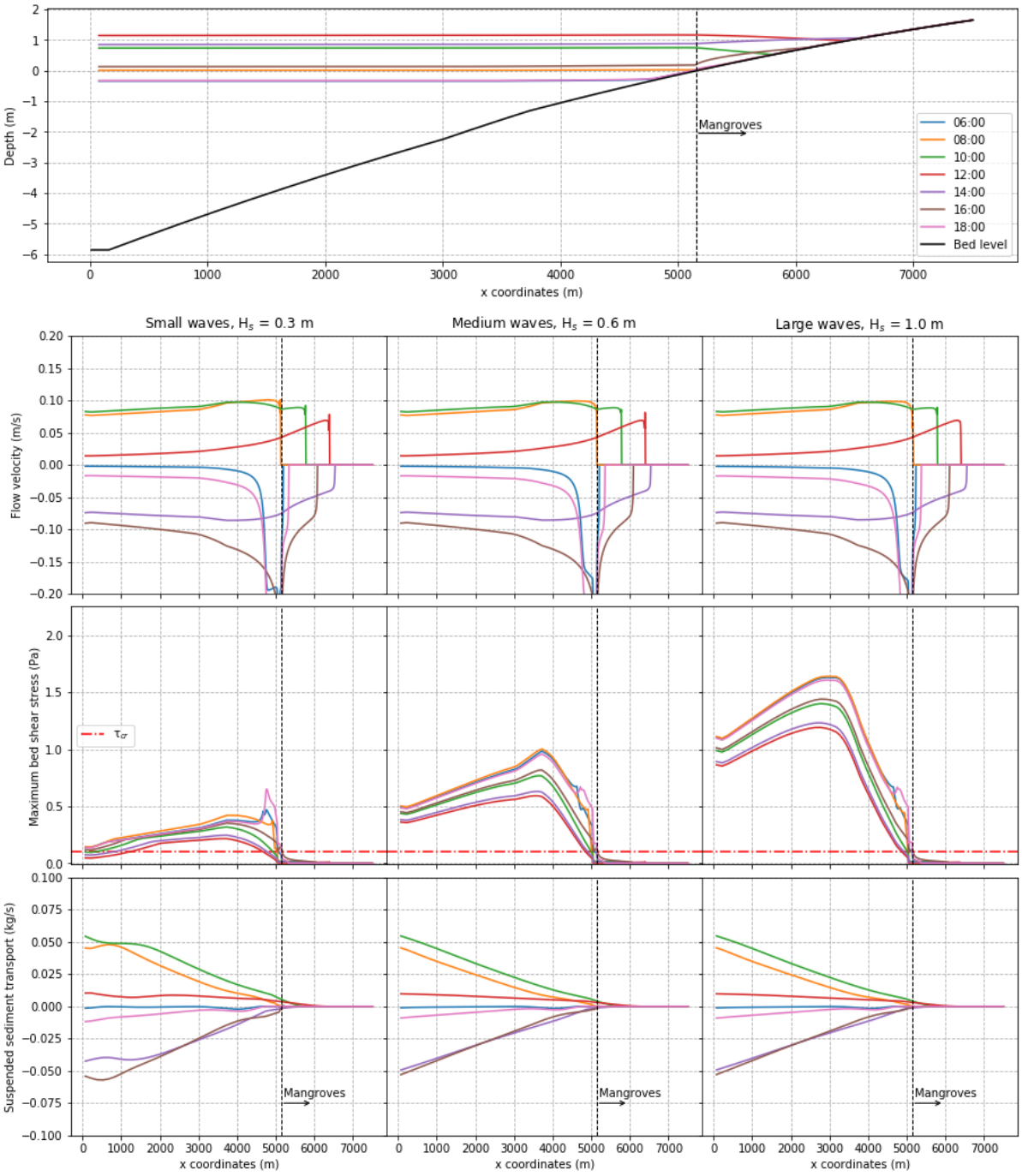

Figure B.35: Cross-shore overview of sea level rise simulation, 0.4 m SLR. Tidal range 0.8-1.5 m. Convex bottom profile, snapshots in time during spring tide.

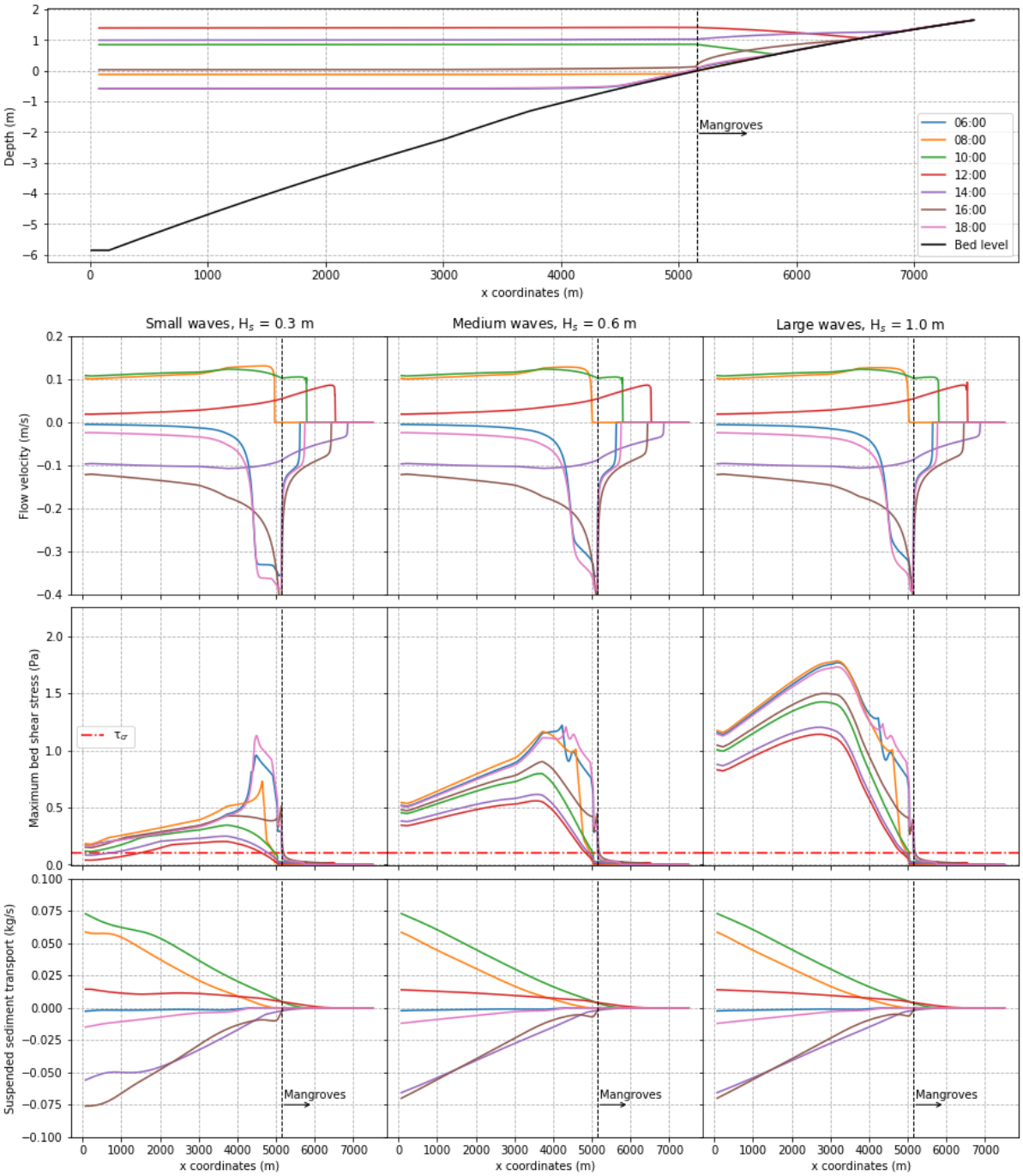

Figure B.36: Cross-shore overview of sea level rise simulation, 0.4 m SLR. Tidal range 1.0-2.0 m. Convex bottom profile, snapshots in time during spring tide.

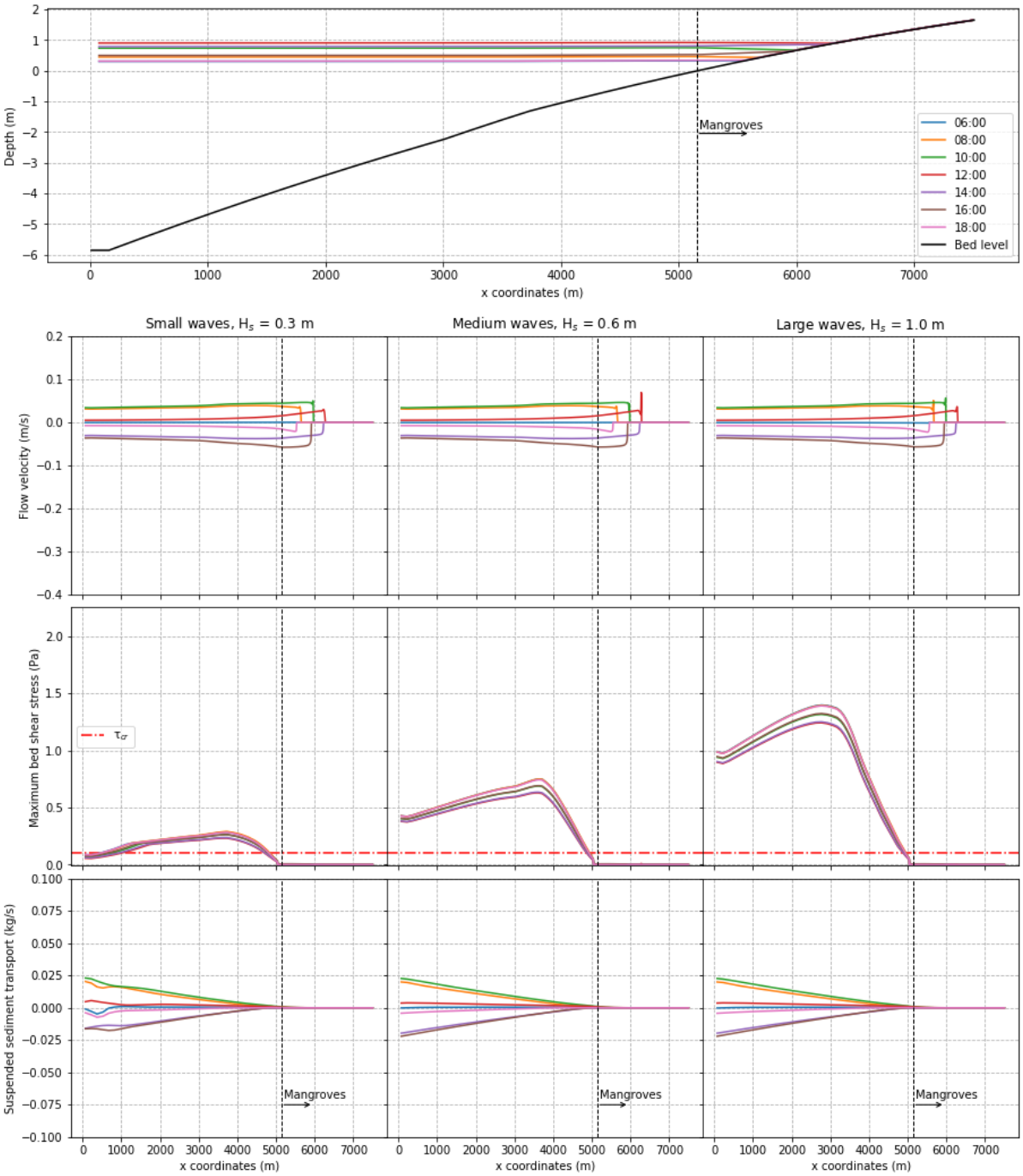

Figure B.37: Cross-shore overview of sea level rise simulation, 0.4 m SLR. Tidal range 0.4-0.6 m. Convex bottom profile, snapshots in time during spring tide.

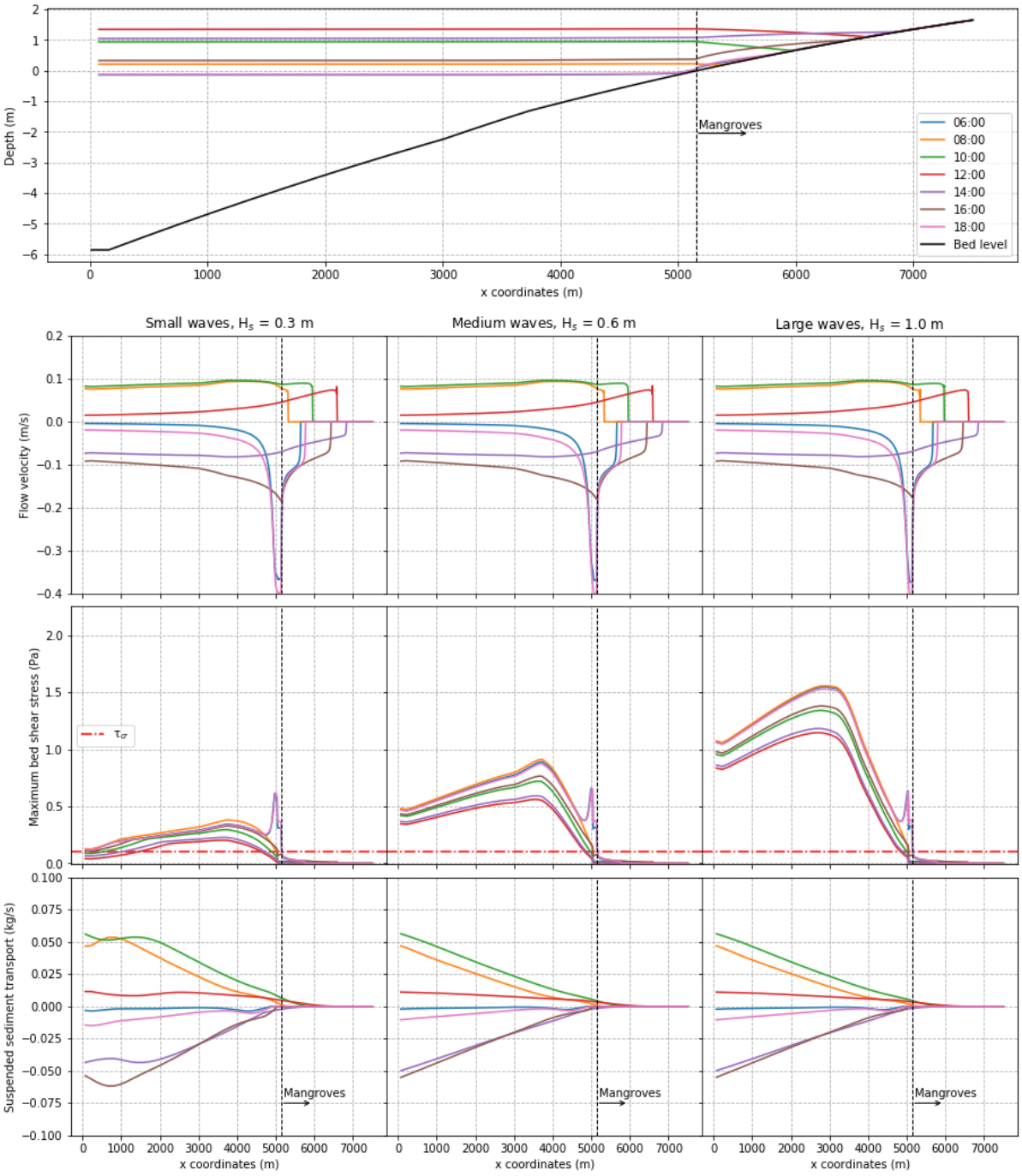

Figure B.38: Cross-shore overview of sea level rise simulation, 0.4 m SLR. Tidal range 0.8-1.5 m. Convex bottom profile, snapshots in time during spring tide.

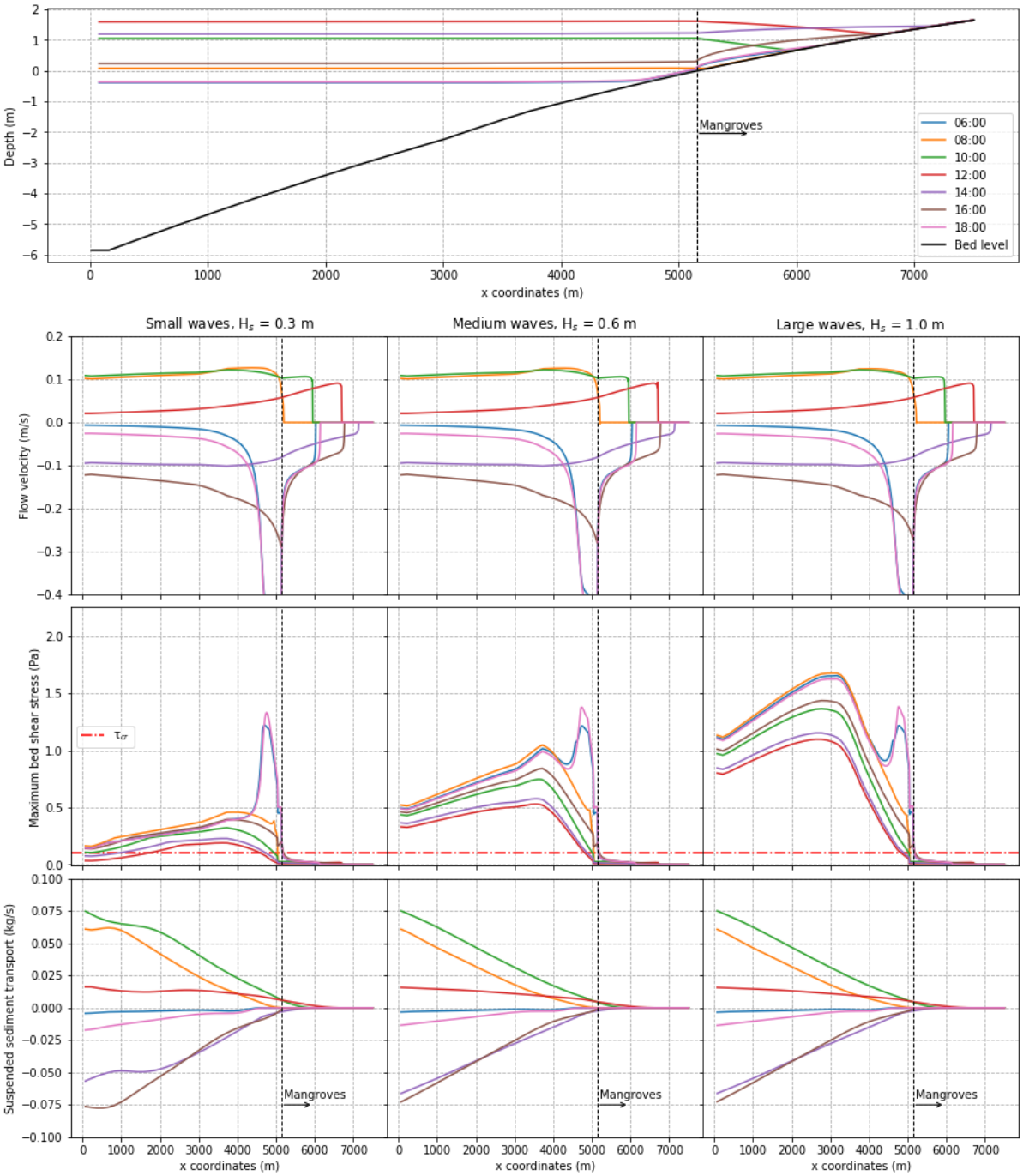

Figure B.39: Cross-shore overview of sea level rise simulation, 0.4 m SLR. Tidal range 1.0-2.0 m. Convex bottom profile, snapshots in time during spring tide.

Appendix C

Plots of sediment nourishments on a mangrove coast

In this appendix, the cross-shore overview plots of the different nourishment strategies (chapter 5) are presented.

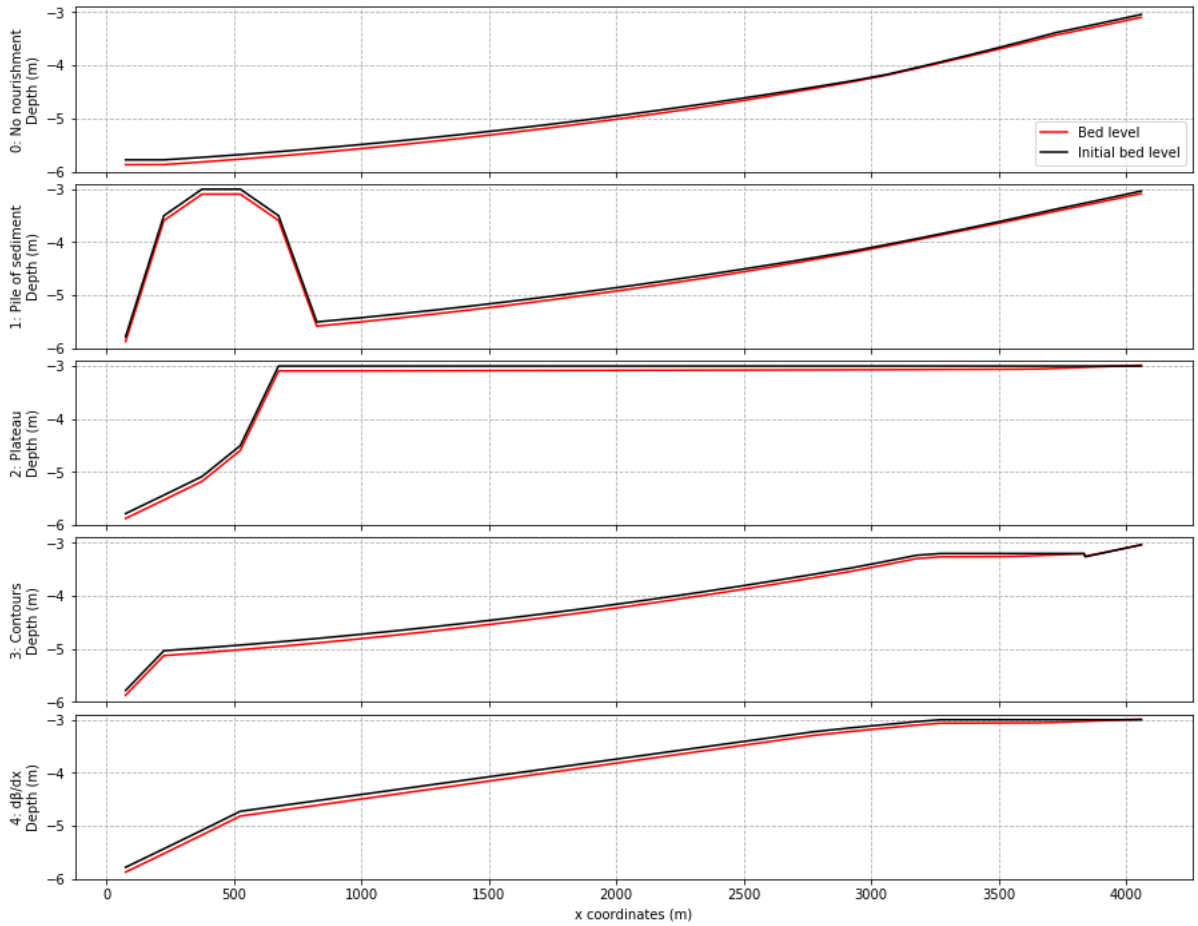

Figure C.1: Cross-shore overview of the erosion of the nourishment strategies after one tidal cycle, tidal range 0.8-1.5 m and wave height 0.6 m.

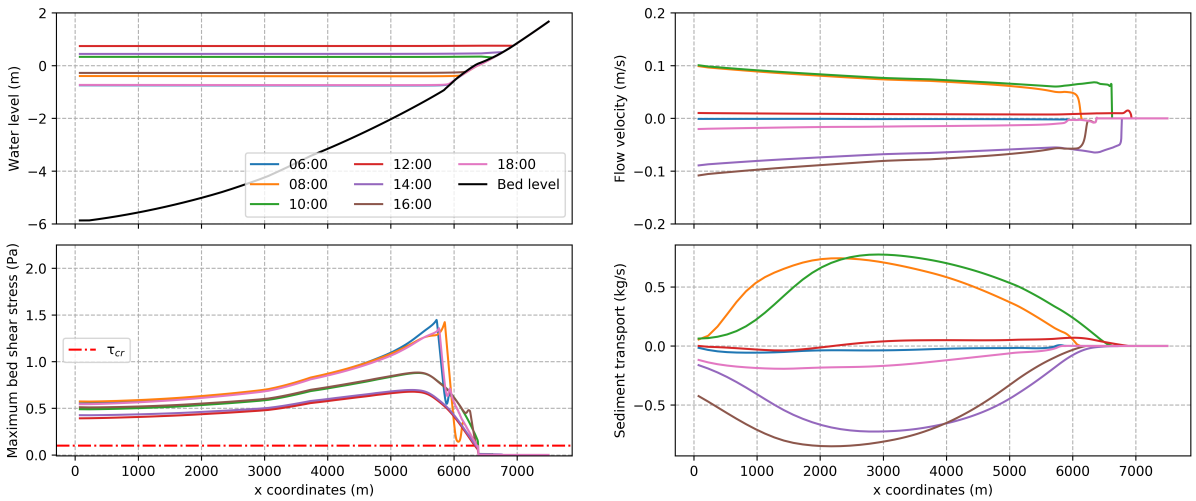

Figure C.2: Cross-shore overview of strategy 0: no nourishment. Tidal range 0.8-1.5 m, wave height 0.6 m. Snapshots in time during spring tide.

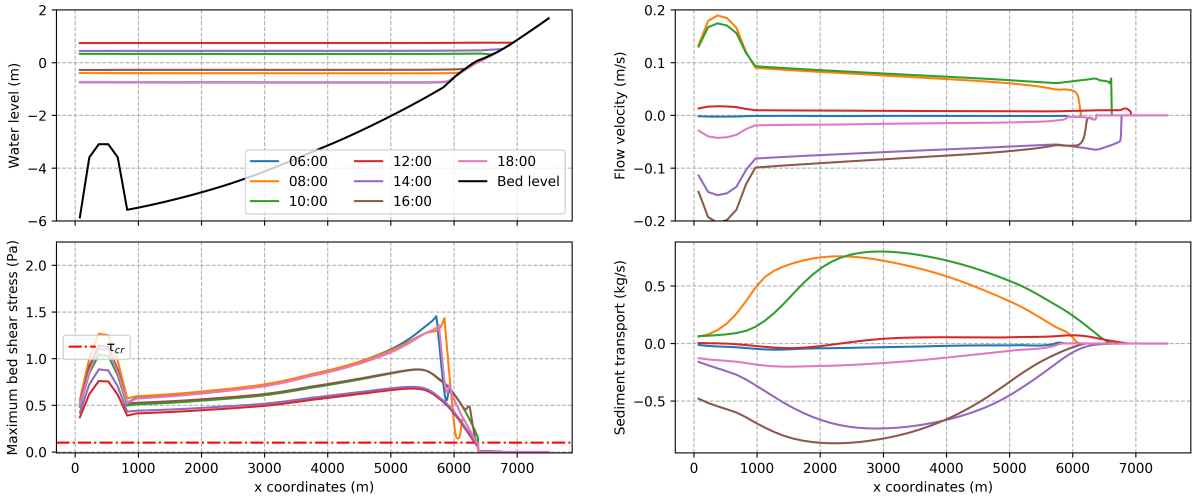

Figure C.3: Cross-shore overview of strategy 1: pile of sediment. Tidal range 0.8-1.5 m, wave height 0.6 m. Snapshots in time during spring tide.

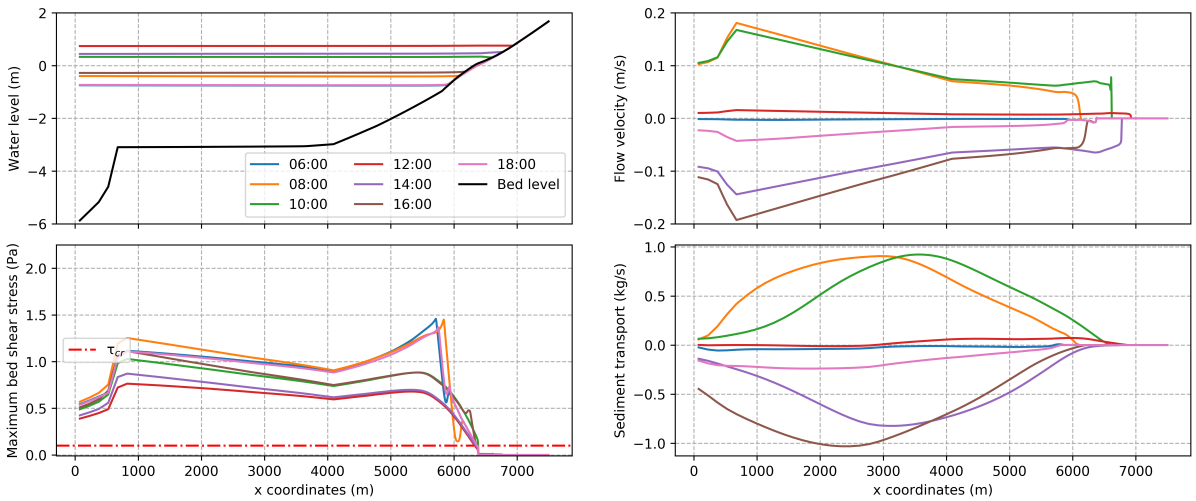

Figure C.4: Cross-shore overview of strategy 2: plateau of sediment. Tidal range 0.8-1.5 m, wave height 0.6 m. Snapshots in time during spring tide.

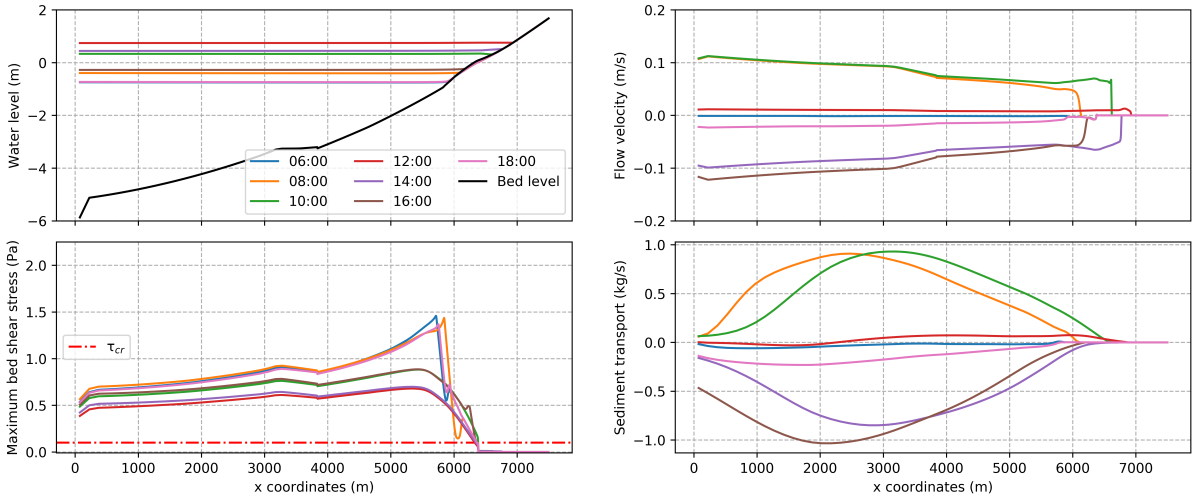

Figure C.5: Cross-shore overview of strategy 3: contours. Tidal range 0.8-1.5 m, wave height 0.6 m. Snapshots in time during spring tide.

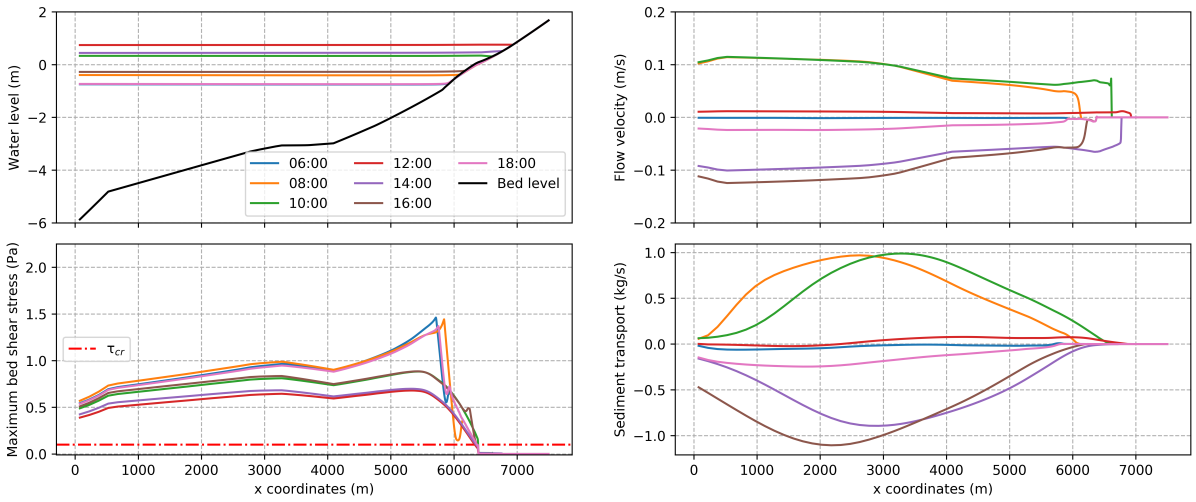

Figure C.6: Cross-shore overview of strategy 4: dβ/dx. Tidal range 0.8-1.5 m, wave height 0.6 m. Snapshots in time during spring tide.